Copper and Copper Alloys:
Studies of Additives

Igor Volov

Submitted in partial fulfillment of the requirements for the degree of Doctor of Philosophy
in the Graduate School of Arts and Sciences

COLUMBIA UNIVERSITY

2013

© 2012
Igor Volov
All rights reserved

Abstract

Copper and Copper Alloys:
Studies of Additives

Igor Volov

Electrodeposition of copper is used extensively for the fabrication of electrical interconnects in semiconductor device manufacturing and in printed circuit board production, as well as other industries. Copper is often plated from an acidic copper sulfate electrolyte with a number of inorganic and organic constituents. Electrolyte enables filling of complex surface geometries with desired internal and surface properties. Continuing miniaturization of modern microelectronics requires a highly controlled electrodeposition process and also requires interconnect materials with improved electromigration and stress migration resistances. Thus, current research deals with two avenues that have a potential to improve the process of copper electroplating and extend copper technology to meet the challenges of future device dimensions.

The improvement in the plating process of copper is being sought by the integration of an iron redox couple (Fe^{3+}/Fe^{2+}) to copper electrolytes. Certain benefits of incorporating

Fe^{3+}/Fe^{2+} subsystem in combination with inert anode to the electrolyte have been previously recognized, though without regards to the impact that Fe^{3+}/Fe^{2+} can exert on the behavior of additives. Organic additives are essential constituents of all copper plating baths. Therefore, we studied how the presence of Fe^{3+}/Fe^{2+} affects organics additives, with focus on two representative components: polyethylene glycol (PEG) and bis(3-sulfopropyl)-disulfide (SPS).

Electrochemical studies on a rotating disk electrode (RDE) and microfluidic device showed that the behavior of PEG during copper deposition is not affected in the presence of Fe^{3+} and Fe^{2+} ions. Kinetics of adsorption and desorption of PEG on copper electrode were also unaffected. In contrast, the activity of SPS increased when Fe^{3+}/Fe^{2+} were present in a copper-plating bath. By means of the electrochemical analysis and investigation by high performance liquid chromatography (HPLC), it was revealed that the Fe^{3+}/Fe^{2+} redox couple reacts with SPS to form 3-mercaptopropyl sulfonate (MPS) in the bulk solution. The ratio of Fe^{3+}/Fe^{2+} determined the reducing power of the electrolyte by changing the concentration of MPS derived from SPS. The estimates of the standard reduction potential of SPS to MPS reduction, based on equilibrium calculation with reference to HPLC results, put the reduction potential in the range between 0.3 – 0.4 V *vs.* standard hydrogen electrode (SHE).

To facilitate the study SPS/MPS equilibrium in the presence of ferrous and ferric ions, a new chromatographic method was developed for the detection of SPS, MPS, monoxide-of-SPS, and dioxide-of-SPS from a copper electrolyte. An HPLC tool was coupled with an electrochemical detector, which enabled concentration sampling in a range of just a few parts per billion (ppb). Due to its low limit of detection and effective separation of detectable compounds, this method can prove crucial for plating bath control, where very

little amount of certain byproducts may significantly decrease performance of the electrolyte.

As technology advances to create smaller microelectronics, copper interconnects are becoming more prone to failures by electromigration and stress migration effects. Copper can potentially be made less susceptible to these effects if alloyed with about one weight percent of another metal. Accordingly our research examined copper-silver (Cu-Ag) and copper-tin (Cu-Sn) alloys as two possible applications in interconnect technology.

The main challenge for depositing silver from copper plating electrolytes, which contain about 50 ppm of chloride, is the low solubility of silver ions with chloride. Together with other additives, chloride is a crucial component promoting defect-free filling of surface features. To overcome this challenge, it was shown that the application of pulse-plating instead of direct current plating enabled the use of chloride at a substantial concentration, while also allowing a wide range of Cu-Ag alloy compositions. Theoretical estimates of alloy compositions were in agreement with experimental values at various pulse frequencies and duty cycles, electrode rotation speeds, and electrolyte concentrations. However, organic additives decreased incorporation of Ag into the alloy due to a possible complexing effect on silver ion. It was also discovered that salt of copper ($CuSO_4 \cdot 5H_2O$) from a number of major chemical suppliers contains Ag as an impurity. Pulsating conditions were responsible for an unwanted increased in surface roughness of the plated film alloys. However, the addition of a leveling agent polyvinylpyrrolidone (PVP) at 10 ppm of chloride improved roughness and surface quality of the deposited Cu-Ag thin films.

Electrodeposits of copper-tin alloy thin films were prepared from acidic copper sulfate electrolytes by polarizing copper deposition into the region where Sn deposition

became possible. The ability to polarize copper deposition demonstrated with the use of EPE, poly(ethylene glycol)-*block*-poly(propylene glycol)-*block*-poly(ethylene glycol), and bromide in comparison to several other chemistries. Sn content between 0 – 7 at% was obtained above the reduction potential of Sn^{2+}. High Sn content of up to 20 at% was achieved when Cu deposition was suppressed below the deposition potential of Sn^{2+} by the combination of Br and EPE. A positive correlation between Sn content and concentration of Sn^{2+} in the electrolyte was observed. Higher tin content in the alloy was also correlated with low rotation speeds.

Table of Contents

CHAPTER 1

INTRODUCTION ………………………………………………………………………. 1

Overview of Copper Interconnect Technology ………………………………..... 1
Copper Electroplating Electrolyte and Additives …………………………….... 2
Iron Redox Couple for Copper Deposition ……………………...………….... 3
Electrodeposition of Copper Alloys ………………………………………...….... 4

CHAPTER 2

INVESTIGATION OF COPPER PLATING AND ADDITIVE INTERACTIONS IN THE PRESENCE OF FE3+/FE2+ REDOX COUPLE …..….. 11

ABSTRACT ……………………………………………………………………….... 11
INTRODUCTION ………………………………………………………………….... 12
EXPERIMENTAL …………………………………………………………………... 14
RESULTS AND DISCUSSION ……………………………………………………. 16
CONCLUSIONS …………………………………………………………………….. 21

CHAPETER 3

INTERACTION BETWEEN SPS AND MPS IN THE PRESENCE OF FERROUS AND FERRIC IONS ………………………………………………..…….. 38

ABSTRACT ……………………………………………………………………….... 38
INTRODUCTION ………………………………………………………………….... 39
EXPERIMENTAL …………………………………………………………………... 42
RESULTS AND DISCUSSION ……………………………………………………. 44
CONCLUSIONS …………………………………………………………………….. 51

CHAPTER 4

CHROMATOGRAPHY OF BIS-(3-SULFOPROPYL) DISULFIDE AND ITS BREAKDOWN PRODUCTS BY HPLC COUPLED WITH ELECTROCHEMICAL DETECTION 65

ABSTRACT 65
INTRODUCTION 66
MATERIALS AND METHODS 68
RESULTS AND DISCUSSION 70
CONCLUDING REMARKS 74

CHAPTER 5

PULSE-PLATING OF COPPER-SILVER ALLOYS FOR INTERCONNECT APPLICATIONS 86

ABSTRACT 86
INTRODUCTION 87
EXPERIMENTAL 88
RESULTS AND DISCUSSION 92
CONCLUSIONS 102
LIST OF SYMBOLS 102

CHAPTER 6

ELECTRODEPOSITION OF COPPER-TIN FILM ALLOYS FOR INTERCONNECT APPLICATIONS 117

ABSTRACT 117
INTRODUCTION 118
EXPERIMENTAL 120
RESULTS AND DISCUSSION 123
CONCLUSIONS 128

CHAPTER 7

CONCLUSSIONS 143

List of Figures and Tables

Chapter 2

Table I. Current efficiency measurements in the presence of the Fe^{3+}/Fe^{2+} couple without plating bath additives. Plating was performed on a Pt RDE at -15 mA cm^{-2} at a rotation speed of 300 rpm.

Figure 1. SEM cross sections of TSV (diameter = 5 μm, height = 25 μm) filling keeping all conditions the same except for Fe^{3+} concentration and anode material: (a) Cu anode, no Fe^{3+} ions; (b) inert anode, 0.47 g L^{-1} (0.0084 M) Fe^{3+}; (c) inert anode, 2 g L^{-1} (0.036 M) Fe^{3+}.

Figure 2. Schematic diagram of the microfluidic device (μ-cell), showing key dimensions.

Figure 3. Results of linear sweep voltammetry measured on a platinum surface inside the μ-cell and RDE. The electrolyte contained dissolved Fe^{3+} (0.5 g L^{-1} or 0.009 M) in 0.5 M H_2SO_4; scan rate was 10 mV s^{-1}. Graph shows mass diffusion limited currents at different flow conditions, and demonstrates that the mass flux inside the μ-cell was considerably higher than on the RDE.

Figure 4. Current as a function of time for an applied potential U = -150 mV *vs.* Ag|AgCl. Results were obtained in the μ-cell: at time = 41 s, additives were introduced to VMS. They are then removed at 150 s. The dashed line represents an experiment with PEG and the redox couple, and the solid line is for introduction of PEG alone. The PEG-Fe^{3+}/Fe^{2+} current density was increased by approximately -2 mA cm^{-2}, due to the reduction of ferric ions.

Figure 5. Current as a function of time for an applied potential U = -50 mV *vs.* Ag|AgCl. Results were obtained on an RDE. At time = 200 s, additives were injected to VMS. Results are shown for an experiment with PEG and the redox couple and for PEG alone. The PEG-Fe^{3+}/Fe^{2+} current density was increased by approximately -2 mA cm^{-2}, due to the reduction of ferric ions.

Figure 6. Current-potential curve on an RDE; potential was scanned from positive to negative at 10 mV s^{-1}. Results are shown for electrolytes containing: (1) VMS and PEG, (2) Fe^{3+} and PEG, and (3) VMS, PEG, and Fe^{3+}.

Figure 7. Current as a function of time for an applied potential U = -50 mV vs. Ag|AgCl. Results were obtained on an RDE. At time = 200 s, additives were injected to VMS. Results are shown for: (1) PEG and SPS, (2) PEG, SPS, and redox couple (no bath aging), and (3) PEG, SPS and redox couple (six experiments combined for various aging times). Premixing of SPS and Fe^{3+}/Fe^{2+} before injection had a noticeable effect on acceleration of Cu ECD.

Figure 8. Current as a function of time for an applied potential U = -100 mV *vs.* Ag|AgCl. Results were obtained in the μ-cell: at time = 41 s, additives were introduced to VMS. They were then removed at 150 s. The dashed line represents an experiment with PEG and the redox couple, and the solid line is for introduction of PEG alone. Premixing of SPS and Fe^{3+}/Fe^{2+} before injection for 3 h had a noticeable effect on acceleration of Cu ECD.

Figure 9. Current as a function of time for an applied potential U = -50 mV vs. Ag|AgCl. Results were obtained on an RDE. At time = 156 s, additives were injected to VMS. Results are shown for: (1) PEG and SPS (premixed for 1 day), (2) PEG, SPS and Fe3þ (premixed for 1 day), (3) PEG, SPS and Fe^{2+} (premixed for 1 day), (4) PEG, SPS, and MPS. Premixing of SPS and Fe^{3+} before experiment showed no effect on acceleration of Cu ECD. Premixing of SPS and Fe^{2+}, however, did increase acceleration and the result closely follows injection of PEG, SPS and MPS to VMS.

Figure 10. Current as a function of time for an applied potential U = -100 mV *vs.* Ag|AgCl. Results were obtained on an RDE at 900 rpm. The dotted line represents an experiment with PEG, SPS and Fe^{2+} in VMS (aged for 3 h), and the solid line is for PEG and SPS alone. Premixing of SPS and Fe^{2+} before experiment shortened the time to steady state.

Figure 11. Current as a function of time for an applied potential U = -100 mV *vs.* Ag|AgCl. Results were obtained on an RDE at different rotation speeds. The electrolyte contained PEG, SPS, and Fe^{2+} ions, premixed 3 h prior to the experiments. The mass transfer dependency presented here is characteristic of PEG, SPS, and MPS containing electrolytes (not shown).

Chapter 3

Figure 1. Possible reduction and oxidation pathways to certain break-down products of SPS.

Figure 2. HPLC chromatogram obtained from aging of SPS (15 ppm) and Fe^{2+} (10 g L^{-1}) in 0.3 M H_2SO_4. The peak around 17 min was attributed to MPS.

Figure 3. HPLC chromatogram obtained from aging of SPS (15 ppm) and Fe^{3+} (10 g L^{-1}) in 0.3 M H_2SO_4.

Figure 4. HPLC chromatogram obtained from aging of SPS (15 ppm), Fe^{2+} (10 g L^{-1}), and Cu^{2+} (10 g L^{-1}) in 0.3 M H_2SO_4. The peak around 17 min was attributed to MPS. The MPS peak area was reduced in the presence of cupric ions.

Figure 5. Linear sweep voltammetry results obtained at a sweep rate of 10 mV s^{-1}; the potential was swept from positive to negative. Results were obtained on preplated with copper, platinum RDE at 900 rpm, 1 day after bath preparation. The dashed line represents an experiment with PEG and SPS, dotted line is an electrolyte with SPS and Fe^{2+}, and the

solid line is for SPS and MPS (using an MPS concentration taken from HPLC measurements).

Figure 6. Current as a function of time for an applied potential of U = -100 mV *vs.* Ag|AgCl. Data were obtained on an RDE at 900 rpm, 2 – 3 h after bath preparation. Results are shown for a three pair of experiments: at 10, 35, and 65 g L^{-1} of cupric ions in electrolyte. As the level of cupric ions was increased the difference in acceleration in the presence and absence of Fe^{2+} was reduced.

Figure 7. Current as a function of time for an applied potential U = -100 mV *vs.* Ag|AgCl. Data were obtained on an RDE at 900 rpm, 4 h after bath preparation. Results show that the steady state current from the acceleration of copper deposition was only a function of a ratio between ferric and ferrous ions.

Figure 8. Steady state current values, from potentiostatic plating at U = -100 mV, are plotted as a function of the Fe^{3+}/Fe^{2+} ratios. In all experiments, the ferric-ion concentration was 0.5 g L^{-1} and the ratio was varied by changing the ferrous-ion concentration.

Figure 9. Calculated values of MPS equilibrium concentrations as a function of Fe^{3+}/Fe^{2+} ratio using several assumed SPS standard reduction potentials. The initial concentration of SPS was 15 ppm.

Figure 10. Calculated values of MPS equilibrium concentrations as a function of Cu^{2+} concentration. The SPS reduction potential was chosen to be 0.33 V *vs.* SHE, and results are given for various initial concentrations of ferric ions and a set concentration of ferrous ions at 10 g L^{-1}.

Chapter 4

Table 1. Chemical structure of SPS and its by-products.

Figure 1. Scheme of HPLC-ED set-up used for the detection of SPS and its by-products. Samples were mixed with the mobile phase at the autosampler and the effluent was sent directly through the analytical column. Prior to chromatographic measurements, samples were pretreated by passing the solution though an OnGuard II H ion exchange cartridge (not shown).

Figure 2. An integrated pulsed amperometry waveform for the detection of organo-sulfur compounds.

Figure 3. Chromatographic separation of SPS and its detectable by-products with the Atlantis T3 column and 2% acetonitrile in 0.0125M H_2SO_4 as mobile phase (a.u. stands for arbitrary units).

Table 2. Composition and chemical suppliers for all chemicals used in this chapter.

Figure 4. Current as a function of the linear potential sweep at 10 mV s^{-1}. Results were obtained at the rotating platinum disk electrode preplated with a thin copper layer. The electrochemical behavior of known chemical standards in copper electrolyte is shown. A small concentration of MPS had a significant effect on acceleration. Mono-ox-SPS and di-ox-SPS exhibited less acceleration than SPS.

Figure 5. Example of chromatograms of standard addition recorded to evaluate concentrations of SPS, mono-ox-SPS, and di-ox-SPS (curves recorded with a 2% ACN and a detection range of 100 nC). Ordinate has arbitrary units (a.u.).

Figure 6. Chromatography of bath sample before and after plating for 6 Ah L^{-1} (detection range of 100 nC for this set of experiments).

Figure 7. Measurement of reproducibility at various times.

Chapter 5

Figure 1. Linear sweep voltammetry results obtained at a sweep rate of 5 mV s^{-1}; the potential was swept from less to more negative. Data were obtained on a preplated with copper, platinum RDE at 100 rpm. Results illustrate the effect of PEG on the suppression of copper deposition at various concentrations of chloride.

Figure 2. An example of the unipolar pulse-plating waveform that was employed for the deposition of Cu-Ag alloys. At zero current, Cu on the surface is replaced by silver; at negative current both Cu and Ag are galvanostatically plated. Duty cycle for the shown pulse is equal to 9.47% and frequency is 1.38 Hz.

Figure 3. Concentration of Ag as a function of ionic copper from a specific lot of $CuSO_4 \cdot 5H_2O$. Films were plated at 400 rpm, 9.47% duty cycle, 1.38 Hz frequency. Figure shows the presence of Ag, even though Ag was not added to solution. This is because $CuSO_4 \cdot 5H_2O$ already contains Ag as an impurity.

Figure 4. Composition of Ag in the alloy as a function of ionic Ag in the electrolyte, obtained at 400 rpm, 9.47% duty cycle, 1.38 Hz frequency, and i_{on} = -10 mA cm^{-2} (the nominal thickness is 226 nm). Straight line shows the theoretical values (assuming mass transfer controlled Ag deposition). The data demonstrates lower plating rate of Ag in the presence of PEG and SPS, and also how the solubility AgCl affects silver content in the film.

Figure 5. Composition of Ag in alloy as a function of rotation speed. The electrodeposition was performed at 1.38 Hz, 9.47% duty cycle, and i_{on} = -10 mA cm^{-2}. The straight line shows theoretical estimates assuming mass transfer controlled Ag deposition. The nominal thickness was kept at 226 nm.

Figure 6. Effect of duty cycle on the variation of Ag in the alloy. The electrodeposition was performed at 400 rpm, 1.38 Hz, and i_{on} = -10 mA cm^{-2}, while keeping the nominal thickness

at 50 nm. The times labeled above the data points indicate the off-time required to reach an estimated thickness of 50 nm.

Figure 7. Roughness profile of the thin films plated at 400 rpm by (a) pulse-plating from bath with PEG, SPS, and Cl (10 ppm); (b) DC plating with PEG, SPS, and Cl (10 ppm). Pulse plating was done at duty cycle of 9.47% and frequency of 1.38 Hz.

Figure 8. Scanning electron images taken at the center of the Cu-Ag alloy thin films before heat treatment. Samples were plated at 400 rpm and 9.47% duty cycle from the electrolyte containing PEG, SPS, PVP, c_{Ag^+} = 1.7 μM, at two different chloride concentrations. (a) cross-section view, at $c_{Cl^-} = 1$ ppm, nominal thickness 120 nm, 0.3 wt% Ag; (b) cross-section view, $c_{Cl^-} = 10$ ppm, nominal thickness 230 nm, 0.3 wt% Ag.

Figure 9. ToF-SIMS depth profile of the Cu-Ag film plated from an electrolyte with PEG, SPS, PVP, $c_{Cl^-} = 10$ ppm, and $c_{Ag^+} = 1.7$ μM. Film was deposited at 400 rpm and 9.47% duty cycle for a nominal thickness of 230 nm. Silver content shown in the figure is about 0.3 wt%.

Chapter 6

Figure 1. Linear sweep voltametry results conducted at a sweep rate of 5 mV s^{-1} and rotation speed of 100 rpm. Results show the polarization of copper deposition on preplated RDE in the presence of Cl-PEG, Cl-EPE or Br-EPE additive systems. Two different electrolyte compositions were used: Electrolyte A was composed of Cu^{2+} = 0.31 M and H_2SO_4 = 1.53 M and Electrolyte B was composed of Cu^{2+} = 0.63 M and H_2SO_4 = 0.31 M.

Figure 2. Linear sweep voltametry results conducted on preplated RDE at a sweep rate of 5 mV s^{-1} and rotation speed 100 rpm. Results show polarization of Cu deposition by Cl-PEG, Cl-EPE, Br-PEG, and Br-EPE systems with and without SPS. In the presence of Br^- ions, SPS has little to no effect on polarization of Cu^{2+} reduction.

Figure 3. Linear sweep voltametry results conducted on preplated RDE at a sweep rate of 5 mV s^{-1} and rotation speed of 100 rpm. Experiments show the onset of Sn deposition and the influence of additives on polarization of Sn^{2+} deposition.

Figure 4. Linear sweep voltametry results conducted on preplated RDE at a sweep rate of 5 mV s^{-1} and rotation speed 100 rpm. Experiments show that polarization of Cu deposition by different halogen-suppressor pairs is almost unaffected by the presence Sn^{2+} ions at 84.3 mM.

Figure 5. Composition of Sn in the Cu-Sn alloy as a function of current density and Sn^{2+} concentration in the electrolyte containing Cl-EPE additive system. Deposition was conducted at 100 rpm.

Figure 6. Composition of Sn in the Cu-Sn alloy as a function of rotation speed and Sn^{2+} concentration in the electrolyte containing Cl-EPE additive system. Deposition was conducted at $j = -20$ mA cm^{-2}.

Figure 7. Time variation of electrode potential during coupon plating at various current densities. Electrolyte contained 84.3 mM Sn^{2+} and Cl-EPE additive system. Potential was corrected for ohmic drop. The nominal thickness of each deposit was 1 μm.

Figure 8. Composition of Sn in the Cu-Sn alloy as a function of current density and Sn^{2+} concentration in the electrolyte containing Br-PEG additive system. Deposition was conducted at 100 rpm.

Figure 9. Composition of Sn in the Cu-Sn alloy as a function of rotation speed and Sn^{2+} concentration in the electrolyte containing Br-PEG additive system. See legend for the applied current density.

Figure 10. Composition of Sn in the Cu-Sn alloy as a function of current density and Sn^{2+} concentration in the electrolyte containing Br-EPE additive system. Deposition was conducted at 100 rpm.

Figure 11. Composition of Sn in the Cu-Sn alloy as a function of rotation speed and Sn^{2+} concentration in the electrolyte containing Br-EPE additive system. Deposition was conducted at $j = -10$ mA cm^{-2}.

Acknowledgements

I would like to express sincere gratitude to my advisor Alan C. West, whose generous support and guidance made this work possible. It is also an honor to acknowledge contributions from all my coauthors on the academic publications, which lay at the heart of this text. A valuable assistance from Ugur Emekli in understanding copper electrodeposition is much appreciated. I would also like to acknowledge the support from Edward Swanson and Greeshma Gadikota in running ICP experiments. I am very thankful to my laboratory colleagues Asli Sahin, Xiaoxuan Sun, Ugur Emekli, Damla Eroglu, Feng Qiao, Robert J. von Gutfeld, Jun Wu, and Joshua Gallaway for their invaluable support and encouragement during my years in Columbia University.

I thank Atotech USA, Inc. for funding this work, and extend special thanks to Robert Preisser for following the progress of this research and enabling my summer stay at Atotech, Berlin GmbH. A generous help in development of the HPLC method described in chapter 4 from Yvonne Hoenersch and Olivier Mann of Atotech is also appreciated.

Chapter 1

Introduction

Overview of Copper Interconnect Technology

The process of copper electroplating is utilized in the fabrication of many modern technologies, such as printed circuit boards (PCB) and semiconductor devices.[1] Copper metal is preferred due to its low resistivity and good electromigration reliability. Typically copper is deposited from an acidic copper sulfate electrolyte by the application of a direct current. During the electrochemical deposition (ECD) process cupric ions (Cu^{2+}) from electrolyte reduce at the cathode to cupreous ions (Cu^{+}) and then to form copper metal (Cu).[2] This process is shown in reactions 1 and 2.

$$Cu^{2+} + e^{-} \rightleftharpoons Cu^{+} \quad (1)$$

$$Cu^{+} + e^{-} \rightleftharpoons Cu \quad (2)$$

The scope of this work is aimed towards the use of copper electroplating in creating electrical conductors – commonly referred to as interconnects – for integrated circuits.[3, 4] Copper has become a metal of choice in the semiconductor industry since the commercial introduction of a Damascene process in 1997.[5] Interconnect fabrication starts by patterning dielectric (*e.g.* silicon dioxide) with desired surface topography using photolithographic processes. Then, on top of dielectric a diffusion barrier layer (such as tantalum nitride and

titanium nitride) is deposited by physical or chemical vapor deposition under high vacuum.[6,7] Barrier layer prevents the diffusion of Cu into the underlying dielectric. This layer is followed by a copper seed layer, which is also deposited by the vacuum process, and is applied to provide a well conductive surface for the electroplating step. Seed layer may also be used to form copper alloys by providing dopant material into the copper layer with a high temperature step. During the electrochemical deposition, wafer is immersed into a copper plating bath, current is applied across the wafer, and the surface cavities are filled with copper. In the next processing step, overfilled metal is removed with chemical mechanical polishing (CMP) for surface planarization.[8]

Copper Electroplating Electrolyte and Additives

The ability of ECD to fill features defect-free and with desired grain structure is made possible by the interaction of additives contained in the electroplating bath. Mixture of various additives promote bottom-up filling of interconnect features (such as trenches and vias) in a phenomena known as superfilling. During superfilling the rate of copper deposition is accelerated at the bottom of the feature while the rate of plating at the side walls of the feature and top entry is suppressed.[9-11]

Copper electrolytes are composed of inorganic and organic constituents. Inorganic components are copper sulfate salt, sulfuric acid, and halogen. Chloride is a primary halogen used, as it effectively modifies adsorption properties of organic additive.[12] Organic components are usually classified into three categories: suppressor, accelerator, and leveler. Suppressor is typically a polyether (such as polypropylene glycol (PEG) which polarizes Cu deposition in combination with chloride by adsorbing on a copper surface during plating.[13-15] The most commonly utilized accelerator is bis-(3-sulfopropyl) disulfide (SPS); it

precipitates in charge transfer reaction and determines Cu growth profile with major impact on metallurgy.[16-20] SPS is known to alleviate suppression caused by PEG and Cl^-. Lastly, leveling agents are often used to reduce surface roughness by inhibiting growth rate of copper at protrusions.[21-23] There are many variety of levelers, with polyvinylpyrrolidone (PVP) being a model leveler in a variety of publications.[24]

Iron Redox Couple (Fe^{3+}/Fe^{2+}) for Copper Deposition

On-chip metallization of copper can possibly be improved by utilizing an iron redox couple (Fe^{3+}/Fe^{2+}) in copper electrolytes. Fe^{3+}/Fe^{2+} couple is already implemented in PCB industry for filling features such as blind-microvias and through-hole vias.[25-27] Anodic oxidation of Fe^{2+} ions allows for the use of dimensionally stable, insoluble anode materials without the formation of defect causing oxygen bubbles (as oppose to no redox couple and soluble Cu anode).[28] As ferrous ions are oxidized at the anode, ferric ions are reduced on the cathode at a mass transfer limited rate. This results in lower current efficiency of copper reduction on a surface, and relatively higher copper deposition inside a via.[29] For semiconductor chip structures, an additional benefit is that Fe^{3+} ions can contribute to the reduction of overburden thickness, which is favorable for subsequent processing by CMP.

The main motivation to use iron redox mediator chemistry is to (a) reduce additive consumption rate if no membrane (separating anolyte and catholyte) is in place, and (b) incorporate Fe-atoms in the copper structure to enhance electromigration and stress-migration stability. Reduced additive consumption extends bath lifetime and promotes deposition of cleaner copper films.[30] Since copper electroplating on semiconductor devices requires stringent bath control for additive breakdown products, reduced consumption of additives is of real advantage over conventional plating electrolytes.

The goal of this work is to provide a better understanding of the impact that Fe^{3+}/Fe^{2+} couple exerts on the interaction between organic additives that enable superfilling. Since a tight control of additive formulation is necessary for the interconnect fabrication, this investigation may facilitate the introduction of Fe^{3+}/Fe^{2+}–mediated chemistry to commercial plating systems.

Chapter 2 presents mainly electrochemical investigation of the redox couple – additive interactions, which were carried on a conventional rotating disk electrode (RDE) as well in–lab built microfluidic cell (μ–cell).[31-33] Utilization of both electrochemical setups enables system characterization at diverse hydrodynamic conditions. Chapter 3 builds on the study presented in chapter 2 with utilization of a newly developed high performance liquid chromatography (HPLC) method[34] described in chapter 4. The focus of chapter 3 is interaction between SPS and Fe^{3+}/Fe^{2+}, where HPLC and electrochemical investigations are complimented by equilibrium estimates.[35]

Electrodeposition of Copper Alloys

Electromigration is one of the main reliability issues in modern integrated circuits, where copper interconnects are particularly affected.[36-39] Accordingly, new interconnect materials that are less susceptible to electromigration are required. It has been shown that co-deposits of Cu with other metals (such as Ag, Sn, Co, and Mg) can potentially mitigate both electro- and stress-migration.[40-42] The content of the alloying metal needs to be small since the resistivity of the interconnect increases with the addition of foreign metals.[41] Various copper alloy compositions are possible with the application of controlled co-electrodeposition of cupric and other metallic ions. In this study, we focus on two candidate

copper alloys as a possible application in interconnect technology: copper-silver (Cu-Ag) and copper-tin (Cu-Sn) alloys.

A large difference in the standard reduction potentials between Cu^{2+} ($U^{\theta} = 0.337\ V$)[43] and Sn^{2+} ($U^{\theta} = -0.136\ V$)[43] is the main challenge for electrodepositing Cu-Sn alloys (standard electrode potentials U^{θ} are given with respect to the standard hydrogen electrode (SHE)). While the main challenge for depositing Cu-Ag alloys is the low solubility of chloride with silver ions (the solubility product of AgCl in water at 25^{0}C is only 1.8×10^{-10} M^{2})[44]. However, the control of the Ag content in deposit can be readily achieved, since Ag^{+} reduction ($U^{\theta} = 0.799\ V\ vs. SHE$)[43] occurs in a mass-transfer-controlled regime during copper deposition.

Chapter 5 demonstrates the application of a pulsating current instead of a direct current as it permits the use of chloride at a substantial concentration, while also allowing a wide range of Cu-Ag alloy compositions. The aim of chapter 5 is to investigate the composition of Cu-Ag alloys at various pulse-plating parameters, such as frequency and duty cycle, as well as various electrolyte concentrations. The role of the displacement reactions in pulse-plating of Cu-Ag is shown by comparing measured alloy compositions with those predicted by theoretical estimates. Additionally, film microstructure and surface quality of the deposited Cu-Ag alloy films is also examined.

Although Cu-Sn deposition have been studied for multiple applications and from various electrolytes,[42, 45-51] the electrochemical deposition of Cu-Sn alloys for the microelectronic applications have received limited attention.[42, 49] Chapter 6 describes investigation into co-deposition of Cu-Sn from acidic copper sulfate solutions at currents below the limiting current of Cu and without the use of complexing agents. The ability to

produce varying Cu-Sn alloy compositions is demonstrated with the use of polyethylene glycol-block-polypropylene glycol-block-polyethylene glycol (EPE) and bromide. Electrodeposition of copper in the presence of EPE-chloride pair[52-54] and Br-suppressor pair[55] has been investigated in the past. This approach enables the use of stronger halogen-suppressor pairs, rather than a conventional Cl-PEG, in order to polarize Cu deposition to a greater extend so that the deposition of Sn becomes possible.

.

References

1. M. Schlesinger and M. Paunovis, *Modern Electroplating*, p. 888, Wiley-Interscience (2000).
2. J. Newman and K. E. Thomas-Alyea, *Electrochemical Systems*, p. 672, Wiley-Interscience (2004).
3. *International Technology Roadmap for Semiconductors*, Interconnect Chapter (2009).
4. T. Osaka, M. Hasegawa, M. Yoshino and N. Yamachika, *Advanced Nanoscale ULSI Interconnects: Fundamentals and Applications*, p. 183, Springer Science & Business Media, LLC, New York (2009).
5. P. C. Andricacos, C. Uzoh, J. O. Dukovic, J. Horkans and H. Deligianni, *IBM Journal of Research & Development*, 42, 567 (1998).
6. J. Baumann, T. Werner, A. Ehrlich, M. Rennau, C. Kaufmann and T. Gessner, *Microelectronic Engineering*, 37â€“38, 221 (1997).
7. G. S. Chen and S. T. Chen, *J. Appl. Phys.*, 87 (2000).

8. J. M. Steigerwald;, S. P. Murarka; and R. J. Gutmann;, *Chemical Mechanical Planarization of Microelectronic Materials*, Wiley-VCH (1997).

9. T. P. Moffat, J. E. Bonevich, W. H. Huber, A. Stanishevsky, D. R. Kelly, G. R. Stafford and D. Josell, *Journal of The Electrochemical Society*, 147, 4524 (2000).

10. A. C. West, S. Mayer and J. Reid, *Electrochemical and Solid-State Letters*, 4, C50 (2001).

11. T. P. Moffat, D. Wheeler, S. K. Kim and D. Josell, *Electrochimica Acta*, 53, 145 (2007).

12. W.-P. Dow and H.-S. Huang, *Journal of The Electrochemical Society*, 152, C67 (2005).

13. J. J. Kelly and A. C. West, *Journal of The Electrochemical Society*, 145, 3477 (1998).

14. J. J. Kelly and A. C. West, *Journal of The Electrochemical Society*, 145, 3472 (1998).

15. J. P. Healy, D. Pletcher and M. Goodenough, *Journal of Electroanalytical Chemistry*, 338, 155 (1992).

16. M. Tan and J. N. Harb, *Journal of The Electrochemical Society*, 150, C420 (2003).

17. J. J. Kim, S.-K. Kim and Y. S. Kim, *Journal of Electroanalytical Chemistry*, 542, 61 (2003).

18. E. E. Farndon, F. C. Walsh and S. A. Campbell, *Journal of Applied Electrochemistry*, 25, 574 (1995).

19. T. P. Moffat, D. Wheeler, M. D. Edelstein and D. Josell, *IBM J. Res. Dev.*, 49, 19 (2005).

20. T. P. Moffat, D. Wheeler and D. Josell, *Journal of The Electrochemical Society*, 151, C262 (2004).

21. J. J. Kelly, C. Tian and A. C. West, *Journal of The Electrochemical Society*, 146, 2540 (1999).

22. S. K. Kim, D. Josell and T. P. Moffat, *Journal of The Electrochemical Society*, 153, C616 (2006).

23. M. Hasegawa, Y. Negishi, T. Nakanishi and T. Osaka, *Journal of The Electrochemical Society*, 152, C221 (2005).

24. M. J. Willey, J. Reid and A. C. West, *Electrochemical and Solid-State Letters*, 10, D38 (2007).

25. S. Kenny and B. Reents, in *Proceedings of the CPCA* (2005).

26. S. Kenny, B. Reents and J. Zosel, in *Proceedings of the CPCA* (2003).

27. S. Kenny and K. Matejat, in *EPC 2000 Proceedings of the European PCB Convention*, p. 10 (2000).

28. J. Barthelmes, in *Electronics Circuits World Convention 8* (1999).

29. B. Roelfs, S. Kenny and T. Fujiwara, *JPCA* (2008).

30. J. D. Adolf, R. Preisser and U. Landau, *ECS Meeting Abstracts*, 902, 2163 (2009).

31. M. J. Willey and A. C. West, *Electrochemical and Solid-State Letters*, 9, E17 (2006).

32. M. J. Willey and A. C. West, *Journal of The Electrochemical Society*, 153, C728 (2006).

33. I. Volov, T. Saito and A. C. West, *Journal of The Electrochemical Society*, 158, D384.

34. I. Volov, O. Mann, Y. Hoenersch, B. Wahl and A. C. West, *Journal of Separation Science*, 34, 2385 (2011).

35. I. Volov and A. C. West, *Journal of The Electrochemical Society*, 158, D456.

36. J. R. Lloyd, *Microelectronic Engineering*, 49, 51 (1999).

37. S. R. Wilson, C. J. Tracy and J. L. Freeman, *Handbook of Multilevel Metallization for Intergrated Circuits*, p. 910, William Andrew (1994).

38. C. M. Tan, *Electromigration in ULSI Interconnections*, p. 312, World Scientific Publishing Company (2012).

39. A. Heryanto, K. L. Pey, Y. K. Lim, W. Liu, N. Raghavan, J. Wei, C. L. Gan, M. K. Lim and J. B. Tan, *Journal of Applied Physics*, 109, 9 (2011).

40. C.-K. Hu, M. Angyal, B. C. Baker, G. Bonilla, C. Cabral, D. F. Canaperi, S. Choi, L. Clevenger, D. Edelstein, L. Gignac, E. Huang, J. Kelly, B. Y. Kim, V. Kyei-Fordjour, S. L. Manikonda, J. Maniscalco, S. Mittal, T. Nogami, C. Parks, R. Rosenberg, A. Simon, Y. Xu, T. A. Vo and C. Witt, in *STRESS-INDUCED PHENOMENA IN METALLIZATION: 11th International Workshop*, E. Zschech, P.S. Ho and S. Ogawa Editors, p. 57 (2010).

41. S. Strehle, J. W. Bartha and K. Wetzig, *Thin Solid Films*, 517, 3320 (2009).

42. D. Padhi, S. Gandikota, H. B. Nguyen, C. McGuirk, S. Ramanathan, J. Yahalom and G. Dixit, *Electrochimica Acta*, 48, 935 (2003).

43. L. L. Shreir, R. A. Jarman and G. T. Burstein, Corrosion (3rd Edition) Volumes 1-2, in, Elsevier (1994).

44. J. A. Dean, Lange's Handbook of Chemistry (15th Edition), in, McGraw-Hill (1999).

45. G. I. Medvedev, N. A. Makrushin and O. V. Ivanova, *Russian Journal of Applied Chemistry*, 77, 1104 (2004).

46. A. Survila, Z. Mockus, S. KanapeckaitÄ—, V. JasulaitienÄ— and R. JuÅ¡kÄ—nas, *Electrochimica Acta*, 52, 3067 (2007).

47. O. Galdikiené and Z. Mockus, *Journal of Applied Electrochemistry*, 24, 1009 (1994).

48. S. D. Beattie and J. R. Dahn, *Journal of The Electrochemical Society*, 150, A894 (2003).

49. J. Horkans, I. C. H. Chang, P. C. Andricacos and H. Deligianni, *Journal of The Electrochemical Society*, 142, 2244 (1995).

50. Hiroaki Nakano, Satoshi Oue, Daisuke Yoshihara, Hisaaki Fukushima, Yoshifumi Saka, Shigeru Sawada and Y. Hattori, *Materials Transactions*, 52, 1237 (2011).

51. Zhiqing Qiao, Wei Shang, Xin Zhang and C. Wang, *Analytical and Bioanalytical Chemistry*, 381, 1467 (2005).

52. J. W. Gallaway, M. J. Willey and A. C. West, *Journal of The Electrochemical Society*, 156, D146 (2009).

53. J. W. Gallaway, M. J. Willey and A. C. West, *Journal of The Electrochemical Society*, 156, D287 (2009).

54. J. W. Gallaway and A. C. West, *Journal of The Electrochemical Society*, 155, D632 (2008).

55. M. Hayase, M. Taketani, T. Hatsuzawa and K. Hayabusa, *Electrochemical and Solid-State Letters*, 6, C92 (2003).

Chapter 2

Investigation of Copper Plating and Additive Interactions in the Presence of Fe^{3+}/Fe^{2+} redox couple*

Abstract

The impact of the ferric/ferrous (Fe^{3+}/Fe^{2+}) redox couple on the behavior of polyethylene glycol (PEG) and bis-(3-sulfopropyl) disulfide (SPS) during copper electrodeposition is investigated. The Fe^{3+}/Fe^{2+} couple is used in plating of copper onto printed circuit boards and may have advantages when implemented for on-chip metallization of copper. Experiments show that in the presence of Fe^{3+}/Fe^{2+} the suppressing behavior of PEG does not change; in contrast, the accelerating activity of SPS increases when Fe^{3+}/Fe^{2+} is present in a copper-plating bath. Furthermore, potentiostatic experiments suggest that SPS interacts with Fe^{2+} ions in the bulk electrolyte, probably to produce 3-mercapto-1-propane sulfonic acid (MPS) at low ppb levels.

---

* This work was done in collaboration with Tadashi Saito

Introduction

Copper interconnects are used extensively in semiconductor device manufacturing[1] and in printed circuit board (PCB) production.[2] They are fabricated using an electrochemical deposition (ECD) procedure from an acidic $CuSO_4$ electrolyte with organic and inorganic constituents.[3,4] The success of ECD in creating copper interconnects is attributed to its ability to fill gaps void free with desired internal and surface properties.[5] Copper features are produced by a phenomenon known as superfilling, whereby the rate of copper deposition is accelerated at the bottom of the feature while the rate of plating at the side walls of the feature and top entry is suppressed.[6]

Superfilling is made possible by a synergetic interplay of organic additives placed in a plating bath.[7, 8] Most common additives encountered in PCB and wafer industries can be classified into three groups: suppressor, accelerator, and leveler. Suppressors are typically molecules like polyethylene glycol (PEG) that lower Cu deposition rates in the presence of chloride ions.[9–16] Accelerators, such as bis-(3-sulfopropyl) disulfide (SPS) and 3-mercapto-1-propane sulfonic acid (MPS), are known to lower the suppression, leading to an accelerated copper deposition.[17–22] The role of a leveling agent, such as polyethyleneimine or Janus Green B, is often to improve surface topography.[23–26]

An iron redox couple (Fe^{3+}/Fe^{2+}) has been extensively utilized in copper electrolytes for filling features on printed circuit boards, such as through-holes and blind-microvias.[27–29] It is known that for the PCB level metallization of copper, the anodic oxidation of Fe^{2+} ions allows for the use of a dimensionally stable, insoluble anode without the formation of oxygen bubbles. Formation of oxygen bubbles is undesired because it can lead to surface defects, such as bubble entrapment in vias.[30] At the same time Fe^{3+} ions can be reduced on

the cathode at a mass transfer limited rate. This results in lower current efficiency of copper reduction on a surface and, because of differing mass transfer rates to an outer surface and into a surface feature, a relatively higher copper deposition of copper inside the via.[31]

For semiconductor chip structures, such as interconnect lines and vias, and through-silicon vias (TSV), the application of iron redox mediator chemistry may offer a number advantages over the conventional plating setups[32,33] including the use of insoluble, dimensionally stable anodes,[30] and a reduced consumption rate of accelerator.[34] Possibly, with fewer accelerator breakdown products, cleaner copper films can be deposited. An added benefit is that Fe^{3+} ions can contribute to the reduction of overburden thickness, which is beneficial for subsequent processing by chemical mechanical planarization.[4]

For example, deposition from a plating bath with the Fe^{3+}/Fe^{2+} couple has shown thinner copper thicknesses on the top surface and wider openings of through-silicon vias (Fig. 1). With 0.47 g L^{-1} of Fe^{3+}, via openings are wider, while the vias remained void free. At the higher concentration of Fe^{3+}, openings are even wider and the overburden is thinner.

The impact of the Fe^{3+}/Fe^{2+} couple on surface reactions and organic additives in the plating bath has not been systematically investigated. Since a tight control of additive formulation is necessary for the on-chip metallization of copper,[1] investigation of the impact of the Fe^{3+}/Fe^{2+} redox couple on plating bath additives may facilitate the introduction of an iron-mediated system to commercial electrolytes. In this chapter we present the results of electrochemical investigations of the redox couple–additive interactions, which were carried on a rotating disk electrode (RDE) and an in–lab built microfluidic cell (μ–cell). Utilization of both electrochemical setups enabled the characterization of the system under substantially different hydrodynamic conditions.

Experimental

Beaker scale

Current efficiency measurements were performed on a platinum RDE (Pine Corporation) dipped inside a 100 ml beaker with 50 ml of the copper electrolyte (termed here VMS) containing: 0.55 M $CuSO_4.5H_2O$ (Fisher Scientific, Inc.), 0.3 M H_2SO_4 (EMD Chemicals, Inc.), and 1.4 mM HCl. Platinum wire (diameter = 0.5 mm) was used as a counter electrode and Ag|AgCl as a reference electrode (BASi Re-5). Plating was performed at a constant current of -15 mA cm^{-2} for 350 s at 300 rpm. The copper was then stripped at 15 mA cm^{-2} in concentrated phosphoric acid (H_3PO_4), and the stripping time was recorded. Consequently, the current efficiency was calculated by dividing the time of stripping by the time of plating, and multiplying the resulting ratio by 100%. Electrodes were removed within 10 s of plating, and we assumed that any Cu dissolution during removal had negligible impact on current efficiency results.

Injection experiments were performed at constant potential. For the injection measurements on an RDE, the experimental procedure was standardized by preplating Pt RDE in VMS at -40 mA cm^{-2} for 4 min and 900 rpm. Then, a constant potential of -50 mV was applied and the working electrode was allowed to plate for another 200 s. At which point, additives were injected into the plating bath from an air displacement micropipette. The impact of Fe^{3+}/Fe^{2+} couple on each additive was then observed for another 400 s. Fe^{2+} and Fe^{3+} ions were added as $FeSO_4{\cdot}7H_2O$ (Sigma-Aldrich) and $Fe_2(SO_4)_3{\cdot}xH_2O$ (Sigma-Aldrich), respectively. The two organic additives used in this chapter were: PEG 3350 g L^{-1} (Sigma-Aldrich) and SPS (Raschtig GmbH).

The electrolytes prepared with SPS and Fe^{3+}/Fe^{2+} couple were found to exhibit a time dependent behavior; therefore the contact time between SPS and Fe^{3+}/Fe^{2+} prior to an experiment was recorded and is indicated where appropriate.

Microfluidic

A microfluidic device (μ-cell) to measure an electrode response to rapid changes in composition of an electrolyte was also employed. The device was first developed by Willey *et al.*[35–37] and subsequently improved to its current form (Fig. 2) by Gallaway *et al.*[38] The channel design allows for the electrochemical monitoring of rapid changes in the electrolyte composition while plating copper onto a working electrode with minimal ohmic losses.

The microfluidic channels were molded from polydimethylsiloxane (PDMS) over a negative pattern formed on a silicon chip by photolithography. There were two parallel channels: a working channel with two inlets containing working (d = 100 μm) and counter (d = 250 μm) platinum electrodes and a parallel channel containing Ag|AgCl reference electrode (BASi RE-6). Both channels had a rectangular cross section ~500 μm wide and ~180 μm tall, and solution was passed through them at 0.5 mL min^{-1}, corresponding to an average velocity of ~8.3 cm s^{-1}. The electrode wires are embedded ~600 μm apart in Spurr low-viscosity embedding media (Polysciences, Inc.). The embedding mold with cross-sectioned wires was polished with silicon carbide sandpaper (Leco), and the electrode epoxy structure formed the floor of the m-cell.

Additive transition experiments in the μ-cell were conducted by switching between the two inlets leading to a working channel. At the beginning of each experiment, VMS was passed through the working channel to pre-plate the Pt working electrode with copper at -15

mA cm^{-2} for 175 s. The applied potential was then set, and after 45 s of plating in VMS, the electrolyte was switched to the one containing plating additives. After 105 s the flowing solution was switched back to VMS. In this way a single experiment was used to study both the adsorption and desorption behavior of additives.

Results and Discussion

Effect of current efficiency and mass transfer of the Fe^{3+}/Fe^{2+} couple on Cu ECD

Current efficiency measurements were conducted, as deviations from 100% may affect filling performance. Reduction of ferric ions is more likely to happen at the employed cathodic current, due to a significant difference in overpotentials, where $U^{\theta}_{Cu^{2+}\rightarrow Cu} = 0.145\ V$ and $U^{\theta}_{Fe^{3+}\rightarrow Fe^{2+}} = 0.57\ V$ *vs.* Ag|AgCl reference. As seen in Table I, current efficiency measurements in VMS containing Fe^{2+} (12 g/L or 0.215 M) and Fe^{3+} (0.5 g/L or 0.009 M) showed that about 9% of the applied current was consumed by the reduction of ferric to ferrous ions rather than the reduction of cupric ions to copper metal. When Fe^{3+} ions are present at 1.0 g L^{-1} (0.018 M), the current efficiency decreased further to 81%. The current efficiency results were consistent with analysis assuming a mass-transfer limited reduction rate of Fe^{3+} and with experimental studies (Fig. 3) of the redox couple on platinum RDE.

The current efficiency measurements in the presence of the Fe^{3+}/Fe^{2+} redox couple have also been carried out inside the µ-cell. However, the results were substantially different from measurements with the RDE. For example after a galvanostatic current of -15 mA cm^{-2} was applied, there was no copper deposit, and even the pre-plated copper film had been stripped (i.e., copper was etched by the excess of Fe^{3+} ions near the electrode surface). This

can be explained by realizing that the hydrodynamics of the μ-cell were very different from that of the RDE. Figure 3 clearly shows the difference in mass flux of ferric ions to the electrode surface between the RDE and the μ-cell arrangements.

As shown in Fig. 3, the limiting current plateaus on the RDE were much smaller than the current plateau obtained inside the μ-cell. For the experimental results presented below, it was found that inside the μ-cell the same mass diffusion limited current attained on an RDE for Fe^{3+} concentration of 0.5 g L^{-1} (0.009 M) and a rotation rate at 300 rpm could be achieved if the concentration of Fe^{3+} ions was decreased to 0.024 g/L or 0.00043 M (note that the ratio of Fe^{3+}/ Fe^{2+} was kept the same).

Potentiostatic additive transition study

Two common additives used in plating electrolytes are polyethylene glycol (PEG) and bis-(3-sodiumsulfopropyl) disulfide (SPS). To determine the impact of the Fe^{3+}/Fe^{2+} couple on these species, potentiostatic additive injection experiments were carried out inside the μ-cell and also at the RDE setup. In the μ-cell, changes in composition were achieved by switching between the two inlet syringes leading to the working channel (Fig. 2). Similar experiments are discussed in detail elsewhere.[16,36–39]

Potentiostatic response to the introduction of 300 ppm of PEG with and without the Fe^{3+}/Fe^{2+} couple inside the μ-cell is shown in Fig. 4. The addition of PEG caused rapid decrease in the observed current, followed by stable period of suppression, and subsequently by slow desorption after the removal of PEG from VMS. When the same experiment was repeated with the addition of PEG and Fe^{3+}/ Fe^{2+}, the curve simply shifted vertically by -2 mA cm^{-2}, which was the value of the mass-transfer-limited current from the reduction of

Fe^{3+} ions. In addition, after the removal of PEG and Fe^{3+}/Fe^{2+} from VMS, the desorption behavior of PEG was the same as without Fe^{3+}/Fe^{2+}. Hence, these electrochemical data suggests that adsorption, suppression and desorption of PEG was unaffected by the Fe^{3+}/Fe^{2+} couple.

Figure 5 shows current density as a function of time in response to the injection of additives from pipette to a beaker with immersed RDE at a potential of -50 mV vs. Ag|AgCl. The two curves represent injection of PEG to VMS and injection of PEG and the Fe^{3+}/Fe^{2+} couple to VMS. As in the μ-cell, the only difference between the two curves was the additional current from the reduction of ferric ions (see Fig. 3). We conclude again that the inhibition of copper deposition by PEG was unaffected by the Fe^{3+}/Fe^{2+} couple.

Electrochemical investigation was carried out further to assess the role ferric ion reduction on the behavior of PEG across a potential range. As shown in Fig. 6, linear sweep voltammetry experiments were performed in three different electrolytes: (1) VMS and PEG, (2) PEG and Fe^{3+}, and (3) VMS, PEG, and Fe^{3+}. It was seen that the ferric reduction precedes cupric ion reduction as was expected from a difference in reduction potentials between the two reactions. Furthermore, we see that the copper reduction takes off at the same potential in both VMS and PEG and VMS, PEG, and Fe^{3+} electrolytes.

Potentiostatic injections of additives were also performed to characterize the influence of the Fe^{3+}/Fe^{2+} couple on SPS. As shown in Fig. 7, the introduction of PEG and SPS to VMS caused a rapid decrease in the observed current, followed by a relatively slow increase in current due to the action of the accelerating agent. The accelerating effect becomes more pronounced at higher potentials (not shown), as SPS is known to exhibit potential or current-dependent behavior.[15] When the same experiment was conducted with

an injection of PEG, SPS, and Fe^{3+}/Fe^{2+}, the accelerating effect showed no change (the curve shifted by the value of the Fe^{3+} mass transfer limited current). However, if the additives were premixed and allowed to sit for some time before injection (as indicated on Fig. 7) a considerable increase in acceleration was observed. These two observations led us to hypothesize that: (1) the Fe^{3+}/Fe^{2+} couple had no or minimal impact on the surface reactions associated with the action of SPS and (2) the Fe^{3+}/Fe^{2+} couple did have an impact on the bulk composition of the electrolyte, which in turn was responsible for the observed increase in acceleration.

Figure 8 compares the behavior of SPS and PEG with and without Fe^{3+}/Fe^{2+} in the μ-cell. Again, a noticeable change in acceleration of copper deposition was observed when the Fe^{3+}/Fe^{2+} couple and SPS were premixed in electrolyte for 3 h.

An increase in acceleration of Cu deposition can possibly be attributed to an increase in the concentration of cuprous ions as predicted from the equilibrium between dissolved oxygen, Fe^{2+} and Cu^{2+} (according to Reaction 1 and 2), since an accumulation of cuprous complexes near the surface has been linked to the acceleration mechanism of SPS.[40] An increase in acceleration can also be explained by the interaction between ferrous ions and SPS molecules in the bulk electrolyte according to Reaction 3

$$Cu^{2+} + Fe^{2+} \rightleftarrows Fe^{3+} + Cu^{+} \qquad (1)$$

$$\frac{1}{4}O_2 + H^{+} + Fe^{2+} \rightleftarrows \frac{1}{2}H_2O + Fe^{3+} \qquad (2)$$

$$SPS + 2H^{+} + 2Fe^{2+} \rightleftharpoons 2MPS + 2Fe^{3+} \qquad (3)$$

The reduction of the disulfide bond (such as found in SPS) to its two monomers (MPS being a monomer of SPS) has been observed in other systems, such as the cysteine-cystine couple.[41,42] The equilibrium analogous to Reaction 3, but between cysteine and

cystine instead of SPS and MPS, respectively, has also been investigated in the past.[43] Since MPS is known to accelerate copper deposition faster than SPS, either due to faster adsorption or through higher impact upon adsorption, the stabilization of a small amount (e.g., low ppb range) of MPS in the bulk can explain the observed increase in acceleration of copper electrodeposition. The Reactions 1, 2, and 3 can also have a significant impact on previously proposed reactions that affect equilibrium between SPS and MPS.[44,45]

The Reactions 1, 2, and 3 were indirectly studied by performing potentiostatic additive injections with each reactant and product. As shown in Fig. 9, the injection of PEG, SPS, and Fe^{3+} to VMS produced no increase in acceleration of Cu ECD, since the curve simply shifted vertically due to the reduction of ferric ions. The injection of PEG, SPS, and Fe^{2+} to VMS produced an increase in acceleration of Cu ECD (a vertical shift was likely due to the generation of Fe^{3+} ions in a concentrated master solution of $FeSO_4 \cdot 7H_2O$ that was used for dilution after a span of 1 day). The last injection was performed with PEG, SPS, and MPS and it produced a signal that followed closely the response from the injection of PEG, SPS, and Fe^{2+}. All three observations were consistent with Reaction 3.

Investigation of SPS and Fe^{2+} interaction by amperometry on RDE

The potentiostatic behavior of the VMS, PEG, and SPS and VMS, PEG, SPS, and Fe^{2+} electrolytes was examined further. The additives were added to VMS three hours prior to an experiment. Then, after three hours of idle time separate from the electrodes, an experiment was performed by recording a change in current as a function of time at a constant potential of -0.1 V vs. Ag|AgCl. The electrochemical behavior presented in Fig. 10,

followed closely the result presented by Tan *et al.*[18] that showed the impact of adding small amounts of MPS along with PEG and SPS.

Potentiostatic experiments in VMS containing PEG, SPS, and Fe^{2+} (aged for 3 h) when performed on an RDE also revealed a mass-transfer dependence that was not observed for VMS containing PEG and SPS additives (not shown). As shown in Fig. 11, at relatively low rotation speeds the current response was strongly dependent on mass transfer; at higher rotation speeds, however, the response saturated, as little change was observed by increasing rotation. This behavior was also emblematic of PEG, SPS, and MPS containing electrolytes (not shown). The generation of Fe^{3+} ions via oxidation of Fe^{2+} ions by dissolved oxygen could not be attributed to the differences between curves at low rotation speeds. As Fe^{3+} reduction current produced only about 0.3 mA cm^{-2} difference at the specified rotation speeds, when measured by linear sweep voltametry experiments in VMS, PEG, and Fe^{2+} electrolyte, also aged for 3 h.

Conclusions

The effect of the ferric/ferrous redox couple on copper electrodeposition from acidic cupric sulfate electrolytes containing Cl^-, PEG, and SPS was examined using an RDE and a microfluidic device. The copper-deposition current efficiency was lower due to the reduction of ferric ions. The impact of ferric ions was also shown to be strongly dependent on mass transfer rates to the cathode. Different transport rates of Fe^{3+} to the cathode surface had to be considered in the design of experiments, to allow the transfer of knowledge from a microfluidic setup to RDE (and eventually to a full scale plating tool).

The inhibition of copper metal deposition by PEG was not affected by Fe^{3+}/Fe^{2+} ions. Kinetics of adsorption and desorption of PEG on copper electrode were also unaffected by the Fe^{3+}/Fe^{2+} redox couple. The activity of SPS during copper deposition was found to change in the presence of Fe^{2+} ions but not Fe^{3+} ions. Ferrous ions were believed to affect SPS primarily through interactions in the bulk electrolyte. The electroanalytical response from the baths containing Fe^{2+} suggested the appearance of MPS in solution via oxidation of SPS by Fe^{2+}.

References

1. P. Andricacos, D. S. Chung, H. Deligianni, J. E. Fluegel, K. T. Kwietniak, P. S. Locke, D. D. Restaino, S. C. Seo, P. M. Vereecken, and E. G. Walton, Void-Free Damascene Copper Deposition Process and Means of Monitoring Thereof, IBM Corp., United States, 7678258 (2010).
2. T. Kobayashi, J. Kawasaki, K. Mihara, and H. Honma, Electrochim. Acta, 47, 85 (2001).
3. J. Reid, S. Mayer, E. Broadbent, E. Klawuhn, and K. Ashtiani, Solid State Technol., 43, 86 (2000).
4. T. Osaka, M. Hasegawa, M. Yoshino, and N. Yamachika, Advanced Nanoscale ULSI Interconnects: Fundamentals and Applications, p. 183, (Springer Science & Business Media, LLC, New York, USA, 2009).
5. P. C. Andricacos, C. Uzoh, J. O. Dukovic, J. Horkans, and H. Deligianni, IBM J. Res. Dev., 42, 567 (1998).
6. A. C. West, S. Mayer, and J. Reid, Electrochem. Solid-State Lett., 4, C50 (2001).

7. T. P. Moffat, J. E. Bonevich, W. H. Huber, A. Stanishevsky, D. R. Kelly, G. R. Stafford, and D. Josell, J. Electrochem. Soc., 147, 4524 (2000).
8. W.-P. Dow and H.-S. Huang, J. Electrochem. Soc., 152, C67 (2005).
9. J. J. Kelly and A. C. West, J. Electrochem. Soc., 145, 3477 (1998).
10. J. D. Reid and A. P. David, Plat. Surf. Finish., 74, 66 (1987).
11. V. D. Jovic and B. M. Jovic, Copper Electrodeposition From a Copper Acid Baths in the Presence of PEG and NaCl, p. 18, Serbian Chemical Society, Belgrade, SERBIE (2001).
12. J. P. Healy, D. Pletcher, and M. Goodenough, J. Electroanal. Chem., 338, 155 (1992).
13. J. J. Kelly and A. C. West, J. Electrochem. Soc., 145, 3472 (1998).
14. K. R. Hebert, S. Adhikari, and J. E. Houser, J. Electrochem. Soc., 152, C324 (2005).
15. T. P. Moffat, D. Wheeler, and D. Josell, J. Electrochem. Soc., 151, C262 (2004).
16. J. W. Gallaway and A. C. West, J. Electrochem. Soc., 155, D632 (2008).
17. P. M. Vereecken, H. Deligianni, K. T. Kwietniak, P. C. Andricacos, R. A. Binstead, J. Wu, R. Mikkola, and J. M. Calvert, Abstract Philadelphia, PA; May 13, 2002. The 201st Meeting Electrochem. Soc. 2002.
18. M. Tan, C. Guymon, D. R. Wheeler, and J. N. Harb, J. Electrochem. Soc., 154, D78 (2007).
19. M. Tan and J. N. Harb, J. Electrochem. Soc., 150, C420 (2003).
20. E. E. Farndon, F. C. Walsh, and S. A. Campbell, J. Appl. Electrochem., 25, 574 (1995).
21. T. P. Moffat, D. Wheeler, and M. D. Edelstein, IBM J. Res. Dev., 49, 19 (2005).

22. J. J. Kim, S.-K. Kim, and Y. S. Kim, J. Electroanal. Chem., 542, 61 (2003).

23. M. J. Willey, J. Reid, and A. C. West, Electrochem. Solid-State Lett., 10, D38 (2007).

24. S. K. Kim, D. Josell, and T. P. Moffat, J. Electrochem. Soc., 153, C616 (2006).

25. P. Taephaisitphongse, Y. Cao, and A. C. West, J. Electrochem. Soc., 148, C492 (2001).

26. M. Hasegawa, Y. Negishi, T. Nakanishi, and T. Osaka, J. Electrochem. Soc., 152, C221 (2005).

27. S. Kenny and K. Matejat, in Proceedings of the EPC 2000 PCB Convention, CircuiTree, February 2001, p. 10. (2000).

28. S. Kenny and B. Reents, in Proceedings of the CPCA, Atotech Deutschland GmbH (2005).

29. S. Kenny, B. Reents, and J. Zosel, in Proceedings of the CPCA, Atotech Deutschland GmbH (2003).

30. J. Barthelmes, in Proceedings of the Electronics Circuits World Convention 8, Atotech Deutschland GmbH (1999).

31. B. Roelfs and T. Fujiwara, in Proceedings of the JPCA, Atotech Deutschland GmbH (2008).

32. T. D. R. Preisser, and H. Fuerhaupter, Abstract Orlando, FL; October 13, 2003. The 204th Meeting of The Electrochemical Society, Inc., 2003.

33. J. V. Eisden, X. Kang, J. Enloe, C. G. Koh, and R. Preisser, Abstract San Francisco, FL; May 25, 2009, p. 979, The Electrochemical Society Meeting Abstracts, Vol. 901, 2009.

34. J. D. Adolf, R. Preisser, and U. Landau, Abstract Vienna, Australia; October 5, 2009, p. 2163, The Electrochemical Society Meeting Abstracts, Vol. 902, 2009.

35. M. J. Willey and A. C. West, Electrochem. and Solid-State Lett., 9, E17 (2006).

36. M. J. Willey and A. C. West, J. Electrochem. Soc., 153, C728 (2006).

37. M. J. Willey and A. C. West, J. Electrochem. Soc., 154, D156 (2007).

38. J. W. Gallaway, M. J. Willey, and A. C. West, J. Electrochem. Soc., 156, D146 (2009).

39. J. W. Gallaway, M. J. Willey, and A. C. West, J. Electrochem. Soc., 156, D287 (2009).

40. P. M. Vereecken, R. A. Binstead, H. Deligianni, and P. C. Andricacos, IBM J. Res. Dev., 49, 3, (2005).

41. T. R. Ralph, M. L. Hitchman, J. P. Millington, and F. C. Walsh, J. Electroanal. Chem., 375, 17 (1994).

42. C. V. Krishnan, M. Garnett, and B. Chu, Int. J. Electrochem. Sci., 3, 854 (2008).

43. N. Tanaka, I. M. Kolthoff, and W. Stricks, J. Am. Chem. Soc., 77, 2004 (1955).

44. T. P. Moffat, B. Baker, D. Wheeler, and D. Josell, Electrochem. Solid-State Lett., 6, C59 (2003).

45. L. D’Urzo, H. Wang, A. Pa, and C. Zhi, J. Electrochem. Soc., 152, C243 (2005).

Table I.

Solution	**Current efficiency**
VMS	98.2%
VMS–Fe^{2+} (12g L^{-1} or 0.215 M)–Fe^{3+} (**0.5** g L^{-1} or 0.009 M)	89%
VMS–Fe^{2+} (12g L^{-1} or 0.215 M)–Fe^{3+} (**1.0** g L^{-1} or 0.018 M)	81%

Table I. Current efficiency measurements in the presence of the Fe^{3+}/Fe^{2+} couple without plating bath additives. Plating was performed on a Pt RDE at -15 mA cm^{-2} at a rotation speed of 300 rpm.

Figure 1

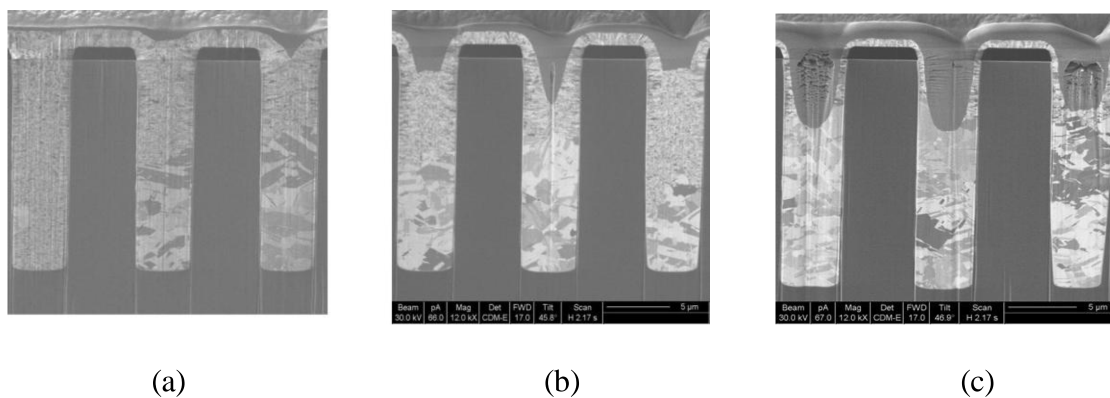

Figure 1. SEM cross section of TSV (diameter = 5 μm, height = 25 μm) filling keeping all conditions the same except for Fe^{3+} concentration and anode material: (a) Cu anode, no Fe^{3+} ions; (b) inert anode, 0.47 g L^{-1} (0.0084 M) Fe^{3+}; (c) inert anode, 2 g L^{-1} (0.036 M) Fe^{3+}.

Figure 2

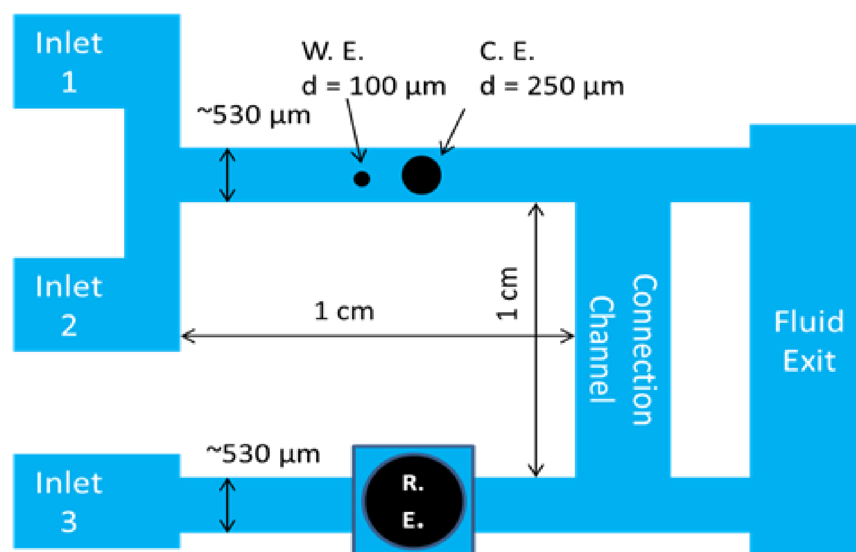

Figure 2. Schematic diagram of the microfluidic device (µ-cell), showing key dimensions.

Figure 3

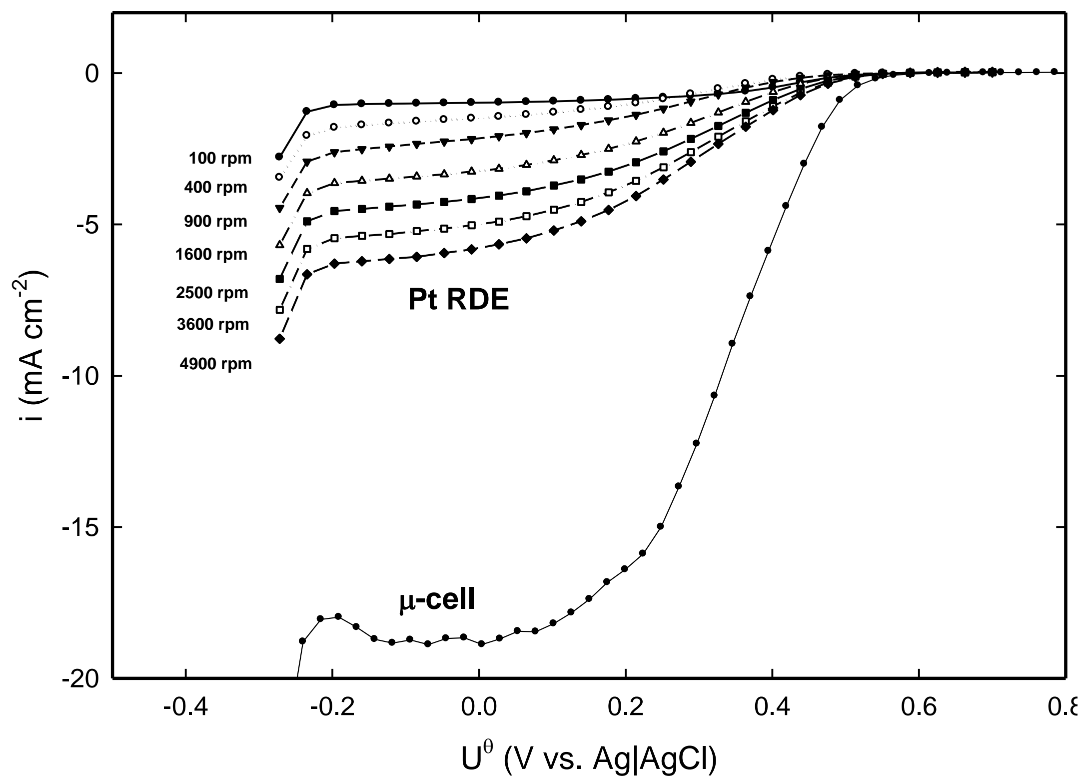

Figure 3. Results of linear sweep voltammetry measured on a platinum surface inside the μ-cell and RDE. The electrolyte contained dissolved Fe^{3+} (0.5 g L^{-1} or 0.009 M) in 0.5 M H_2SO_4; scan rate was 10 mV s^{-1}. Graph shows mass diffusion limited currents at different flow conditions, and demonstrates that the mass flux inside the μ-cell is considerably higher than on the RDE.

Figure 4

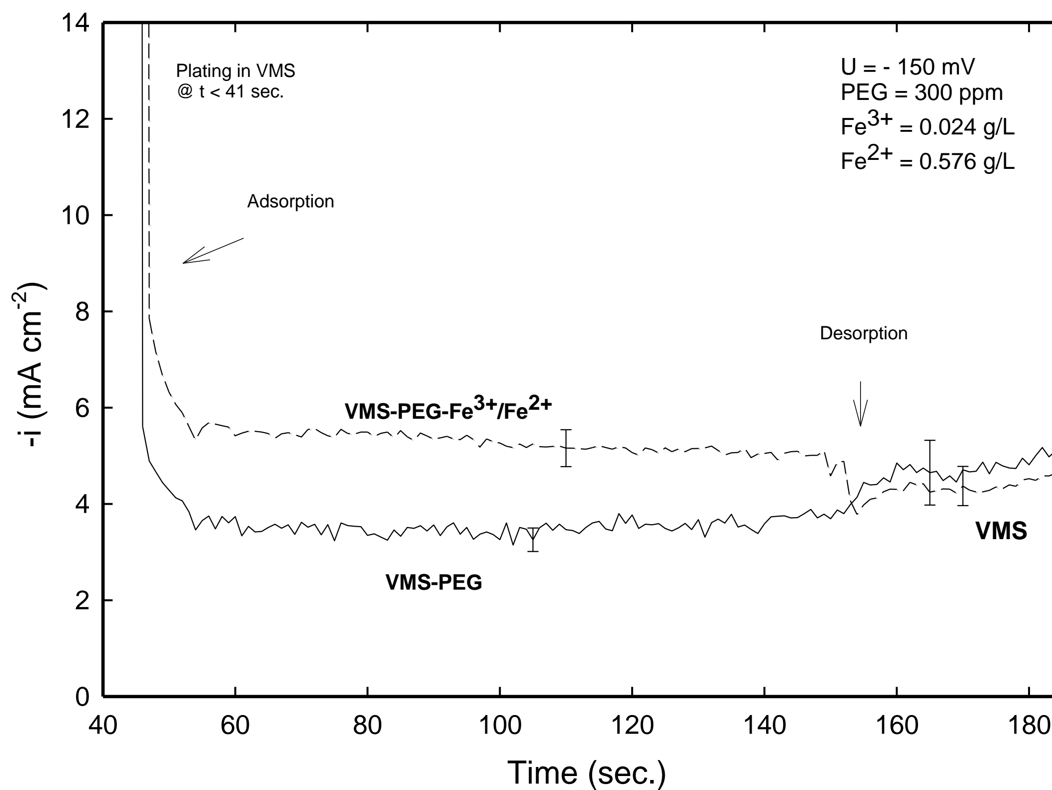

Figure 4. Current as a function of time for an applied potential U = -150 mV *vs.* Ag|AgCl. Results are obtained in the μ-cell: at time = 41 s, additives are introduced to VMS. They are then removed at 150 s. The dashed line represents an experiment with PEG and the redox couple, and the solid line is for introduction of PEG alone. The PEG-Fe^{3+}/Fe^{2+} current density is increased by approximately -2 mA cm^{-2}, due to the reduction of ferric ions.

Figure 5

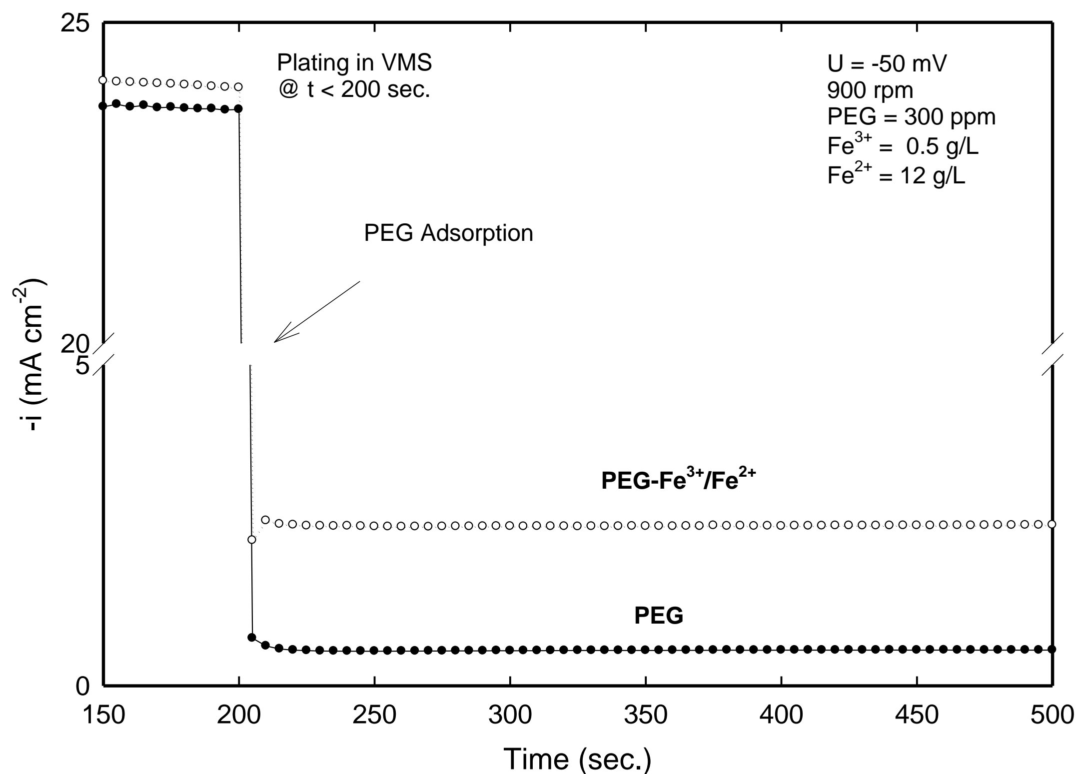

Figure 5. Current as a function of time for an applied potential U = -50 mV *vs.* Ag|AgCl. Results are obtained on an RDE: at time = 200 s, additives are injected to VMS. Results are shown for an experiment with PEG and the redox couple and for PEG alone. The PEG-Fe^{3+}/Fe^{2+} current density is increased by approximately -2 mA cm^{-2}, due to the reduction of ferric ions.

Figure 6

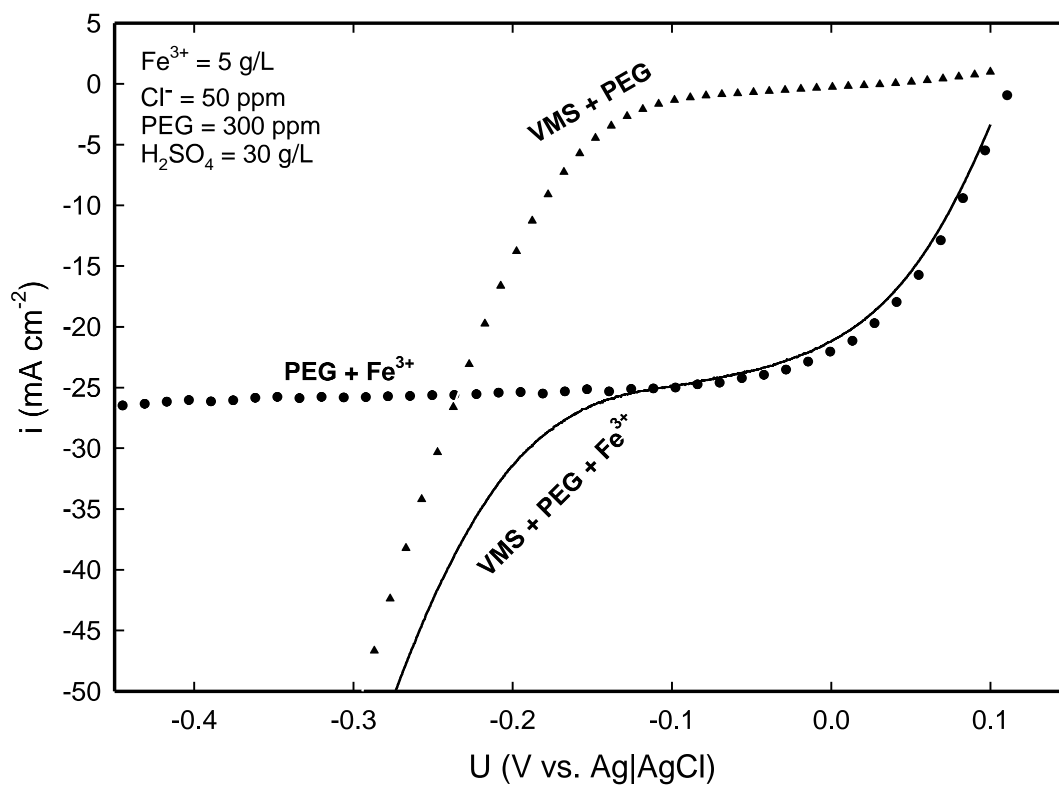

Figure 6. Current-potential curve on an RDE; potential is scanned from positive to negative at 10 mV s^{-1}. Results are shown for electrolytes containing: (1) VMS and PEG, (2) Fe^{3+} and PEG, and (3) VMS, PEG, and Fe^{3+}.

Figure 7

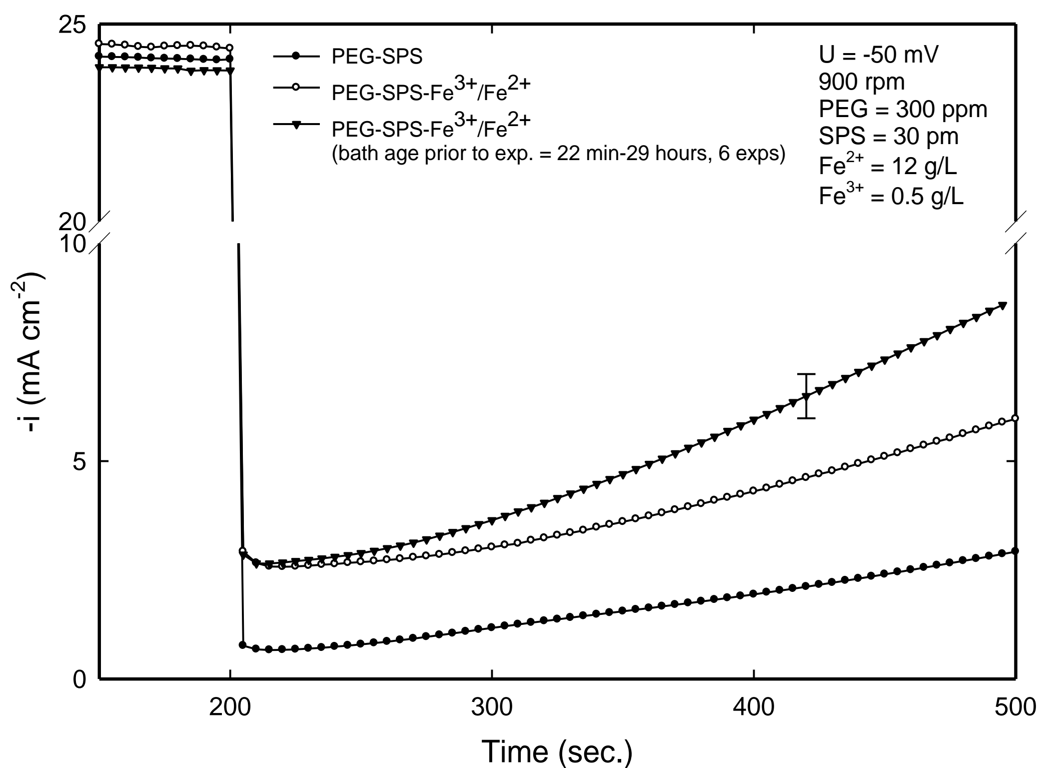

Figure 7. Current as a function of time for an applied potential U = -50 mV *vs.* Ag|AgCl. Results are obtained on an RDE: at time = 200 s, additives are injected to VMS. Results are shown for: (1) PEG and SPS, (2) PEG, SPS, and redox couple (no bath aging), and (3) PEG, SPS and redox couple (six experiments combined for various aging times). Premixing of SPS and Fe^{3+}/Fe^{2+} before injection had a noticeable effect on acceleration of Cu ECD.

Figure 8

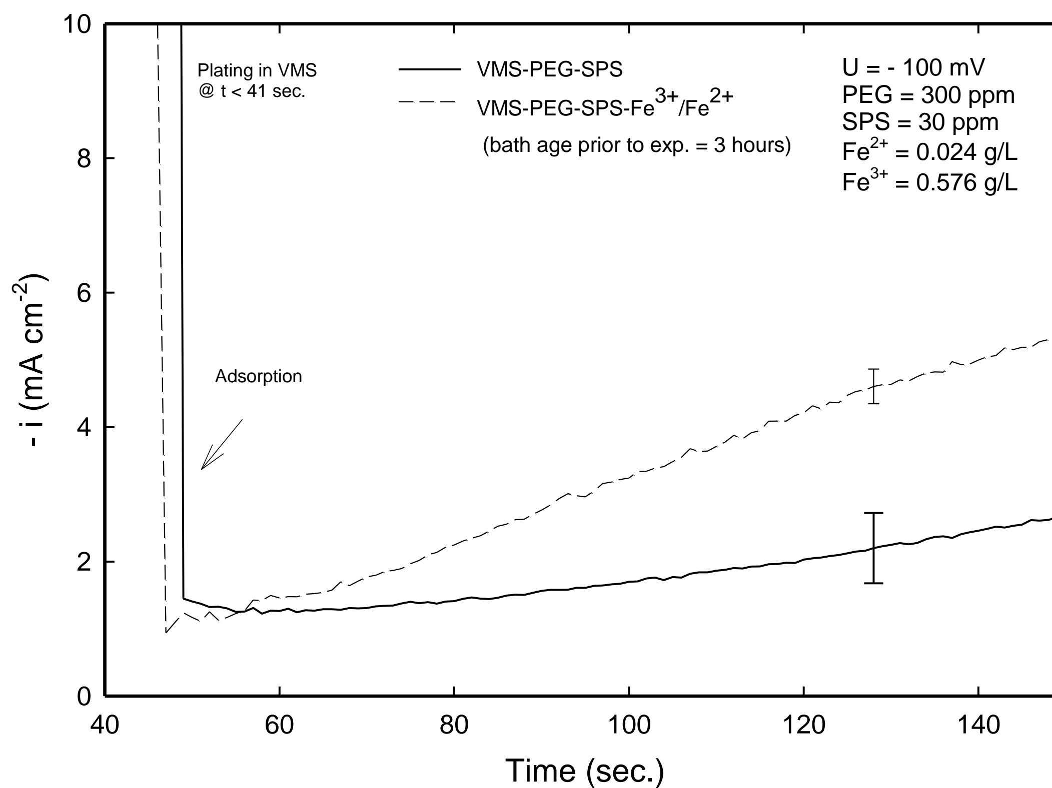

Figure 8. Current as a function of time for an applied potential U = -100 mV *vs.* Ag|AgCl. Results are obtained in the μ-cell: at time = 41 s, additives are introduced to VMS. They are then removed at 150 s. The dashed line represents an experiment with PEG and the redox couple, and the solid line is for introduction of PEG alone. Premixing of SPS and Fe^{3+}/Fe^{2+} before injection for 3 h has a noticeable effect on acceleration of Cu ECD.

Figure 9

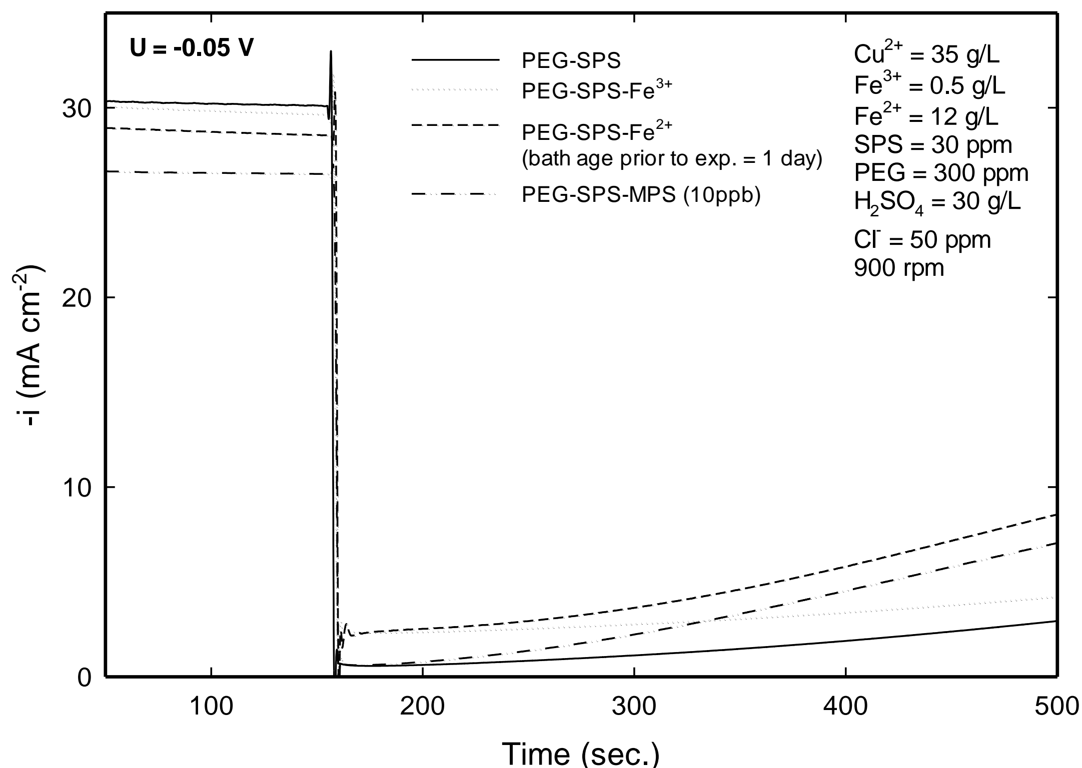

Figure 9. Current as a function of time for an applied potential U = -50 mV *vs.* Ag|AgCl. Results were obtained on an RDE: at time = 156 s, additives were injected to VMS. Results are shown for: (1) PEG and SPS (premixed for 1 day), (2) PEG, SPS and Fe^{3+} (premixed for 1 day), (3) PEG, SPS and Fe^{2+} (premixed for 1 day), (4) PEG, SPS, and MPS. Premixing of SPS and Fe^{3+} before experiment had insignificant effect on acceleration of Cu ECD. Premixing of SPS and Fe^{2+}, however, did increase acceleration and the result closely followed injection of PEG, SPS and MPS to VMS.

Figure 10

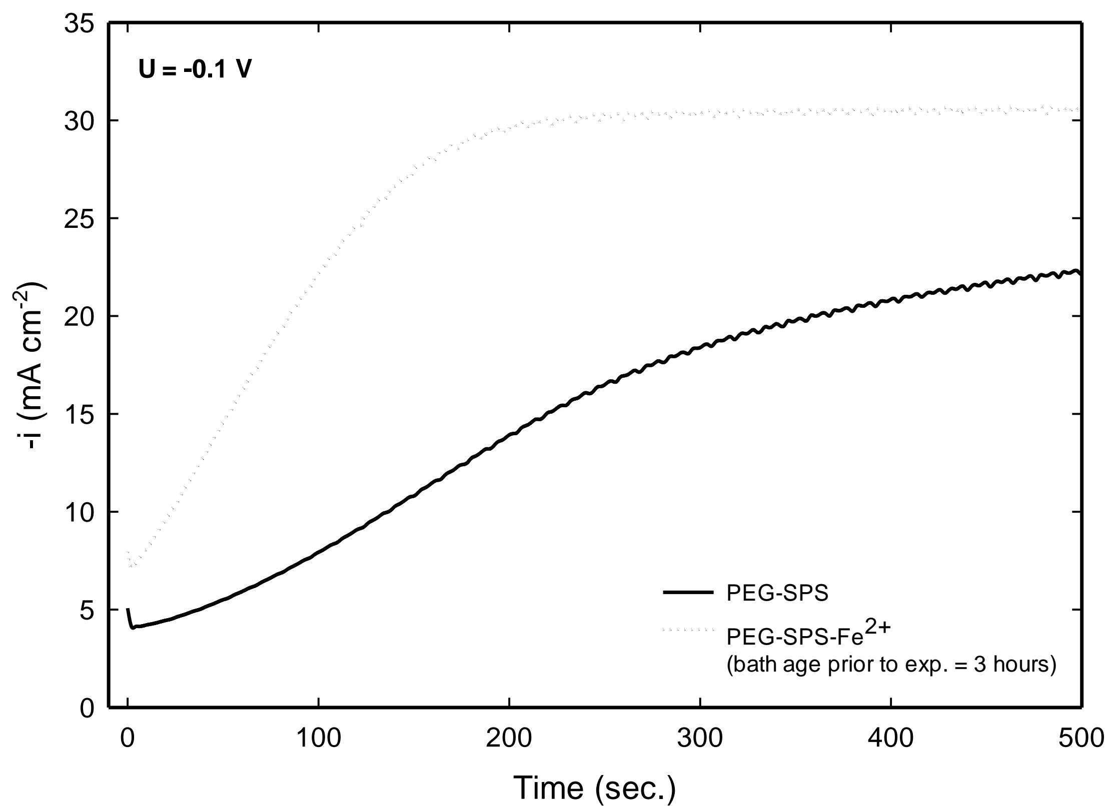

Figure 10. Current as a function of time for an applied potential U = -100 mV *vs.* Ag|AgCl. Results were obtained on an RDE at 900 rpm. The dotted line represents an experiment with PEG, SPS and Fe^{2+} in VMS (aged for 3 h), and the solid line is for PEG and SPS alone. Premixing of SPS and Fe^{2+} before experiment shortened the time to steady state.

Figure 11

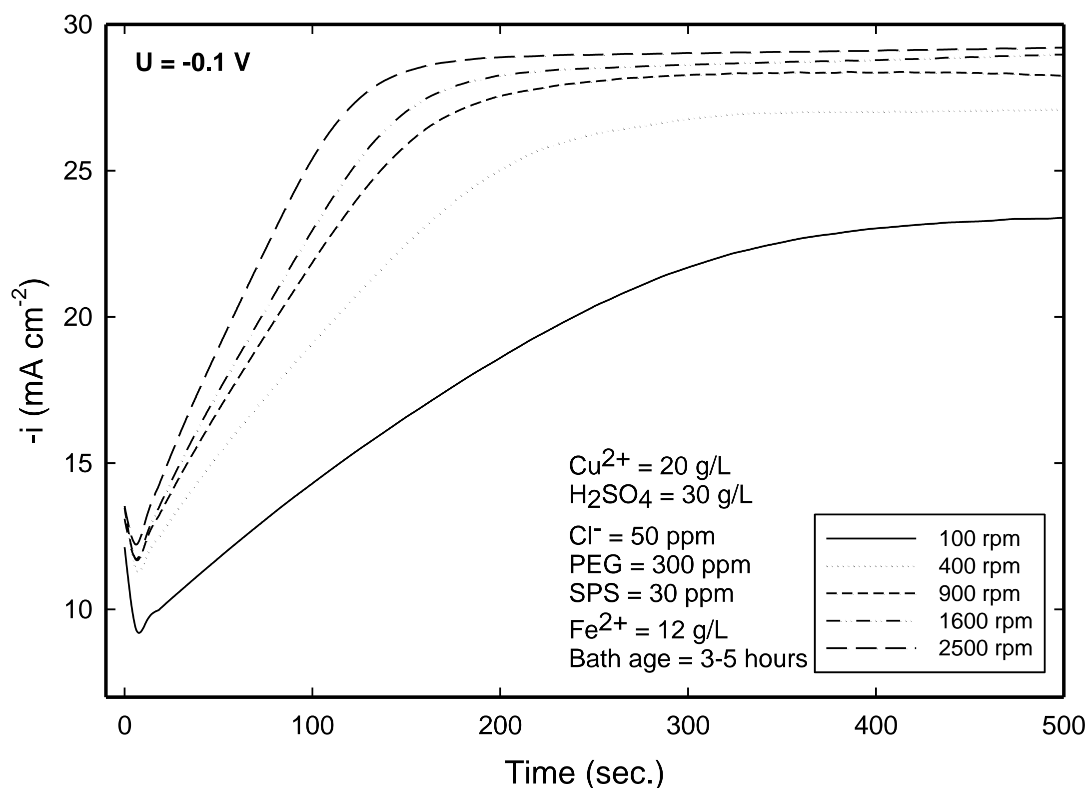

Figure 11. Current as a function of time for an applied potential U = -100 mV *vs.* Ag|AgCl. Results were obtained on an RDE at different rotation speeds. The electrolyte contained PEG, SPS, and Fe^{2+} ions, premixed 3 h prior to the experiments. The mass transfer dependency presented here was characteristic of PEG, SPS, and MPS containing electrolytes (not shown).

Chapter 3

Interaction between SPS and MPS in the Presence of Ferrous and Ferric Ions

Abstract

The ferric/ferrous redox couple interacts with bis-(3-sulfopropyl) disulfide (SPS), leading to increased amounts of 3-mercaptopropyl sulfonate (MPS) in solution. SPS is an essential organic additive in the electrochemical deposition of copper from acidic cupric sulfate electrolytes onto printed circuit boards and integrated circuits. Electrochemical studies showed that the accelerating action of SPS was dependent on the ferric/ferrous concentration ratio, with weakening dependence at increasing cupric sulfate concentration. HPLC and electrochemical results suggested that an increased concentration of MPS in the presence of the redox couple was the primary cause of the increased acceleration. Equilibrium estimates of MPS generation by the introduced redox chemistry partially explained these observations; the standard reduction potential of SPS to MPS reduction was estimated to be in a range between 0.3 and 0.4 V *vs.* SHE. However, the magnitude of acceleration went through a maximum at an intermediate ferric-ferrous ratio, possibly because SPS may be converted to MPS via both an oxidative and reductive pathways.

Introduction

Organic additives play a crucial role in the copper electrodeposition process that is utilized in the fabrication of modern microelectronic devices and printed circuit boards.[1] A synergetic interplay between various organic constituents of the copper plating bath leads to a special filling behavior of inlaid features, often referred to as superfilling or bottom-up filling.[2] Superfilling makes possible the filling of inlaid cavities by electrodeposition without voids and with desired internal and surface properties. Constituents of electrolyte that enable this behavior are able to either suppress or alleviate suppression (*i.e.* accelerate) of copper deposition. The suppressors are normally polyalkene molecules, such as polyethylene glycol (PEG), and the accelerator is almost exclusively bis-(3-sulfopropyl) disulfide (SPS).[3]

Although the interaction between plating additives at the electrode surface and in the bulk electrolyte has been a major topic of research for many years, the behavior of accelerator in particular is still under investigation.[4–9] Moffat *et al.* have shown that aged 3-mercaptopropyl sulfonate (MPS) containing electrolytes exhibit the same electrochemical behavior as SPS containing electrolytes.[10] Using Raman spectroscopy and pH measurements, Kim *et al.* demonstrated the appearance of disulfide bond in the mixture of MPS and Cu^{2+} ions.[11] These and other observations,[12] led researchers to propose the following oxidative dimerization mechanism of MPS to SPS (where $U^{\theta}_{Cu^{2+} \rightarrow Cu^{+}}$ = 0.16 V *vs.* SHE)

$$\frac{1}{2}SPS + Cu^{+} + H^{+} \rightleftarrows Cu^{2+} + MPS \quad (1)$$

It was also proposed that a conversion of SPS to MPS does not occur, because the right side of Reaction 1 is favored due to a continuous consumption of Cu^{+} by dissolved oxygen.[10] D'Urzo *et al.* noted that in the bulk electrolyte and without electrodic activity

MPS molecules can combine to form SPS through the dissolved oxygen in solution, possibly in accordance with Reaction 2.[13] However, Brennan *et al.* saw no evidence for Reaction 2 when they analyzed MPS standards in O_2 sparging water with ion chromatography.[14] Nevertheless, oxygen does play a role in MPS speciation, as evidenced by the data from Brennan *et al.* that shows MPS conversion to mainly SPS and 1,3 propanedisulfonic acid (PDS) in the presence of cupric ions.[14]

$$SPS + H_2O \leftrightarrows 2MPS + \frac{1}{2}\,O_2 \qquad (2)$$

It would seem that there may be multiple pathways by which most MPS is converted to SPS. However, the electrodic activity of SPS is also important.[15,16] Based on the mass-spectrum data obtained by Hung *et al.*[17] and West *et al.*,[18] together with information from Atotech, Berlin GmbH,[19] SPS breakdown in a standard copper electrolytic bath may be summarized by Fig. 1, although more interconversions and other breakdown products were reported.[18] SPS can be either oxidized or reduced in a plating bath during electrodic activity on both the anode and cathode. Both pathways, however, may eventually lead to PDS, which has been shown to be the most stable byproduct of SPS decomposition.[16–18] The reduction of SPS to MPS has also been associated with the catalytic action of SPS through various hypothesized mechanisms, many involving stabilization of cuprous complexes at the electrode surface.[20–26]

The ferric/ferrous redox couple is utilized in copper electrolytes for plating printed circuit boards, and has been considered for implementation in on-chip metallization of copper.[27,28] One advantage of including the Fe^{3+}/Fe^{2+} couple in copper electrolytes is that it allows the use of an insoluble, dimensionally stable anode.[27,29] It has also been found that the consumption of accelerator is significantly reduced when both the Fe^{3+}/Fe^{2+} redox

couple and an insoluble anode are used (as oppose to no redox couple and Cu anode).[30] It may be useful to note that a similar or even better prevention of SPS break down can possibly be achieved by separating anode and cathode compartments with a cation-selective membrane.[10,31]

This chapter builds on the study of interaction between the Fe^{3+}/Fe^{2+} couple and plating bath additives presented in chapter 3.[32] It was suggested that SPS interacts with ferrous ions in solution to generate MPS at sub-ppm concentration levels (possibly in accordance with Reaction 3). The cleavage of the disulfide bond in the presence of various redox couples (that occurs during the reduction of SPS) has also been seen in analogous systems, such as the L-cystine/L-cysteine couple.[33–35]

$$SPS + 2Fe^{2+} + 2H^{+} \rightleftarrows 2Fe^{3+} + 2MPS \quad (3)$$

The redox couple can also potentially influence the equilibrium of Reactions 1 and 2 in favor of MPS. Especially, the concentration of dissolved oxygen can be strongly influenced by the Fe^{3+}/Fe^{2+} couple, due to a thermodynamically favored consumption of dissolved oxygen via oxidation of ferrous ions (where $U^{\theta}_{Fe^{3+} \rightarrow Fe^{2+}} = 0.77V$ *vs.* SHE).

$$\frac{1}{4}O_2 + H^{+} + Fe^{2+} \rightleftarrows \frac{1}{2}H_2O + Fe^{3+} \qquad (\Delta U^{\theta} = 0.458\ V) \quad (4)$$

Furthermore, the amount of Cu^{+}, which has been attributed to the catalytic action of SPS,[23] can be altered either through an impact of the Fe^{3+}/Fe^{2+} couple on the concentration of dissolved oxygen or directly via the reduction of Fe^{3+} to Fe^{2+}.

$$\frac{1}{4}O_2 + H^{+} + Cu^{+} \rightleftarrows \frac{1}{2}H_2O + Cu^{2+} \qquad (\Delta U^{\theta} = 1.076\ V) \quad (5)$$

$$Cu^{2+} + Fe^{2+} \rightleftarrows Cu^{+} + Fe^{3+} \qquad (\Delta U^{\theta} = -0.618\ V) \quad (6)$$

In the previous chapter, no direct measurement of MPS in the bulk electrolyte has been performed.[32] To address this issue, a chromatographic method has been developed for

high performance liquid chromatography coupled with electrochemical detection (HPLC-ED) to allow a resolution of minute quantities of MPS (*i.e.* low ppb levels).[36] A few efforts have been described in the literature for analysis of SPS and its byproducts by HPLC with various detection schemes, such as UV spectroscopy,[13,37] mass spectrometry,[17] and electrochemical detection.[38] However, we are not aware of studies that show an adequate separation of SPS by-products, unambiguously assign chromatographic peaks, and have detection sensitivity in the nano-molar range.

In this chapter we present the results of electrochemical investigation and HPLC-ED examination which were used to determine the action of SPS in the presence of ferric and ferrous ions. Theoretical predictions based on equilibrium constants are also included as a complement to the HPLC and electrochemical results.

Experimental

HPLC-ED

All chromatographic analyses were performed on an in-house developed system at Atotech, Berlin GmbH. A more detailed description of the methodologies is found in chapter 4.[36] The set-up consisted of a K-120 gradient pump (Knauer, Inc.) connected to a PEEK pulsation damper (Metrohm, Inc.), which, over a T-piece, led to a Triathlon Spark auto-sampler (Metrohm, Inc.). At the T-piece, an eluent stream split in two streams: one half was sent to the auto-sampler and the other half was passed through an equivalent back pressure column, to maintain the electrochemical cell under flow when the matrix from an analytical column was directed to waste. At the auto-sampler, an eluent was mixed with a sample of interest and was sent to an analytical column. Atlantis T3 (column dimensions 4.6×100 mm,

particle size 3 μm) C18 reversed-phase analytical column from Waters, Inc. was used for all chromatographic measurements.

The effluent from the analytical column was passed through an ED50A Electrochemical Detector (ED) obtained from Dionex, Inc. with Au working electrode and Ag|AgCl reference electrode. The ED detector worked on a waveform specially designed to oxidize sulfur atoms; therefore PDS could not be detected. The optimal waveform for the integrated pulsed amperometric detection was developed by Atotech, Inc.[39] Each 1 s cycle included an adsorption delay step at U = 0.5 V for 0.1 s, followed by the detection step, where the potential was ramped to 1.7 V in 0.2 s and then decreased back to -0.5 V in 0.2 s; the third and final step was used for electrode cleaning and included a jump in potential to 1.6 V in 0.01 s, keeping potential steady at 1.6 V for 0.1 s, decrease in potential to -0.6 V in 0.01 s, and finally keeping potential steady at -0.6 V for 0.38 s.

To prevent an influence of the matrix, metallic ions were removed from electrolytes by passing a sample through OnGuard II H proton exchange cartridge (Dionex, Inc.). All separations were conducted in an isocratic mode (0.25 ml min^{-1} per column) at room temperature without temperature control. Instrument control and data acquisition were handled by the EZChrom Elite software (Agilent Technologies, Inc.).

The optimal method developed for the Atlantis T3 column allowed for a measurement time of ~70 min per run. Separation of chromatographic peaks was achieved by using a mobile phase that consisted of 2% HPLC grade acetonitrile and 0.0125 M H_2SO_4 in deaerated Millipore water. The retention times of all detectable species have been established with the use of commercially available (SPS and MPS) as well as in-company synthesized (mono-ox-SPS and di-ox-SPS) chemical standards. The retention times were

based on peak matching relative to standards and were found to be as follows: ~11 min for mono-oxide-SPS, ~16.5 min for MPS, ~19 min di-oxide-SPS, and ~64 min for SPS. Further, details on the method development can be found in work by chapter 4.[36]

Electrochemistry

The electrochemical cell consisted of a platinum rotating disk electrode (diameter 3 mm), Ag|AgCl reference electrode (BASi Re-5), and a platinum wire as a counter electrode. Prior to every experiment, the platinum RDE was pretreated in 0.5 M H_2SO_4 solution by cycling the electrode potential repeatedly from -0.173 to 1.2 V at 1 V s^{-1} until a characteristic cyclic voltammogram was observed. Then platinum surface was modified by preplating a thin copper layer from a copper sulfate electrolyte at -40 mA cm^2 for 120 s. At the end of every experiment, a nitric acid solution was used to strip the plated copper from the platinum surface. This electrode preparation procedure led to a highly reproducible polarization data.

Copper baths were prepared from $CuSO_4 \cdot 5H_2O$ (VWR International), $Fe_2SO_4 \cdot 7H_2O$ (Sigma-Aldrich), concentrated H_2SO_4 (EMD Chemicals, Inc.), PEG 3350 g mol^{-1} (Sigma-Aldrich), HCl, SPS (96% mass fraction,[14] Raschig GmbH), and MPS (87.2% mass fraction,[14] Raschig GmbH). The organic additives were individually added to the plating bath through dilution from master solutions that were dissolved in water. PEG was always used in the amount of 300 ppm (9×10^{-5} M). During aging, solutions were kept at a room temperature in a beaker exposed to atmosphere for electrochemical experiments and sealed in plastic containers for HPLC experiments.

Results and Discussion

Chromatographic results

The chromatographic measurements were first performed in 0.3 M sulfuric acid solution with 10 g L^{-1} (0.18 M) of Fe^{2+} and 15 ppm (4.23×10^{-5} M) of SPS, without cupric ions and without electrodic activity. The results of these measurements at 1, 4, and 7 days after sample preparation are shown in Fig. 2. The MPS peak became readily visible in the chromatograms, and the peak area continued to grow even after 4 days, suggesting a slow equilibration time (in contrast to solutions with Cu^{2+}, see below). The SPS peak appeared at 64 min (not shown). The areas of chromatographic peaks seen around 17 min were linked to MPS concentrations via an external calibration of peak areas versus known amounts of MPS (not shown). The concentration of MPS corresponding to the data presented in Fig. 2, are as follows: 78 ppb (4.38×10^{-7}) after 1 day, 240 ppb (1.35×10^{-6}) after 4 days, and 510 ppb (2.88×10^{-6}) after 7 days.

The chromatographic analysis was then performed in a solution with 10 g L^{-1} (0.18 M) of Fe^{3+} and 15 ppm (4.23×10^{-5} M) of SPS in 0.3 M sulfuric acid solution, again without cupric ions and without electrodic activity. Figure 3 shows the results 1, 4, and 7 days after sample preparation. The chromatographs demonstrate the absence of MPS and di-ox-SPS peaks. The absence of MPS could have also been predicted from Reaction 3, since SPS requires ferrous ions (i.e. a reducing agent), to be converted to MPS. However, the absence of di-ox-SPS peak was unclear to us.

Similar to Figs. 2 and 3, the chromatographic measurements were carried out in the 0.3 M sulfuric acid solution of SPS (15 ppm), Fe^{2+} (10 g L^{-1}), and 10 g L^{-1} (0.157 M) of Cu^{2+} ions. As shown in Fig. 4, the magnitude of the chromatographic peak attributed to MPS

decreased in the presence of cupric ions. The peak areas of MPS, after 1, 4 and 7 days, correspond to a concentration value of around 24 ppb (1.35×10^{-7} M) and appear stable over time. The reason for faster equilibration time in solutions containing Cu^{2+} was unclear. It is also worth noting that the peak for di-ox-SPS appears only in the presence of ferrous ions (i.e. solutions with and without Cu^{2+} and/or Fe^{3+} showed no sign of di-ox-SPS).

The small shifts in elution time of the various peaks in Figs. 2 – 4 could be due to several external and internal factors. The elution time depends on the interaction of molecules with stationary and mobile phases. The degree of interaction could be affected by several factors, such as temperature (which was not controlled) and small variations in the concentration of the mobile phase (which could happen upon replenishment of the mobile phase, for example). Since the experiments in Figs. 2 – 4 were performed over a span of 7 days, small changes in elution time were hard to control.

Electrochemical results

An electroanalytical investigation was performed to check whether the electrochemical behavior is consisted with the chromatographic data, and to further investigate the role of Reaction 3 in copper deposition. We hypothesized that MPS was the primary species responsible for the acceleration of copper deposition. Based on this hypothesis, a similar electroanalytical response was expected during the electrochemical deposition of copper from the copper electrolyte of PEG, SPS (15 ppm), and Fe^{2+} (10 g L^{-1}) and the electrolyte of PEG, SPS (15 ppm), and MPS at 24 ppb (as predicted from Fig. 3). Based on linear sweep voltammetry measurements (Fig. 5), the two electrolytes indeed exhibit a similar electrochemical behavior.

Deviation of PEG, SPS, and Fe^{2+} curve from PEG, SPS, and MPS curve, notwithstanding experimental uncertainties and scatter, may be correlated with the presence of di-ox-SPS species in the PEG, SPS, Fe^{2+} electrolyte (as suggested by Figs. 2 and 4). The same deviation can also be attributed to the variation in the bulk concentration of Cu^{+}, which was affected by Fe^{2+} ions in solution.

As measured by HPLC, the bulk concentration of MPS was a function of Cu^{2+} level in electrolyte. To see whether an increase in acceleration due to the presence of ferrous ions was also a function of Cu^{2+} concentration, chronoamperometric plating of copper was conducted at various levels of cupric ions under two conditions: (1) PEG and SPS, and (2) PEG, SPS, and Fe^{2+}. Figure 6 demonstrates that the impact of Fe^{2+} on the acceleration of copper deposition was dependent on amount of cupric ions in solution. As the concentration of Cu^{2+} increased, the increase in acceleration in the presence of Fe^{2+} was diminished. It even appears that at a sufficiently high concentration of cupric ions, ferrous ions had no impact on the acceleration of copper deposition.

It was also expected, based on Reaction 3, that with a decreasing ratio of ferric to ferrous ions, the equilibrium amount of MPS (and hence the degree of acceleration) could increase. However, as shown in Fig. 8, the steady state current only follows this trend at relatively high ratios. As the Fe^{3+}/Fe^{2+} ratio decreases, the steady state current goes through a maximum and then decreases. One possible explanation is the grossly simplified equilibrium considerations.

Based on Fig. 1, it can be hypothesized that, in the presence of the redox couple, MPS was produced via both a reductive pathway (i.e. Reaction 3) and an oxidative

pathways, involving perhaps several of the oxidized SPS species depicted in Fig. 1. Possibly, the existence of both pathways may explain the maximum.

Prediction of MPS concentration based on equilibrium constants

The estimates of equilibrium concentrations (without activity-coefficient corrections) were made as a means of interpreting experimental results. The SPS/MPS equilibrium constant requires knowledge of the reduction potential of a disulfide bond in SPS (Reaction 7). Vereecken *et al.* have tried to experimentally measure the reduction potential at multiple metal electrodes, but were unable to detect the electrochemical reduction of SPS,[23] possibly due to a slow equilibration and adsorption on solid electrode surfaces

$$SPS + 2H^+ + 2e^- \rightleftarrows 2MPS \quad (7)$$

There are analogues to the SPS/MPS couple, including the L-cystine/L-cysteine redox couple.[40] Depending on the method used, the standard reduction potential for L-cystine/L-cysteine was reported to be in the range between 0.02 and 0.191 V *vs.* standard hydrogen electrode (SHE) at pH = 0.[33] Since an identical disulfide linkage is present in SPS molecule, our initial guess for the SPS standard reduction potential was in the same range.

An equilibrium relation between SPS and MPS for a system initially consisting of 15 ppm SPS ($c_{sps,\ o} = 4.23 \times 10^{-5}\ M$) dissolved in water (described by Reaction 2) was used to predict an equilibrium concentration of MPS (c_{MPS}).

$$10^{\frac{U^{\theta}_{SPS} - 1.229}{0.0591}} = \frac{\left(p_{O_2}\right)^{1/4} \times (c_{MPS})}{\left(c_{sps,\ o} - 0.5 c_{MPS}\right)^{1/2}} \quad (8)$$

Chromatographic measurement of the same solution showed no signs of MPS (not shown). For a range of assumed reduction potentials (U^{θ}_{sps}) up to 0.8 V *vs.* SHE, the

equilibrium concentrations of MPS were predicted to be much less than 1 ppb (5.6×10^{-9} M), which are below the limit of detection of the HPLC tool.

As was already noted, the redox couple may impact the equilibrium between SPS and MPS. To check whether the equilibrium estimates can predict the appearance of MPS at the levels measured by HPLC, we modeled system initially consisting of 15 ppm of SPS at specified ratios of the Fe^{3+}/Fe^{2+} couple in 0.3 M sulfuric acid solution and used equilibrium expression for Reaction 3 in the calculation of MPS concentration.

$$10^{\frac{U^{\theta}_{SPS}-0.771}{0.0591}} = \frac{c_{MPS}}{(c_{H^+}) \times (c_{sps,\ o} - 0.5c_{MPS})^{1/2}} \times \left[\frac{c_{Fe^{3+}}}{c_{Fe^{2+}}}\right] \qquad (9)$$

Figure 9 shows that, at values of U^{θ}_{sps} around 0.33 V vs. SHE, the MPS equilibrium concentration reached detectable amounts – at low ppb range and higher, depending on the Fe^{3+}/Fe^{2+} ion ratio. The standard reduction potential of SPS to MPS reduction has not been reported, despite several attempts; therefore we would like to emphasize the estimate of U^{θ}_{sps} using the approach presented here. The Fe^{3+}/Fe^{2+} ratio also had an impact the concentration of dissolved oxygen.

Figure 4 shows that the addition of 10 g L^{-1} (0.157 M) cupric ions to a solution of SPS and Fe^{2+} significantly reduced the MPS peak intensity (from about 500 ppb to about 20 ppm after 7 days). To estimate equilibrium concentration of MPS, starting from 15 ppm of SPS, 10 g L^{-1} of Fe^{2+}, and a range of Cu^{2+} concentrations, two coupled equilibrium relations were solved with Matlab (based on Reaction 3 and Reaction 6) with Cu^{+} and MPS equilibrium concentrations as unknowns. It was however hard to estimate the ferric-ion concentration on time scales of the experiment because $C_{Fe^{3+}}$ was influenced by the rates of ferrous-ion oxidation by dissolved oxygen. Therefore, the solution presented in Fig. 10 for MPS is given at different initial concentrations of ferric ions. The addition of ferrous ions

should immediately lead to ferric ions in solution through Reaction 4. For example, Reaction 4 predicts that 1 mole of oxygen produces 4 moles of ferric ions, so if we assume all dissolved oxygen is consumed, then the initial concentration of Fe^{3+} would be equal to four times the initial concentration of dissolved oxygen ($c_{Fe^{3+},\ o} = 4 \times c_{O_2,o}$), where c_{O_2} was assumed to be 2.6×10^{-4} M.[41] Figure 10 shows that the drop in MPS concentration comparable to chromatographic measurements, when copper level goes from $c_{Cu^{2+}} = 0$ g/L to $c_{Cu^{2+}} = 10$ g/L, could be also be predicted based on equilibrium estimates. The best agreement between estimates and HPLC findings, as seen in Fig. 10, was obtained at low $c_{Fe^{3+},\ o}$ values.

Conclusions

The interaction between SPS and MPS in the presence Fe^{2+} and Fe^{3+} ions was examined using chromatographic and electrochemical methods. The Fe^{3+}/Fe^{2+} ratio was a means of varying the reducing power of the electrolyte, through changing the concentration of MPS derived from SPS in the bulk electrolyte. When 15 ppm of SPS was mixed with 10 g L^{-1} of Fe^{2+} in 0.3 M H_2SO_4, HPLC chromatograms showed a distinct peak corresponding to MPS (~500 ppb, 2.81×10^{-6} M, after 7 days). When the same solution was prepared with 10 g L^{-1} of Cu^{2+}, the MPS peak intensity was significantly reduced (~20 ppb, 1.12×10^{-7} M, after 7 days). A very similar electrochemical response was achieved by adding either Fe^{2+} or MPS, suggesting that the enhanced acceleration by adding redox mediator was the result of elevation of bulk MPS concentration. This enhancement had a maximum at an intermediate Fe^{3+}/Fe^{2+} concentration ratio, suggesting perhaps that MPS was derived from SPS by both reductive and oxidative pathways. The estimates of the standard reduction potential of SPS

to MPS reduction, based on equilibrium calculations with reference to HPLC results, predicted the reduction potential in a range of 0.3 – 0.4 V *vs.* SHE.

References

1. T. Osaka, M. Hasegawa, M. Yoshino and N. Yamachika, in *Advanced Nanoscale ULSI Interconnects: Fundamentals and Applications*, p. 183, Springer, New York (2009).
2. T. P. Moffat, J. E. Bonevich, W. H. Huber, A. Stanishevsky, D. R. Kelly, G. R. Stafford and D. Josell, *Journal of The Electrochemical Society*, **147**, 4524 (2000).
3. T. P. Moffat, D. Wheeler and D. Josell, *Journal of The Electrochemical Society*, **151**, C262 (2004).
4. P. Taephaisitphongse, Y. Cao and A. C. West, *Journal of The Electrochemical Society*, **148**, C492 (2001).
5. A. C. West, S. Mayer and J. Reid, *Electrochemical and Solid-State Letters*, **4**, C50 (2001).
6. J. J. Kelly and A. C. West, *Journal of The Electrochemical Society*, **145**, 3477 (1998).
7. P. C. Andricacos, C. Uzoh, J. O. Dukovic, J. Horkans and H. Deligianni, *IBM Journal of Research & Development*, **42**, 567 (1998).
8. J. W. Gallaway, M. J. Willey and A. C. West, *Journal of The Electrochemical Society*, **156**, D146 (2009).
9. M. J. Willey and A. C. West, *Journal of The Electrochemical Society*, **154**, D156 (2007).

10. T. P. Moffat, B. Baker, D. Wheeler and D. Josell, *Electrochemical and Solid-State Letters*, **6**, C59 (2003).

11. J. J. Kim, S.-K. Kim and Y. S. Kim, *Journal of Electroanalytical Chemistry*, **542**, 61 (2003).

12. L. Y. Valentelis, *Protection of Metals*, **32**, 38 (1996).

13. L. D'Urzo, H. Wang, A. Pa and C. Zhi, *Journal of The Electrochemical Society*, **152**, C243 (2005).

14. R. G. Brennan, M. M. Phillips, L.-Y. O. Yang and T. P. Moffat, *Journal of The Electrochemical Society*, **158**, D178 (2011).

15. A. Frank and A. J. Bard, *Journal of The Electrochemical Society*, **150**, C244 (2003).

16. W.-H. Lee, C.-C. Hung, S.-C. Chang and Y.-L. Wang, *Journal of The Electrochemical Society*, **157**, H131 (2010).

17. C. C. Hung, K. W. Chen and Y. L. Wang, *J. Vac. Sci. Technol. B*, **26(1)**, 255 (2008).

18. T. H. Bailey, Q. Wang and M. West, *ECS Transactions*, **2**, 131 (2007).

19. H. Brunner, *Private Communication*, **Berlin, Germany** (2010).

20. N. Zukauskaite and A. Malinauskas, *Elektrokhimiya*, **24**, 1691 (1988).

21. H. D. Philippe M. Vereecken, Keith T. Kwietniak, Panayotis C. Andricacos, Robert A. Binstead, Janet Wu, Robert Mikkola, Jeffrey M. Calvert, The Role of SPS in Damascene Copper Electroplating, in *201st Meeting of The Electrochemical Society* (2002).

22. E. E. Farndon, F. C. Walsh and S. A. Campbell, *Journal of Applied Electrochemistry*, **25**, 574 (1995).

23. P. M. Vereecken, R. A. Binstead, H. Deligianni and P. C. Andricacos, The chemistry of additives in damascene copper plating, in *IBM Journal of Research & Development*, p. 3, IBM Corporation/IBM Journals (2005).

24. K. Kondo, T. Matsumoto and K. Watanabe, *Journal of The Electrochemical Society*, **151**, C250 (2004).

25. J. P. Healy, D. Pletcher and M. Goodenough, *Journal of Electroanalytical Chemistry*, **338**, 167 (1992).

26. A. Survila, S. Kanapeckaite and R. Pauliukaite, *Chemija (Vilnius)*, 21 (1998).

27. T. D. R. Preisser, and H. Fuerhaupter, in *204th Meeting, The Electrochemical Society, Inc.* (2003).

28. J. Barthelmes, in *Electronics Circuits World Convention 8*, Tokyo, Japan (1999).

29. J. V. Eisden, X. Kang, J. Enloe, C. G. Koh and R. Preisser, *ECS Meeting Abstracts*, **901**, 979 (2009).

30. J. D. Adolf, R. Preisser and U. Landau, *ECS Meeting Abstracts*, **902**, 2163 (2009).

31. C. L. Beaudry and J. O. Dukovic, *Interface*, **13**, 40 (2004).

32. I. Volov, T. Saito and A. C. West, *Journal of The Electrochemical Society*, **158**, D384 (2011).

33. T. R. Ralph, M. L. Hitchman, J. P. Millington and F. C. Walsh, *Journal of Electroanalytical Chemistry*, **375**, 17 (1994).

34. N. Tanaka, I. M. Kolthoff and W. Stricks, *Journal of the American Chemical Society*, **77**, 2004 (1955).

35. P. J. Vandeberg and D. C. Johnson, *Analytical Chemistry*, **65**, 2713 (1993).

36. I. Volov, O. Mann, Y. Hoenersch, B. Wahl and A. C. West, *Journal of Separation Science*, **34**, 2385–2390 (2011).

37. R. Palmans, S. Claes, L. E. Vanatta and D. E. Coleman, *Journal of Chromatography A*, **1085**, 147 (2005).

38. P. Andricacos, D. S. Chung, H. Deligianni, J. E. Fluegel, K. T. Kwietniak, P. S. Locke, D. D. Restaino, S. C. Seo, P. M. Vereecken and E. G. Walton, Void-Free Damascene Copper Deposition Process and Means of Monitoring Thereof, in, IBM Corp, United States (2010).

39. B. Wahl, Bestimmung von Glanzzusätzen in sauren Kupferelektrolyten mittels HPLC und unterschiedlichen Detektionsmethoden, in, Unpublished Master thesis, TFH Berlin (2005).

40. C. V. Krishnan, M. Garnett and B. Chu, *Int. J. Electrochem. Sci.*, **3**, 854 (2008).

41. L. L. Shreir, R. A. Jarman and G. T. Burstein, Corrosion (3rd Edition) Volumes 1-2, in, Elsevier (1994).

Figure 1

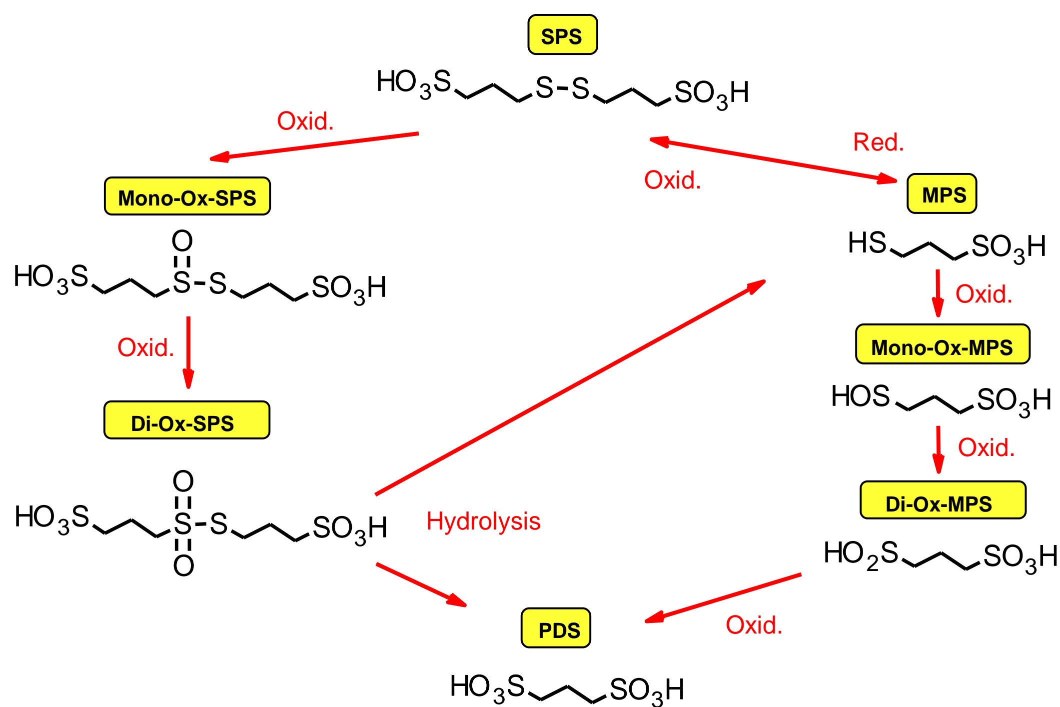

Figure 1. Possible reduction and oxidation pathways to certain break-down products of SPS.

Figure 2

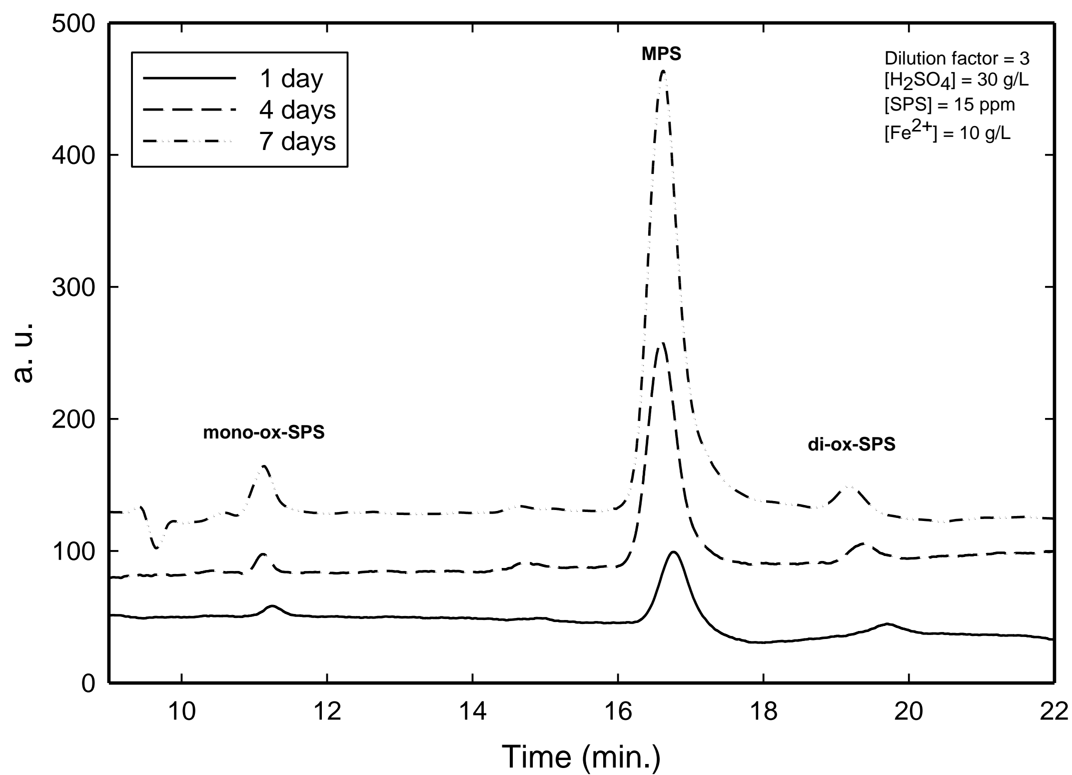

Figure 2. HPLC chromatogram obtained from aging of SPS (15 ppm) and Fe^{2+} (10 g L^{-1}) in 0.3 M H_2SO_4. The peak around 17 min was attributed to MPS.

Figure 3

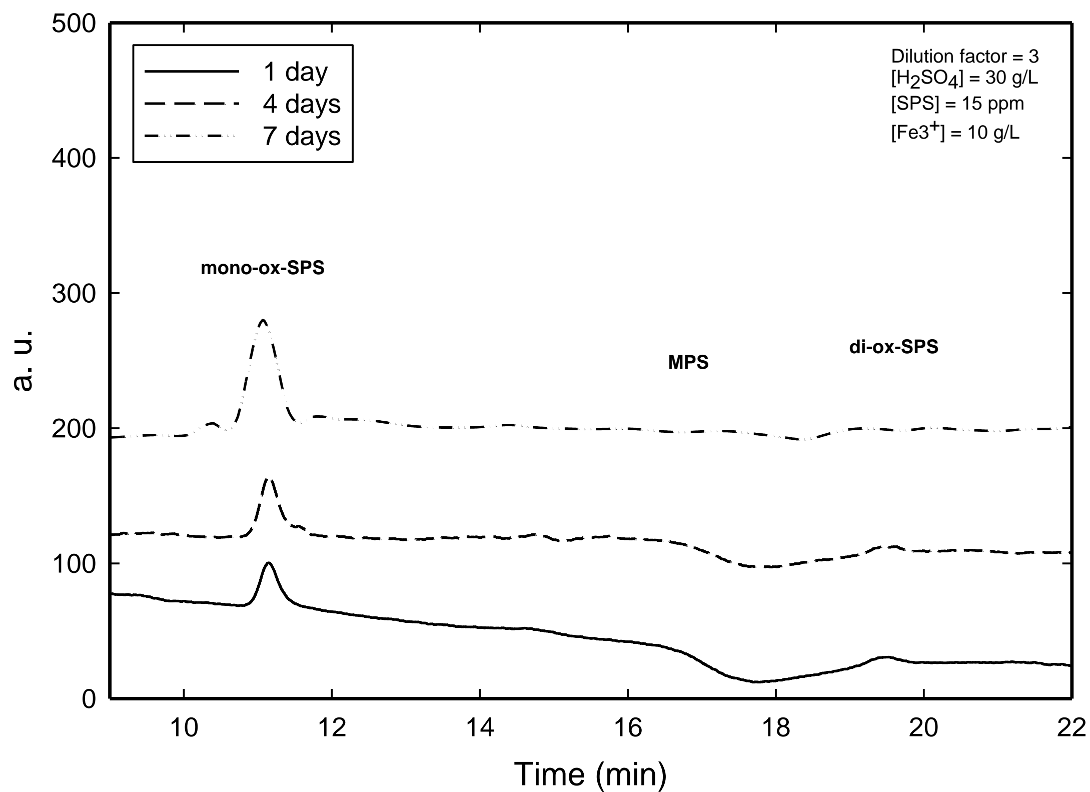

Figure 3. HPLC chromatogram obtained from aging of SPS (15 ppm) and Fe^{3+} (10 g L^{-1}) in 0.3 M H_2SO_4.

Figure 4

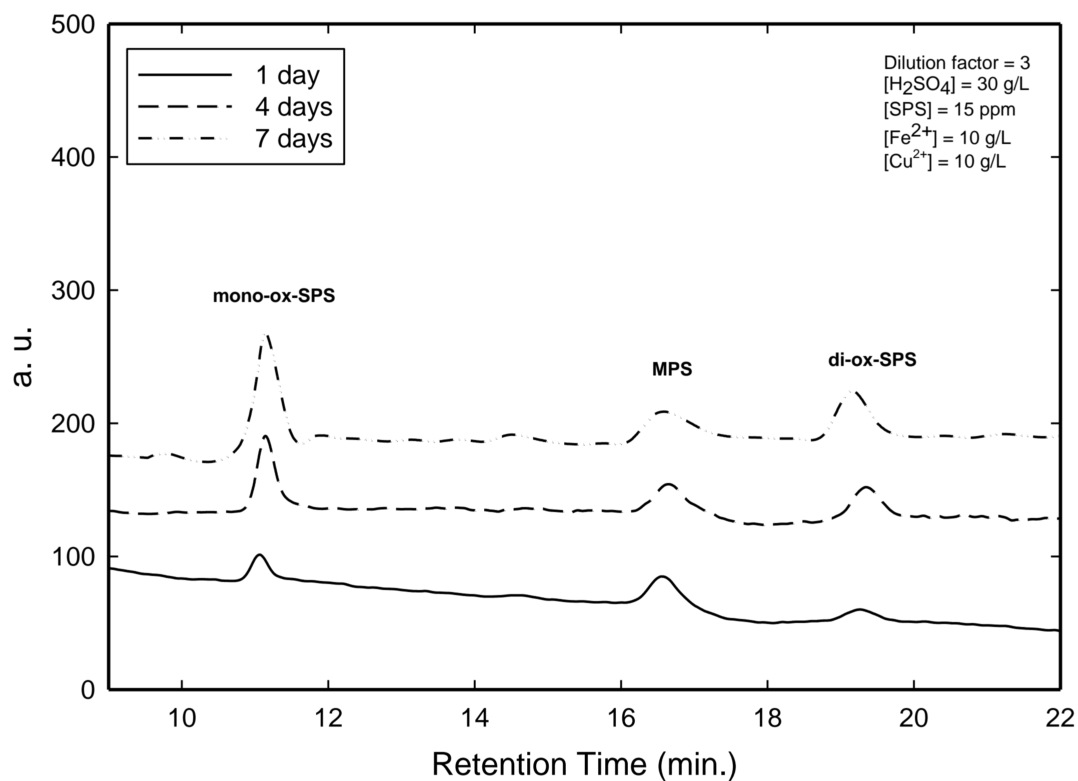

Figure 4. HPLC chromatogram obtained from aging of SPS (15 ppm), Fe^{2+} (10 g L^{-1}), and Cu^{2+} (10 g L^{-1}) in 0.3 M H_2SO_4. The peak around 17 min was attributed to MPS. The MPS peak area was reduced in the presence of cupric ions.

Figure 5

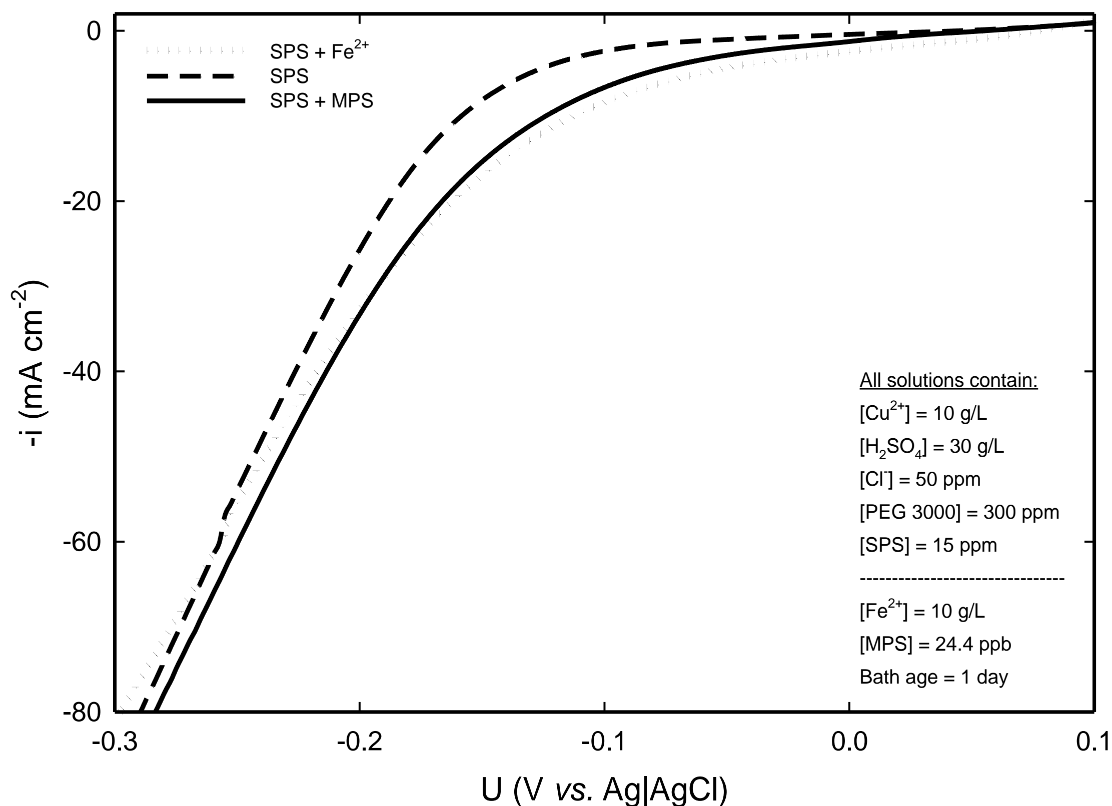

Figure 5. Linear sweep voltammetry results obtained at a sweep rate of 10 mV s^{-1}; the potential was swept from positive to negative. Results were obtained on preplated with copper, platinum RDE at 900 rpm, 1 day after bath preparation. The dashed line represents an experiment with PEG and SPS, dotted line is an electrolyte with SPS and Fe^{2+}, and the solid line is for SPS and MPS (using an MPS concentration taken from HPLC measurements).

Figure 6

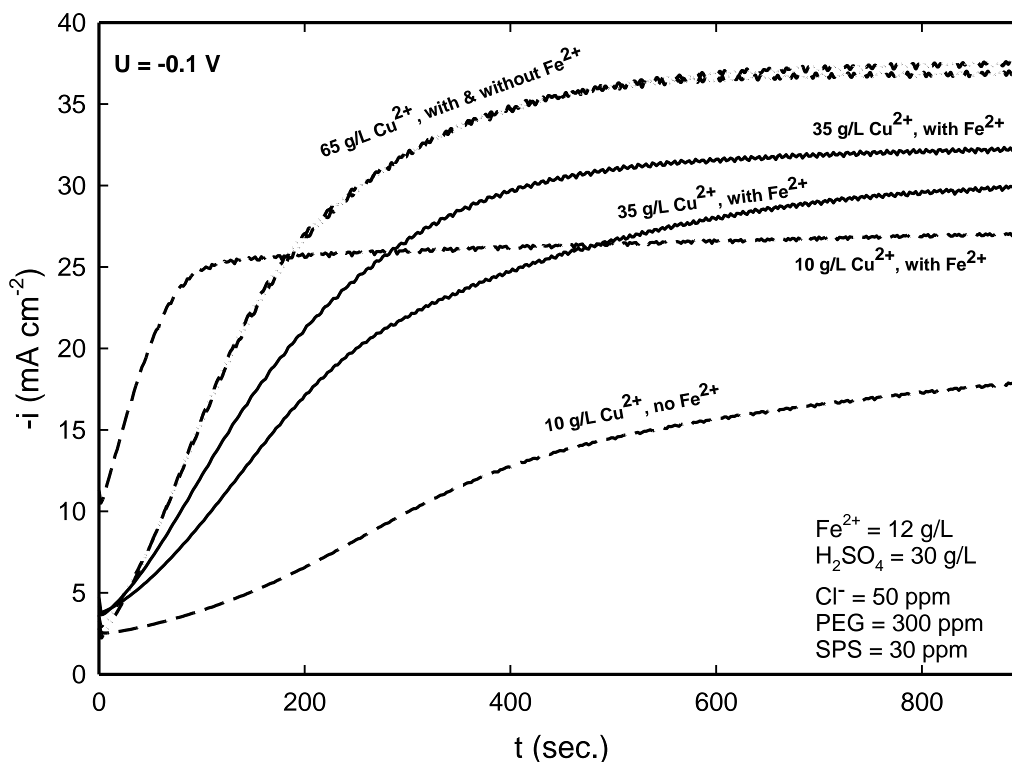

Figure 6. Current as a function of time for an applied potential of U = -100 mV *vs.* Ag|AgCl. Data were obtained on an RDE at 900 rpm, 2 – 3 h after bath preparation. Results are shown for a three pair of experiments: at 10, 35, and 65 g L^{-1} of cupric ions in electrolyte. As the level of cupric ions was increased the difference in acceleration in the presence and absence of Fe^{2+} was reduced.

Figure 7

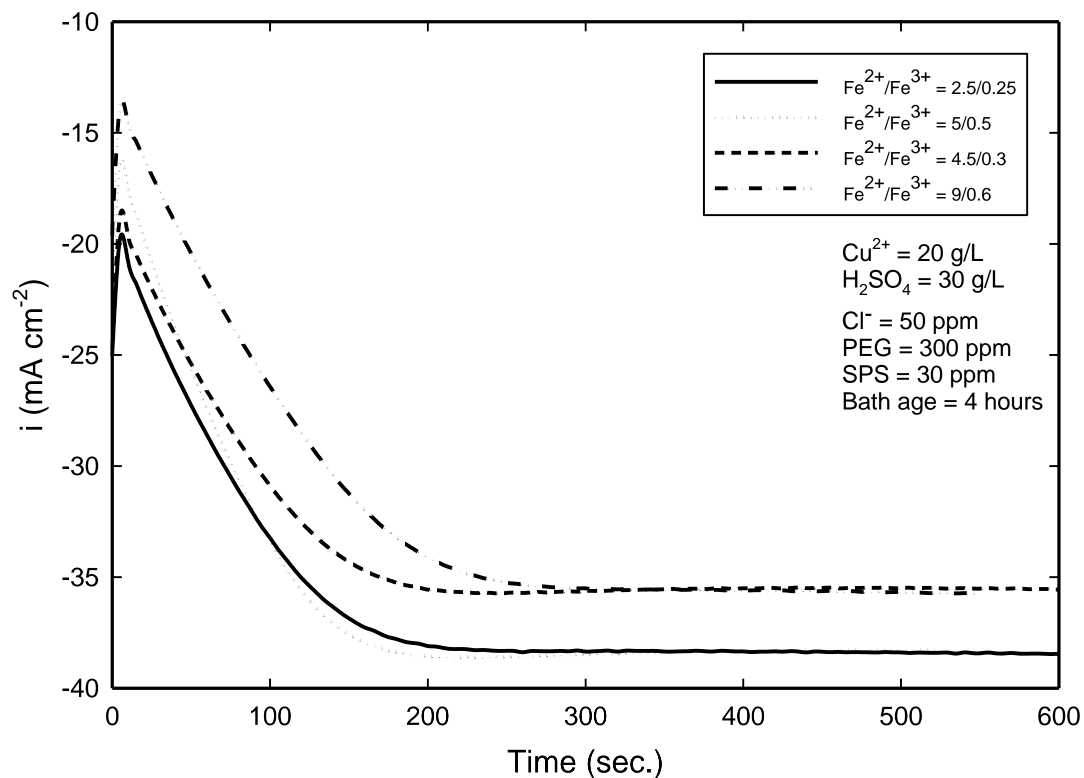

Figure 7. Current as a function of time for an applied potential U = -100 mV *vs.* Ag|AgCl. Data were obtained on an RDE at 900 rpm, 4 h after bath preparation. Results show that the steady state current from the acceleration of copper deposition was only a function of a ratio between ferric and ferrous ions.

Figure 8

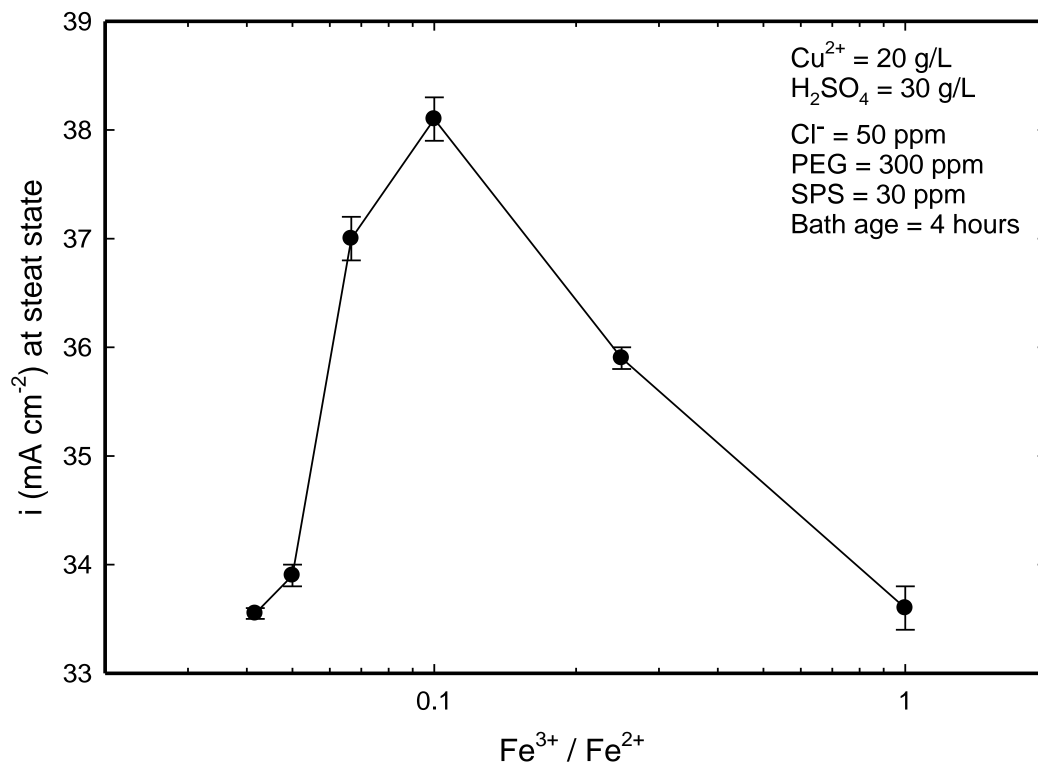

Figure 8. Steady state current values, from potentiostatic plating at U = -100 mV, are plotted as a function of the Fe^{3+}/Fe^{2+} ratios. In all experiments, the ferric-ion concentration was 0.5 g L^{-1} and the ratio was varied by changing the ferrous-ion concentration.

Figure 9

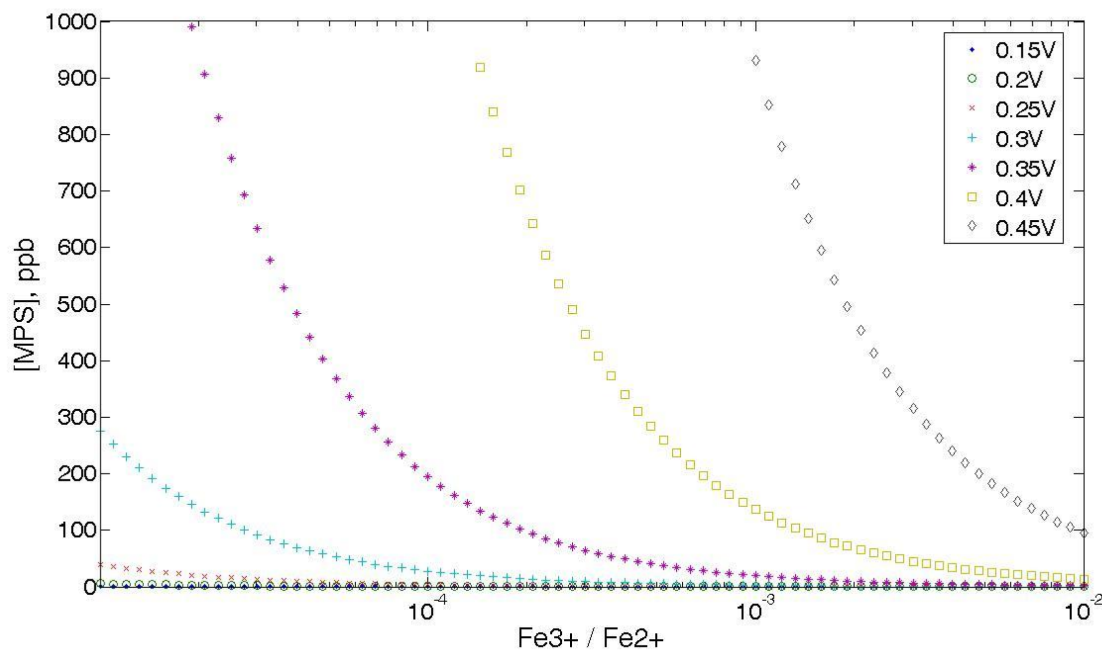

Figure 9. Calculated values of MPS equilibrium concentrations as a function of Fe^{3+}/Fe^{2+} ratio using several assumed SPS standard reduction potentials. The initial concentration of SPS was 15 ppm.

Figure 10

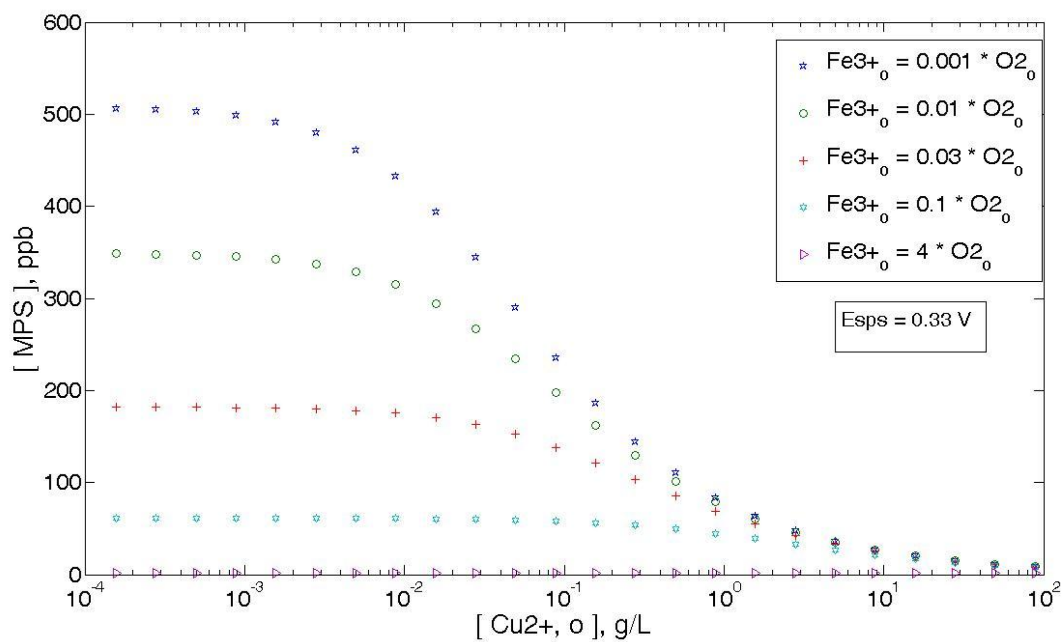

Figure 10. Calculated values of MPS equilibrium concentrations as a function of Cu^{2+} concentration. The SPS reduction potential was chosen to be 0.33 V *vs.* SHE, and results are given for various initial concentrations of ferric ions and a set concentration of ferrous ions at 10 g L^{-1}.

Chapter 4

Chromatography of Bis-(3-Sulfopropyl) Disulfide and Its Breakdown Products by HPLC Coupled with Electrochemical Detection*

Abstract

A chromatographic method for the detection of bis-(3-sulfopropyl) disulfide (SPS), a common additive in acidic copper plating baths, and its breakdown products was demonstrated. The detection scheme involved a combination of solid-phase extraction for sample pre-treatment, C18 reversed-phase high-performance liquid chromatography column for separation, and electrochemical sensor for detection of all non-fully oxidized sulfur containing compounds. We were able to achieve an effective separation and accurately assign chromatographic peaks to all detectable species. Owing to a high sensitivity of the utilized electrochemical detector, detection in low parts per billion range was possible. This can prove crucial for plating bath control, since minute amounts of certain byproducts significantly affect the bath performance.

---

* This work was done in collaboration with Olivier Mann, Yvonne Hoenersch, and Björn Wahl.

Introduction

Copper plating baths are used extensively for the electrochemical deposition (ECD) of copper onto complex surface geometries. The main application of copper ECD is encountered in semiconductor and printed circuit board industries, where copper metal serves as a conductor for wiring purposes.[1] Electrolytic copper plating is performed in acidic copper sulfate solutions with a number of organic constituents, which enable desired filling of surface features. The quality of the deposited copper metal is a major concern for the present and future dual damascene metallization schemes, as well as through-silicon-via (TSV) applications.[2,3] This requires stringent control of the bath composition for inorganic (Cl^-, H_2SO_4, Cu^{2+}) and organic components. Two organic additives that are included in almost all copper plating baths are an accelerator and a suppressor component,[4–10] The accelerator and suppressor decompose during electrolysis as well as during idle periods.[11–14] Owing to the adverse effects of the accelerator breakdown products on copper film properties, in particular, the accelerator and its by-products require frequent monitoring.[15]

The main accelerator used in acidic copper plating electrolytes is the compound bis-(3-sulfopropyl) disulfide, commonly known under the acronym SPS. This additive helps to promote the so-called superfilling or bottom-up fill of fine features with desired metal properties; however, the precise mechanism of action of SPS is still lacking.[16] The main by-products of SPS (Table 1) are thought to include mono-oxide of SPS, di-oxide of SPS, and 1,3-propanedisulfonic acid (PDS) as oxidation by-products, and 3-mercaptopropyl sulfonate (MPS) as a reduction by product.[17]

Currently, the most widely used method for the analysis of the organic additives is cyclic voltammetric stripping (CVS), which relates organic concentration to the copper

plating rate.[18–21] Since cyclic voltammetric stripping works by monitoring the effective activity of each component in the plating process, it does not give a direct measurement of the concentrations of organics and only indirect evidence of species in electrolyte can be obtained. A more reliable and quantitative analysis method for SPS and its breakdown products is possible with high-performance liquid chromatography (HPLC). A few efforts have already been described in the literature for analysis of SPS and its byproducts by HPLC with various detection schemes, such as UV spectroscopy[22,23], mass spectrometry,[17] and others. However, we are not aware of studies that show an adequate separation of SPS by-products, unambiguously assign chromatographic peaks, and have detection sensitivity in the nano-molar range.

In this chpater, the development of an HPLC procedure using a C18 reversed-phase column is presented for analysis of SPS and its breakdown products from an acidic copper plating bath. An electrochemical method of detection (HPLC-ED) has been chosen due to its superior detection sensitivity to the non-fully oxidized sulfur-containing molecules. An HPLC-ED method for plating bath monitoring has been disclosed in US Patent 7 678 258 B2;[15] however, the patent neither does specify detection limits, nor does it accurately identify chromatographic peaks. Moreover, the presented chromatograms showed poor peak separation. In contrast, we were able to achieve a satisfactory separation and unambiguously assign chromatographic peaks to the detectable species, while lowering the limit of detection to only a few parts per billion (ppb). Another unique feature of this work is the use of chemical standards specifically synthesized for precise determination of all chromatographic peaks. This technique has already been utilized in chapter 3 to study the impact of an iron redox couple on SPS.[24]

Material and Methods

Chromatographic set-up

All chromatographic analyses were performed on in-house developed system (Fig. 1) at Atotech, Berlin GmbH. The set-up consisted of a K-120 Pump (Knauer), a PEEK Pulsation Damper (Metrohm), a T-piece, a Triathlon Spark Auto-Sampler (Metrohm), two Atlantis T3 columns (4.6×100 mm, 3 mm, Waters, Inc.), an electrically driven 6-port-3-channel valve A1370 with valve drive K-6 (both Knauer), and an ED50A Electrochemical Detector (Dionex) equipped with a thin-layer channel cell containing Au working electrode and Ag|AgCl reference electrode (1 M KCl plus 1 M HCl). To protect the electrochemical cell from matrix impact, the liquid flow was split before sample introduction with a T-piece. One path was used for the analytical separation, and the other to maintain the electrochemical cell under flow when the matrix from the analytical column was directed to waste. This was realized by a switching valve. The similar flow rates on both paths were obtained by using two identical columns (Fig. 1). The electrochemical detector (ED) operated with a waveform specially designed to detect non-fully oxidized sulfur-containing molecules (Fig. 2). To further prevent the influence of the matrix, metal ions were removed from the sample by passing it through a proton exchange cartridge OnGuard II H (Dionex) prior to the chromatographic analysis. All separations were conducted in an isocratic mode at room temperature. The flow rate through the system was 0.5 mL min^{-1} and the injection volume was 20 mL. Instrument control and data acquisition were handled by the EZChrom Elite Software (Agilent Technologies).

Electrochemical detection with ED cell

The knowledge of SPS and its by-products concentrations is a problem of critical significance for predicting the filling performance of a plating bath.[15,17] These organic sulfur-containing compounds can be separated from the interfering matrix by using reverse-phase chromatography; however, the UV detection is hindered by poor spectroscopic properties.[22, 25] An alternative method is based on electrochemical detection with Au working electrode, which is commercially available and has been used in determination of sulfur-containing amino acids[26] and pesticides.[27]

It has been previously established that the most suitable electrochemical technique for the detection of organic sulfur-containing compounds is integrated pulsed amperometric detection (IPAD).[25] In this technique a repetitive potential pulse is applied to a noble metal electrode – oxidizing the analyte molecules at its surface and the resulting current is measured. In this way, compounds in which the sulfur atom has an unshared pair of electrons are detectable (e.g. thiols and disulfides), but sulfur-containing molecules with fully oxidized sulfur atoms (e.g. PDS) cannot be detected.

An optimal IPAD waveform for the use with the present ED (Fig. 3) was developed at Atotech, Berlin GmbH by Mr. Wahl (details are available in unpublished Master Thesis, TFH Berlin, 2005). The waveform consisted of a 1-s cycle, which included an adsorption delay, detection, and a cleaning step. The adsorption delay step began at U = -0.5 V for 0.1 s, followed by the detection step, where the potential was ramped to 1.7 V in 0.2 s and then decreased back to -0.5 V in 0.2 s. The third and final step was used for the surface cleaning and included a jump in potential to 1.6 V in 0.01 s, keeping the potential steady at 1.6 V for

0.1 s, a decrease in potential to -0.6 V in 0.01 s, and finally a constant potential of -0.6 V for 0.38 s.

Plating set-up

Plating experiments were performed under air agitation in a 10-L cell composed of two soluble copper anode plates (1.5 dm^2 active area) between which the sample to be plated was under horizontal motion. Plain copper printed circuit boards were plated for 90 min at a current density of 1 A dm^{-2} to achieve a plating thickness of ~20 μm. Between each test the plating bath was continuously in operation in order to increase the concentrations of byproducts. Overnight, the plating bath was on idle time.

Chemicals and standards

The suppliers and composition of all chemicals used for the chromatographic runs and bath sample preparation are summarized in Table 2.

This study benefits from the use of in-house synthesized chemical standards: OxSPS_1 (mainly mono-oxidation product of SPS) and OxSPS_2 (mainly di-oxidation product of SPS). The synthesis of these compounds was conducted with H_2O_2 and specific catalysts. Both standards were characterized by liquid chromatography coupled with mass spectrometry (LC-MS) by the organic synthesis group at Atotech, Berlin GmbH. OxSPS_1 was found to be mainly composed of mono-oxidation product of SPS (~80%), relatively high percentages of SPS (~10%) and its di-oxidation product (~10%), and a small amount of PDS. OxSPS_2 was determined to be composed of a mixture of SPS (~23%), its di-oxidation product (~77%), with small amount of the mono-ox-SPS and PDS.

Results and Discussion

Method development for HPLC-ED

The choice of an analytical column and a mobile phase was the key to the separation of SPS and its by-products. For example, our first choice was a C18 reversed-phase column the Puroshper Star RP-18e, 4×55 mm, 3 mm (Merck) and 0.0125 M H_2SO_4 as the mobile phase. The chromatograms at these conditions showed well-defined MPS and SPS peaks, with a relatively short measurement time of ~18 min (SPS showed the longest retention time of 15.4 min). However, it was found later that MPS and mono-ox-SPS could not be adequately separated with this column.

A better separation was achieved with another C18 reversed-phase analytical column the Atlantis T3, 4.6×100 mm, 3 mm (Waters). The run of an SPS standard solution with 0.0125 M H_2SO_4 as the eluent showed an unacceptably long retention time for SPS (over 110 min). Acetonitrile (ACN) was then added to increase the elution strength of the eluent (and reduce the run time). It is worth noting that at 1% ACN in 0.0125 M H_2SO_4 mobile phase, chromatographic peaks (from mono-ox-SPS, di-ox-SPS, SPS, and MPS) showed a good separation, but the retention time of SPS was still long (95 min). At 3% and 4% ACN in 0.0125 M H_2SO_4 eluent, the retention time of SPS was 45 and 35 min, respectively; however, MPS and di-ox-SPS could not be adequately separated.

Finally, the optimal method developed for Atlantis T3 column allowed for a measurement time of ~70 min per run with 2% ACN and 0.0125 M H_2SO_4 in de-gassed DI water. With this method, the retention times of mono-ox-SPS, di-ox-SPS, SPS, and MPS were successfully established (Fig. 3) by making use of known chemical standards dissolved

in water (see legend of Fig. 3). As shown in Fig. 3, the retention times were ~11 min for mono-ox-SPS, ~16.5 min for MPS, ~19 min for di-ox-SPS, and ~64 min SPS.

From the results shown in Fig. 3, the relative polarity of SPS and its oxides became apparent. Mono-ox-SPS was the most polar, since it eluted first from a reversed-phase column, and SPS was the least polar, since it eluted last. The retention time of SPS peak showed a considerable sensitivity to the concentration of ACN in a mobile phase. As such, the SPS peak slightly drifted each time the eluent was replenished. The data presented here were corrected to show all SPS peaks eluting at precisely the same time.

A relative electrochemical impact of mono-ox-SPS, di-ox-SPS, SPS, and MPS on the electrodeposition of copper is shown in Fig. 4. The curve with a single suppressor (PEG) was shown as a reference for the degree of catalytic activity of the other accelerating species. The behavior of SPS and MPS, as shown in Fig. 4, has been previously established.[28] To the best of our knowledge, the degree of acceleration (*i.e.* increase in the current density at a given potential) provided by mono-ox-SPS and di-ox-SPS has not been reported previously. Both oxides exhibit less acceleration than SPS alone, information that may prove useful for understanding the behavior of the aged baths containing a significant degree of SPS by-products.

HPLC-ED measurement of real bath samples

Figure 5 shows chromatograms recorded for a freshly collected sample from a test plating bath typically composed of inorganic constituents: 45 g L^{-1} Cu^{2+}, 40 ppm Cl, and 150 g L^{-1} H_2SO_4; as well as of organic constituents: SPS and PEG (3000 g mol^{-1}) present in the low and high ppm range, respectively, and a N-containing leveler at ppm concentrations. As

previously mentioned, the high sensitivity of the Au working electrode with respect to matrix effects necessitates the use of standard addition to quantify the concentrations of bath constituents. As observed in these chromatograms, the signals of mono-ox-SPS, di-ox-SPS, and SPS, respectively, increase upon standard additions. Therefore, by integrating each peak, concentrations of mono-ox- SPS, di-ox-SPS, and SPS could be extrapolated.

Figure 6 represents typical chromatograms obtained for a freshly prepared electrolyte before plating and for a sample collected after plating (equivalent to 6 Ah L^{-1} bath age). The before-plating curve shows the presence of a predominant peak with an elution time of 62 min assigned to SPS, as well as the presence of a rather small peak around 11 min. According to standard chromatograms presented in Fig. 3, this small peak was attributed to mono-ox-SPS. After plating an equivalent of 6 Ah L^{-1}, a peak assigned to di-ox-SPS was observed, coupled with the notable increase in the mono-ox-SPS peak and the decrease in the SPS peak. Using standard addition method for quantification, concentrations of mono-ox-SPS and di-ox-SPS increased from 0.21 to 0.55 ppm and 0 to 0.07 ppm before and after plating, respectively, whereas the SPS concentration decreased from 0.55 to 0.18 ppm.

It is worth noting the absence of any trace of MPS in the chromatograms before and after plating. MPS was expected to be produced during the catalytic activity of SPS in a course of copper deposition.[28] The absence of MPS may either be due to the instability of MPS in a Cu-bath (as cupric ions drive oxidative dimerization of MPS back to SPS)[13] or to the concentration of MPS itself, which may be below the limit of detection.

Three experiments have been performed in order to evaluate the reproducibility of the measurement process (from sampling to pretreatment) for each compound (Fig. 7). For this purpose, three samples were collected from the same plating bath and pretreated prior to

determining the concentration of the ingredients by HPLC and electrochemical detection. As observed in Fig. 7, mono-ox-SPS and di-ox-SPS exhibited a good reproducibility with a relative standard deviation (RSD) of ~7% and ~3%, respectively. In contrast, SPS presented a relatively high RSD of ~13%. Those deviations can be due on one hand to the stability (reactivity) of the compounds to be detected or on another hand to the high sensitivity of the electrochemical response to changing conditions of the electrode surface (i.e. surface contamination).

Concluding remarks

A new chromatographic method for the determination of SPS and by-products (MPS, mono-ox-SPS, and di-ox-SPS) has been developed. The retention times of the four species were successfully established with purchased as well as in-house synthesized chemical standards. A reverse-phase C_{18} analytical column the *Atlantis T3* (Waters, Inc.) with mobile phase consisting of 2% acetonitrile in 0.0125M H_2SO_4 provided optimal separation. Solid-phase extraction with a cation exchange cartridge (OnGuard II H, Dionex) allowed a convenient and effective measurement of the real bath samples by reducing matrix interference. ED (ED50-A Electrochemical Detector, Dionex) on the one hand allowed the detection of sulfur-containing compounds but on the other hand limited the range of detectable by-products (e.g. molecules such as PDS could not be detected). Standard addition was found to be the most suitable method for the analysis of analyte concentrations due to the elimination of matrix interferences and changing electrode conditions.

References

1. Paunovic, M., Schlesinger, M., *Fundamentals of Electrochemical Deposition*, John Wiley & Sons, Inc., 2006.

2. International Technology Roadmap for Semiconductors,*Interconnect Chapter*, 2009.

3. Beica, R., Sharbono, C., Ritzdorf, T., *Electronic Components and Technology Conference 2008*, 58, 577.

4. Kondo, K., Yamakawa, N., Tanaka, Z., Hayashi, K., *J. Electroanal. Chem.* 2003, 559, 137.

5. Vereecken, P. M., Binstead, R. A., Deligianni, H., Andricacos, P. C., *IBM Journal of Research & Development*, 2005, 3.

6. Healy, J. P., Pletcher, D., Goodenough, M., *J. Electroanal. Chem.* 1992, 338, 155.

7. Healy, J. P., Pletcher, D., Goodenough, M., *J. Electroanal. Chem.*1992, 338, 167.

8. Moffat, T. P., Wheeler, D., Huber, W. H., Josell, D., *Electrochem. and Solid-State Lett.* 2001, C26.

9. Moffat, T. P., Wheeler, D., Josell, D., *J. Electrochem. Soc.* 2004, 151, C262.

10. Willey, M. J., West, A. C., *J. Electrochem. Soc.*2007, 154, D156.

11. Frank, A., Bard, A. J., *J. Electrochem. Soc.*2003, 150, C244.

12. Lee, W.-H., Hung, C. C., Chang, S. C., Wang, Y. L., *J. Electrochem. Soc.* 2010, 157, H131.

13. Moffat, T. P., Baker, B., Wheeler, D., Josell, D., *Electrochem. and Solid-State Lett.*2003, 6, C59.

14. Volov, I., Saito, T., West, A. C., *J. Electrochem. Soc.* 2011,158, D384.

15. Andricacos, P., Chung, D. S., Deligianni, H., Fluegel,J. E., Kwietniak,K. T., Locke,P. S., Restaino,D. D., Seo,S. C., Vereecken,P. M., Walton, E. G., *Patent 7678258*, IBM Corp, United States, 2010.

16. Moffat, T. P., Wheeler, D., Kim, S. K., Josell, D., *Electrochim. Acta*. 2007, 53, 145.

17. Hung,C. C. , Chen,K. W., Wang, Y. L., *J. Vac. Sci. Technol. B,* 2008, 26(1), 255.

18. Chalyt, G., Bratin, P., Pavlov, M., Kogan, A., Perpich, M., *Patent 6572753*, ECI Technology, Inc., United States, 2003.

19. Shalyt, E., Pavlov, M., Bratin, P., Kogan, A., Perpich, M. J., *Patent 7186326*, ECI Technology, Inc., U.S., 2007.

20. Tench, D., Ogden, C., *J. Electrochem. Soc. 1978,* 125, 194.

21. Taephaisitphongse, P., Cao, Y., West, A. C., *J. Electrochem. Soc. 2001,* 148, C492.

22. D'Urzo, L., Wang, H., Pa, A., Zhi, C., *J. Electrochem. Soc. 2005,* 152, C243.

23. Palmans, R., Claes, S., Vanatta, L. E., Coleman, D. E., *J. Chromatogr. A,* 2005, 1085, 147.

24. Volov, I., West, A. C., *J. Electrochem. Soc.*2011, 158 (7), D456-D461.

25. Owens,G.S., LaCourse, W. R., *Current Separations*. 1996, 14, 82.

26. Vandeberg, P. J., Johnson, D. C., *Anal. Chem.* 1993, 65, 2713.

27. Ngoviwatchai, A., Johnson, D. C., *Anal. Chim. Acta.* 1998, 215, 1.

28. Tan, M., Guymon, C., Wheeler, D. R., Harb, J. N., *J. Electrochem. Soc.* 2007, 154, D78.

Table 1

Abbreviation	Structure
SPS	HO_3S … S - S … SO_3H
Mono-ox-SPS	HO_3S … S(=O) - S … SO_3H
Di-ox-SPS	HO_3S … S(=O)(=O) - S … SO_3H
MPS	HO_3S … SH
PDS	HO_3S … SO_3H

Table 1. Chemical structures of SPS and its by-products.

Table 2

Chemical	Supplier	Composition
SPS	Raschig GmbH (Germany)	>94%
MPS	Raschig GmbH (Germany)	>85%
PEG (3350 g L^{-1})	Sigma-Aldrich	n/a
OxSPS_1	Atotech, Berlin GmbH (Germany)	80% mono-ox-SPS, 10% di-ox-SPS, 10% SPS
OxSPS_2	Atotech, Berlin GmbH (Germany)	77% di-ox-SPS, 23% SPS
$CuSO_4 \cdot 5H_2O$	Manica SPA (Italy).	>99.5%
H_2SO_4	Merck (Germany)	98%
Acetonitrile	Merck (Germany)	HPLC Grade
DI water	Millipore Gradient System	High purity, 18.2 mΩ cm

Table 2. Composition and chemical suppliers for all chemicals used in this chapter.

Figure 1

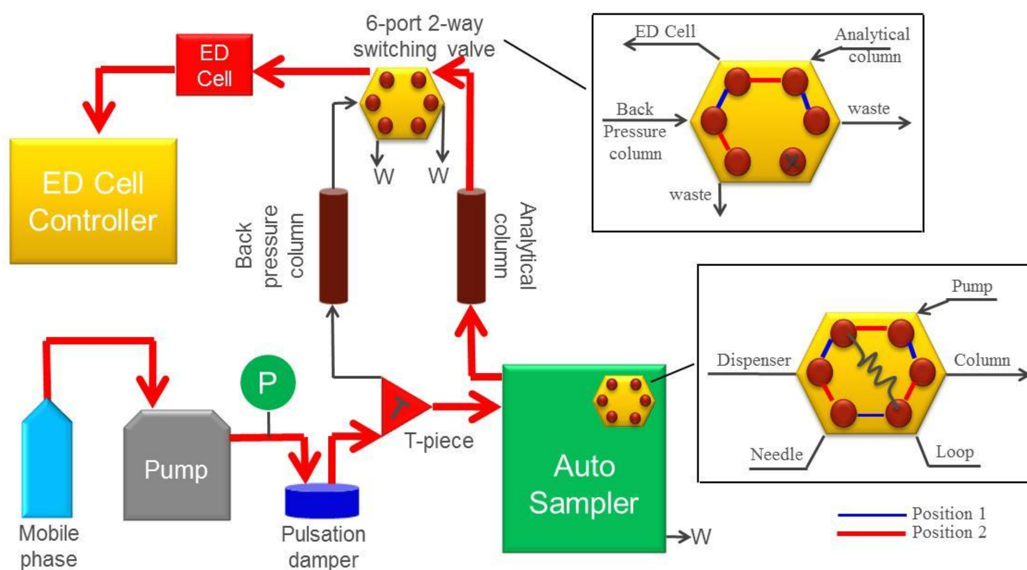

Figure 1. Scheme of HPLC-ED set-up used for the detection of SPS and its by-products. Samples were mixed with the mobile phase at the autosampler and the effluent was sent directly through the analytical column. Prior to chromatographic measurements, samples were pretreated by passing the solution though an OnGuard II H ion exchange cartridge (not shown).

Figure 2

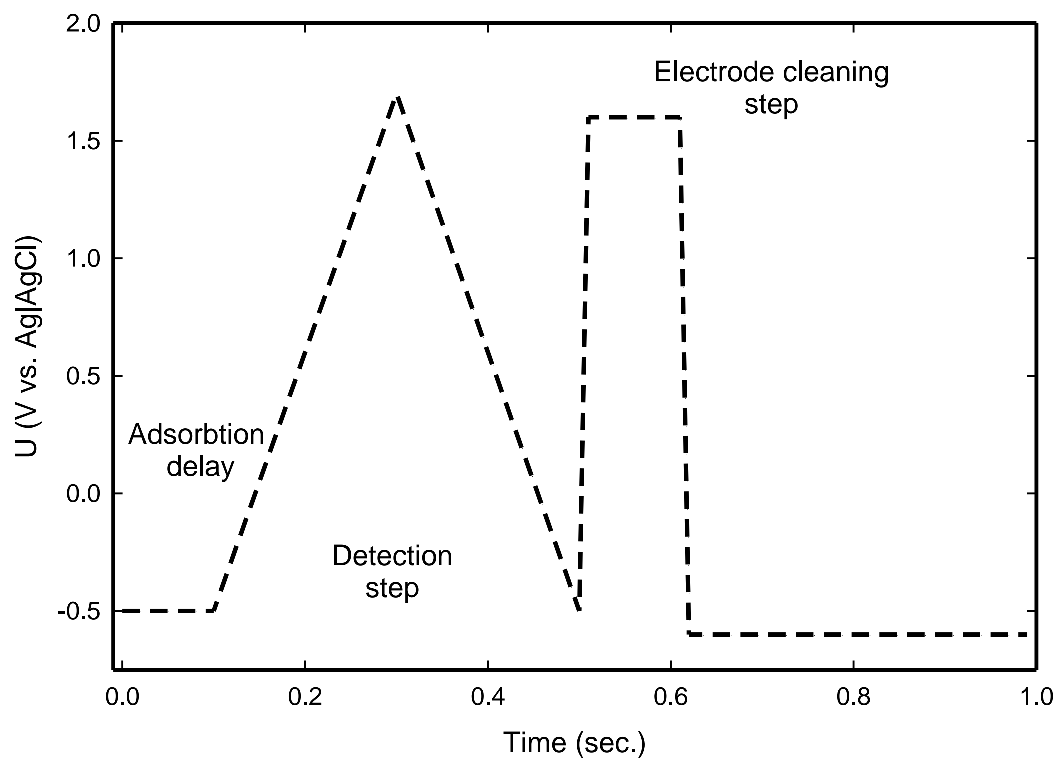

Figure 2. An integrated pulsed amperometry waveform for the detection of organo-sulfur compounds.

Figure 3

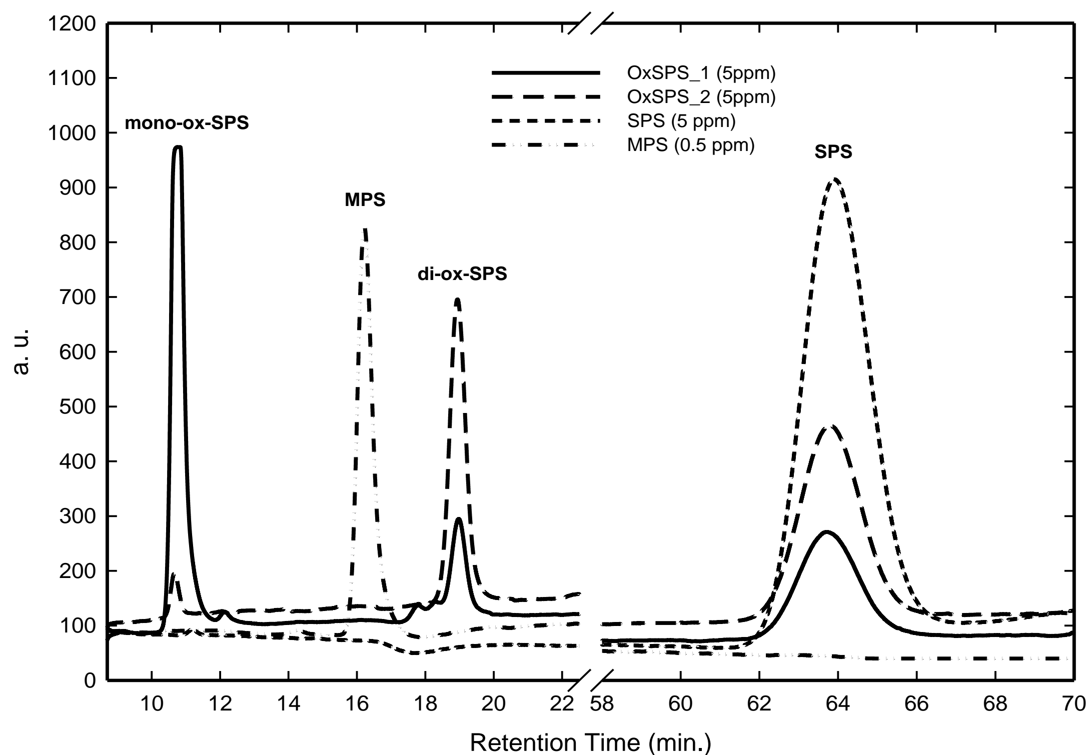

Figure 3. Chromatographic separation of SPS and its detectable by-products with the Atlantis T3 column and 2% acetonitrile in 0.0125M H_2SO_4 as mobile phase (a.u. stands for arbitrary units).

Figure 4

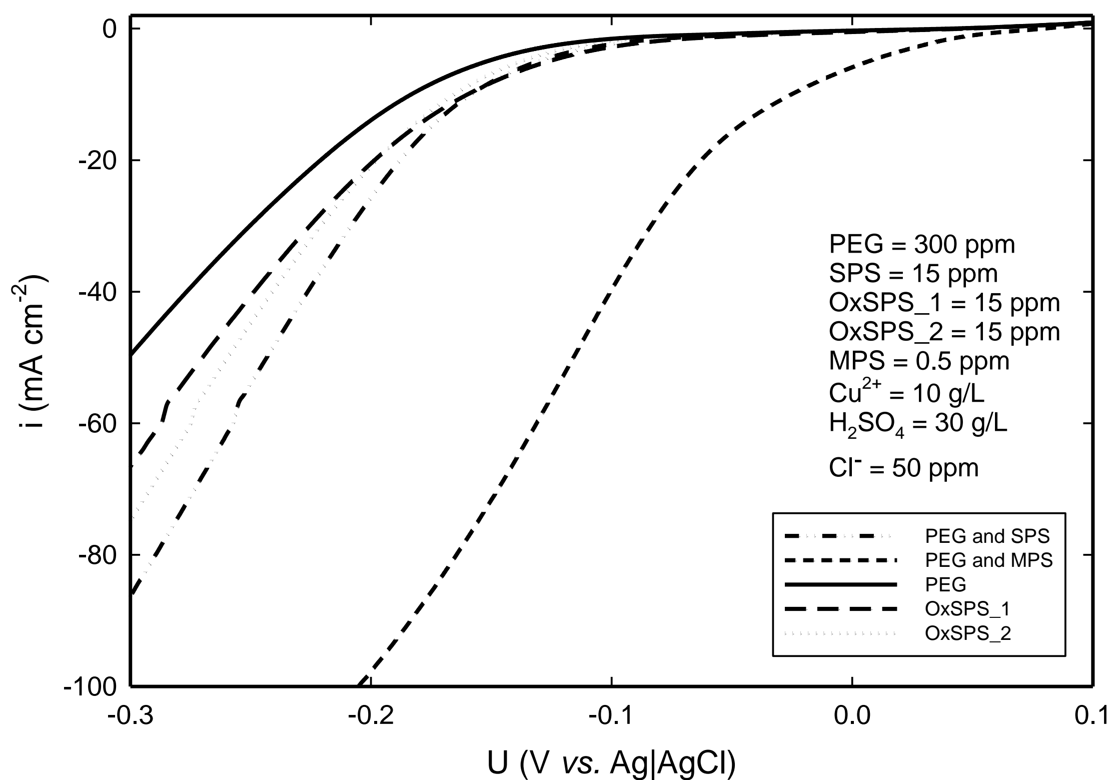

Figure 4. Current as a function of the linear potential sweep at 10 mV s^{-1}. Results were obtained at the rotating platinum disk electrode preplated with a thin copper layer. The electrochemical behavior of known chemical standards in copper electrolyte is shown. A small concentration of MPS had a significant effect on acceleration. Mono-ox-SPS and di-ox-SPS exhibited less acceleration than SPS.

Figure 5

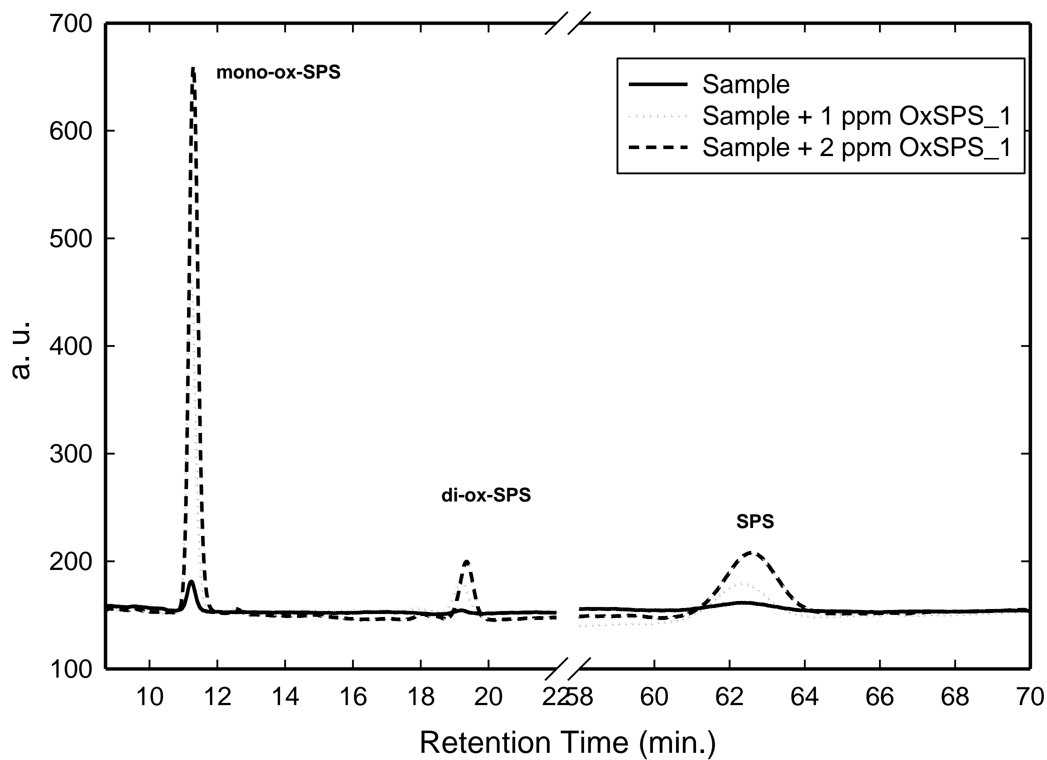

Figure 5. Example of chromatograms of standard addition recorded to evaluate concentrations of SPS, mono-ox-SPS, and di-ox-SPS (curves recorded with a 2% ACN and a detection range of 100 nC). Ordinate has arbitrary units (a.u.).

Figure 6

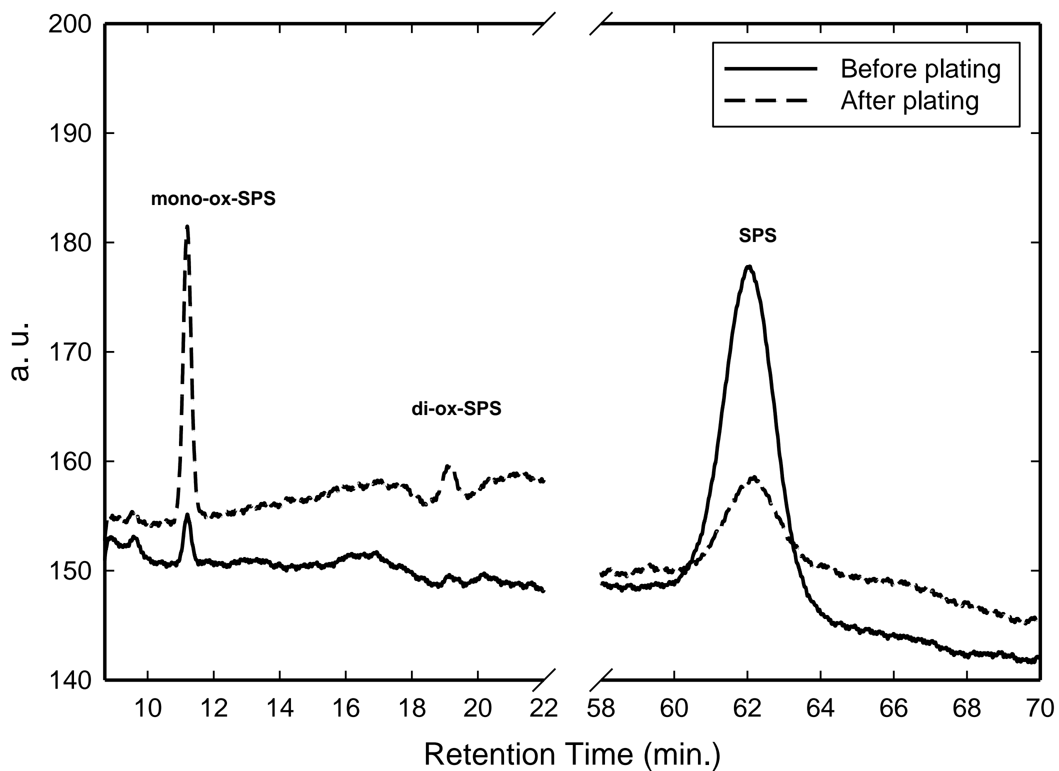

Figure 6. Chromatography of bath sample before and after plating for 6 Ah L^{-1} (detection range of 100 nC for this set of experiments).

Figure 7

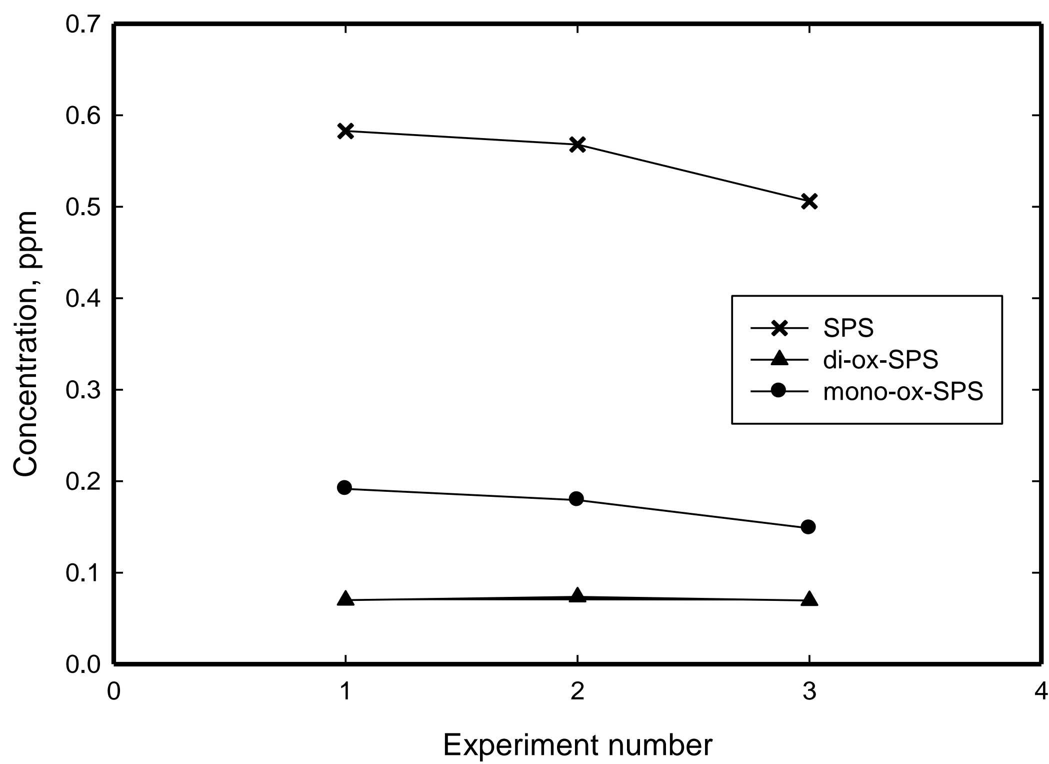

Figure 7. Measurement of reproducibility at various times.

Chapter 5

Pulse-plating of Copper-Silver Alloys for Interconnect Applications

Abstract

The electrodeposition of Cu-Ag alloys was studied as a possible application for interconnect technology, where Cu-Ag alloys may be less susceptible to electromigration than Cu alone. The presence of chloride in state-of-the-art copper plating electrolytes limited the solubility of Ag. However, pulse-plating approach enabled a wide range of Cu-Ag alloy compositions at substantial chloride concentration levels. The deposition of Ag was driven by the displacement reactions between the metallic copper and ionic silver during the off-time. Measured alloy compositions were consistent with theoretical estimates at various electrolyte concentrations, electrode rotation speeds, pulse frequencies and duty cycles. However, organic additives decreased incorporation of Ag into the alloy. It was also discovered that $CuSO_4 \cdot 5H_2O$ from a number of major chemical suppliers contained Ag as an impurity. The roughness of the films was significant when produced by pulsed plating, but was shown to be substantially reduced in the presence of a leveling agent. Additionally, the concentration of chloride in the electrolyte was shown to significantly affect surface quality of the deposited Cu-Ag thin films.

---

* This work was done in collaboration with Edward Swanson, Brendan O'Brien, Steven W. Novak, Ruud van den Boom, and Kathleen Dunn

Introduction

With the continuing miniaturization of microelectronics, electromigration effects in copper interconnect systems are becoming a major factor in determining device lifetime and reliability.[1-3] Accordingly, there is a need for interconnect materials with improved electromigration resistance, while maintaining adequate electrical resistivity. It has been shown that co-deposits of Cu with small amount of other metals (such as Ag, Sn, Co, and Mg) can potentially mitigate both electro- and stress-migration.[4-8] However, the resistivity of the interconnect increases with the addition of foreign metals. The International Technology Roadmap of Semiconductors (ITRS) has set the resistivity criterion at $\rho < 2.2$ μΩ·cm,[9] only slightly above the bulk resistivity of pure copper at 1.68 μΩ·cm. Alloying copper with silver (ρ_{Ag} = 1.59 μΩ·cm) was shown to increase the resistivity of post-anneal electrochemically deposited Cu-Ag films the least when compared to other copper alloys.[10] For Ag content between 0.17 and 3.2 wt% the resistivity ranges 1.8 to 3.1 μΩ·cm.[10] For this reason Cu-Ag alloys, especially at the lower Ag weight percentages, are potential candidates for the fabrication of interconnects in microelectronic devices.

Acidic copper-sulfate electrolytes containing chloride have been successfully applied for many years to the electrochemical fabrication of copper interconnects.[11-13] Chloride in these electrolytes is known to be one of the critical constituents enabling defect-free filling of surface features.[14-20] The main challenge for depositing silver from copper-plating electrolytes, which contain about 50 ppm of chloride, is the low solubility of silver in the presence of chloride ions (the solubility product of AgCl in water at 25°C is 1.8×10^{-10} M^2).[21] While Strehle *et al.* demonstrated a controlled electrodeposition of Cu-Ag alloys from

chloride-free acidic copper sulfate electrolytes,[22] the deposition in the presence of chloride is probably necessary.

We demonstrate that the application of a pulsating current instead of a direct current permits the use of chloride at a substantial concentration, while also allowing a wide range of Cu-Ag alloy compositions. The literature contains numerous descriptions of pulse-plating of different binary and ternary metal alloys with copper from a variety of electrolytes: Cu-Co from citrate and boric acid electrolyte,[23] Cu-Ni from trisodium citrate electrolyte,[24] Cu-Sn from Lucent's SnTech line of electroplating baths,[25] Cu-Mg from ammonium sulfate electrolyte,[26] Ni-Cu-Mo from ammonia citrate electrolyte,[27] *etc*. However, this is the first investigation to look at the pulse-plating approach for the electrochemical deposition of Cu-Ag thin films from the conventional copper plating electrolytes containing chloride and organic additives.

The aim of chapter 5 is to investigate the composition of Cu-Ag alloys at various plating conditions, electrolyte concentrations, and applied pulse parameters. We show the role of the displacement reactions in pulse-plating of Cu-Ag by comparing measured alloy compositions with those predicted by theoretical estimates. Additionally, the film microstructure and film quality of the deposited alloys was also examined.

Experimental

Electrochemistry on rotating disk electrode

For the electrochemical investigation, a three-electrode cell was employed. The working electrode was a platinum rotating disk electrode (RDE) with 4 mm diameter (Pine Corporation). The counter electrode was a gold wire. A double junction reference electrode

$Hg|Hg_2SO_4$ (Pine RREF0026) was chosen to avoid problems associated with leakage from such reference electrodes as Ag|AgCl. Prior to each experiment, the platinum surface of the RDE was electrochemically treated in 0.5 M H_2SO_4 solution by cycling the electrode potential repeatedly from -0.66 V to 8.5 V at 1 V s^{-1} until a characteristic cyclic voltammogram developed. Then, the working electrode was modified by plating about 1.8 μm layer of copper from a copper sulfate electrolyte without additives at - 40 mA cm^{-2}.

Copper oxidation was found to be an important parameter during pulse-plating. The measurement of the oxidation rate of copper was conducted in 0.63 M $CuSO_4{\cdot}5H_2O$ and 0.3 M H_2SO_4 electrolyte. First, a copper film was electrochemically plated at -10 mA cm^{-2} onto platinum RDE for 271.5 s at 400 rpm. According to Faraday's law, this corresponds to a film thickness of about 1 μm. Then, current was switched to zero and, depending on the desired experiment, the electrode was either immediately rinsed with DI water or allowed to stay in the electrolyte for 15 min at 400 rpm. Afterwards, the RDE was transferred to a concentrated phosphoric acid; there copper was stripped from RDE at 10 mA cm^{-2} and the stripping time was recorded (it was previously demonstrated that stripping of Cu in H_3PO_4 occurs nearly at 100% current efficiency).[28] The time required to dissolve copper was determined by observing a sharp potential increase at the completion of the dissolution process, when the potential reached 1.39 V vs. $Hg|Hg_2SO_4$ up from a dissolution potential of -0.325 V. Comparing the time of deposition to the time of stripping allowed for the determination of the oxidation rate of copper.

Electroplating of alloy films

Coupon squares were used for the electrochemical deposition of thin films. Coupons were cleaved from 300 mm silicon wafer that had Ta/TaN barrier layer and PVD plated copper-seed layer (thickness of 50 nm) on the surface. After cleaving the wafer, the coupon was cleared of dust by blowing pre-purified compressed nitrogen to the surface. Then, the coupon was attached to the coupon holder, designed by Atotech USA, Inc., to approximate an RDE. The electrical contact to the wafer segments was achieved by applying Cu adhesive tape to all four sides of the square coupon, and then Kapton tape was applied to define a circular surface area of deposition. A hole in the Kapton tape was cut using a craft punch (Marvy Uchida), with 5/8 inch hole diameter (surface area 1.98 cm^2).

After attaching the coupon, the holder was mounted on a rotatory shaft at the RDE stand (Pine), rinsed in deionized (DI) water (18.2 MΩ·cm), and immersed in a 200 ml of electrolyte contained in a 325 ml Pyrex crystallizing dish for the deposition experiment. The counter electrode for the preparation of thin films was a gold wire. The entire stand was inclined 5 degrees to prevent the entrapment of air bubbles on the coupon surface during the immersion of coupon into solution. A pulse current was controlled through Nova 1.5 electrochemical software (Metrohm Autolab B.V.), by FRA2 μAutolab Type III potentiostat/galvanostat (Metrohm Autolab B.V.). After the deposition experiment, the coupon was rinsed with DI water and blown dry with compressed nitrogen. Composition of the alloy was examined by inductively coupled plasma – atomic emission spectroscopy (ICP-AES). For this analysis, the whole deposit (including the seed layer) was dissolved in 1 ml of 35% concentrated nitric acid, and afterwards diluted in DI water to make 10 ml of volume for analysis by ICP-AES.

Electrolytes for all plating experiments were prepared using the following materials: $CuSO_4.5H_2O$, 99+ % (Fisher Scientific, Acros Organics), H_2SO_4, 95-98% (EMD Chemicals, Inc.), $AgNO_3$, 99.9+ % (Alfa Aesar), PEG 3350 g/mol (Sigma-Aldrich), HCl, 12.1 M (VWR, BDH Aristar), SPS, 96% mass fraction[29] (Raschig GmbH), Polyvinylpyrrolidone 29,000 g/mol (Sigma-Aldrich). For all experiments conducted in this chapter, the concentration of PEG was 300 ppm (8.95×10^{-5} M), the concentration of SPS was 30 ppm (8.46×10^{-4} M), and the concentration of PVP was 200 ppm (6.9×10^{-6} M). The organic additives, silver, and chloride were individually added to the plating bath through dilution from concentrated solutions made with DI water.

Metrology

ICP-AES tool (Horiba Jobin Yvon) controlled by ACTIVAnalyst 5.4 software was used to determine the total amount of silver in the electroplated films. The quantification of the silver concentration was done through the calibration of the signal intensities with known amounts of silver. Calibration standards were prepared using 1000 ppm silver ICP standard, silver nitrate in 3% nitric acid (Ricca Chemical Company). The emission wavelength for silver analysis was chosen to be 328.068 nm.

The surface quality and thickness of plated films were examined by plan view and cross-sectional imaging in an FEI Nova NanoLab 600 Dual Beam Focused Ion Beam-Scanning Electron Microscope (FIB-SEM). The SEM column was operated at 5 kV for imaging while the FIB column was operated at 30kV for cross sectioning. Depth profiling of the film composition was determined by IonTOF 5-300 Time-of-flight Secondary Ion Mass spectrometry (ToF-SIMS). The analysis beam was pulsed 1nA Bi+ at 25keV and 45 degrees

incidence across a 50 μm area. The sputtering beam was 100 nA Cs+ at 2 keV and 45 degrees incidence. The analysis and sputtering beams were used in interlace mode. Negative secondary ions were monitored with a mass resolution of about 4000. Calibration of the depth scales and conversion of ion counts to concentrations were made using an ion implanted Cu standard. Calculated concentrations should be accurate to within 15% and depth scales should be accurate to within 5%.

Results and Discussion

Rationale for choosing pulse-plating approach

The electrochemical deposition of Ag from copper electrolytes that contain chloride ions as a critical component is made difficult by the low solubility of silver ions with chloride (K_{sp} of AgCl in water is 1.8×10^{-10} M^2 at room temperature[21]). One possible way to avoid the issue of AgCl solubility is to find a substitute for chloride. Bromide has been reported to have a similar effect as chloride when used with organic additives,[30] however AgBr is even less soluble (K_{sp} = 5×10^{-13} M^2) than AgCl. Another halogen, fluoride was tested by linear sweep voltametry technique to observe whether it exerts any effect on organic additives. The critical suppression of copper deposition by PEG was not achieved in the presence of fluoride ions. The solubility of AgCl can be improved by complexing or chelating Ag^+ ions. However, known chelating agents for Ag^+ (such as ammonia, thiosulfate, and EDTA) adversely affect and/or complex cupric ions, which are present in much larger concentration levels than silver ions. Yet another way to avoid the problem of low solubility of AgCl, is to find organic additives that enable feature filling without chloride. However, most reported organic additives are used in the presence of chloride.[31]

Suppressors, such as PEG, PPG, EPE, PEP, [32, 33] were tested by linear sweep voltammetry to evaluate their behavior in the absence of chloride during the electrodeposition of Cu. The experimental results showed that all these substances do not to provide an adequate suppression without chloride.

In order to deposit Cu-Ag alloys, the approach taken in the present chapter was to maintain a silver concentration below the solubility limit of AgCl, while keeping the concentration of chloride, $c_{Cl^-} \geq 10$ ppm (2.82×10^{-4} M). The surface quality of the plated films was found to be adversely affected at lower chloride concentration levels (discussed below). Additionally, Dow *et al.* has shown that in order to obtain good filling of fine features a $c_{Cl^-} \geq 10$ ppm must be maintained.[34]

Electroanalytical investigation was carried out to observe how the suppression of copper deposition by PEG is affected by the concentration of chloride, and more importantly to determine if adequate suppression can be obtained at $c_{Cl^-} = 10$ ppm. Polarization curves in Figure 1 show the effect of chloride at different potentials. Until the potential reached about 0.67 V *vs.* Hg|Hg_2SO_4, the suppression of copper deposition at $c_{Cl^-} = 10$ ppm (2.82×10^{-4} M) and the conventionally used $c_{Cl^-} = 50$ ppm (1.41×10^{-3} M) was almost unchanged.

According to K_{sp} value of AgCl in water and at 10 ppm of Cl^-, the concentration of silver ions (c_{Ag^+}) at saturation is 9.87×10^{-7} M. However, in higher ionic strength solutions, such as sulfuric acid based copper electrolytes, solubility of Ag^+ may be somewhat higher. To determine the effect of copper electrolyte on the solubility of AgCl, 4.63×10^{-4} M of Ag^+ and 4.63×10^{-4} of Cl^- were combined in 0.63 M $CuSO_4.5H_2O$ and 0.3 M H_2SO_4 solution. Silver chloride precipitate began forming almost instantaneously upon the contact. After

several days, about 10 ml of solution at the top was withdrawn and filtered through Steriflip-GV, 0.22 μm (Millipore) to ensure that no precipitate was left in the saturated solution. From the measured silver concentration, K_{sp} value of AgCl in the specified copper electrolyte was 5.4×10^{-10} M^2. Based on this solubility product, c_{Ag^+} cannot exceed 1.9 μM before AgCl would precipitate.

Since the concentrations of copper and silver have to be so different, the plating mode required careful consideration. The direct-current (DC) deposition would limit the possible fraction of Ag in a Cu-Ag alloy. For example, based on Faraday's law, the mass fraction of Ag in a 100 nm film would be limited to 0.26 wt% if the deposition were to be carried at the saturation concentration of Ag^+ (c_{Ag^+} = 1.9 μM) and a typical applied current density of -10 mA cm^{-2} and 400 rpm.

Description of the pulse-plating method

We thus investigated pulse-plating as a more promising option. Figure 2 shows an example of the unipolar pulse-plating waveform that was chosen for the deposition of Cu-Ag alloys. The current is pulsed between i_{off} = 0 mA cm^{-2} (*i.e.* off-time) and i_{on} = -10 mA cm^{-2} (*i.e.* on-time). During the off-time, metallic copper on the surface is expected to be spontaneously replaced by silver (reaction 1), driven by the difference of standard reduction potentials between silver (U^{θ} = 0.799 V vs. SHE) and copper (U^{θ} = 0.337 V vs. SHE) reactions. During the on-time, both Cu^{2+} and Ag^+ ions are electrolytically plated on the cathode surface. Based on reaction 1, during the off-time, for every one atom of Cu leaving the surface two atoms of Ag are deposited.

$$\mathrm{Cu} + 2\mathrm{Ag}^+ \rightarrow \mathrm{Cu}^{2+} + 2\mathrm{Ag} \qquad (1)$$

The amount of Ag versus Cu in the alloy can be controlled by varying the duty cycle of the pulse (equation 2) and by regulating the pulse amplitude. However, to allow for the adequate deposition of Ag, duty cycle needs to be low (*e.g.* below 15%). The distribution of silver in the alloy can possibly be controlled by changing frequency of the pulse (equation 3), as was demonstrated by other researchers for similar systems.[23, 35] Due to the self-limiting nature of the displacement reactions and to ensure uniform metal distribution between Ag and Cu, the frequency was chosen as to deposit less than a monolayer of silver during a single pulse cycle based on Faraday's law.

$$\text{Duty Cycle} = \frac{\text{time on}}{\text{time on} + \text{time off}} \tag{2}$$

$$\text{Frequency} = \frac{1}{\text{time on} + \text{time off}} \tag{3}$$

To gain insight about the surface composition during deposition of Ag, the potential of the working electrode was measured at zero current. The measurements of the open-circuit potential (OCP) were performed at different concentrations of silver after an initial 30 seconds of plating at -10 mA cm^{-2}. The thermodynamic difference between the reversible potentials of Cu and Ag is 0.46 V. However, the difference between the OCP of copper in the presence of a copper sulfate electrolyte without silver and the electrolyte with various amounts of silver (0.01 M, 0.0001 M, and 0.00001 M) was only about 7 mV. This behavior probably indicates that Ag does not form a complete monolayer on the Cu surface.

Estimation of the Cu-Ag alloy composition

The transport of silver ions to the surface can be well understood theoretically since the deposition of Cu-Ag films was conducted in a rotating disk electrode configuration. Based on the concentration of silver used, the flux of silver ions to the surface is mass-

transport-limited and can be calculated using the Levich equation for a given c_{Ag^+} and rotation speed. In calculating the flux of ions, the kinematic viscosity was taken to be that of water, ν = 0.01 cm^2 s^{-1}. The diffusion coefficient of silver ion D_{Ag^+} in various supporting electrolytes, such as KNO_3 and $HClO_4$, ranges from 1.53×10^{-5} to 1.62×10^{-5} cm^2 s^{-1} at 25 °C.[36] Hotlos *et al.* measured diffusion coefficients of silver ion at various concentrations of $CuSO_4$ and H_2SO_4.[37] For the calculations of the limiting current of silver ions, D_{Ag^+} $=1.03\times10^{-5}$ cm^2 s^{-1} was used, which was determined by Hotlos *et al.* in the electrolyte of similar composition to that used in this chapter.

During both on- and off- times silver ions discharge on the cathode at its limiting current. Accordingly, the rate of silver incorporation into the alloy can be directly calculated based on Faraday's law. For example, starting with c_{Ag^+} = 3.0 μM and rotation of 400 rpm, the limiting current is -1.18 μA cm^{-2} and the plating rate of Ag is then 2.62 ng s^{-1}. Thus, to achieve an appreciable Ag content, the time-average Cu deposition rate must be substantially lowered. At such a slow deposition rate, one may worry about the practicality of the present deposition scheme. However, the rate is not unreasonable if one-wt% alloys are to be deposited in the narrow geometries of microelectronic devices where feature sizes may be less than 20 nm.[9] For the subsequent deposition of the overburden where the Ag incorporation rate is not important, a DC plating protocol could be adopted to increase the deposition rate.

The weight percent of Ag in the Cu-Ag alloy was predicted by accounting for the mass-transfer-controlled deposition of Ag during both the off- and on-times, the galvanostatic deposition of Cu based on 100% current efficiency, and the oxidation of Cu during the off-times as shown in equation 4 (where *w* corresponds to the weight of species).

$$c_{Ag}\,(wt\%) = \frac{\left(W^{Ag}_{time\ off} + W^{Ag}_{time\ on}\right)}{\left(W^{Ag}_{time\ off} + W^{Ag}_{time\ on}\right) + \left(W^{Cu}_{time\ on} - W^{Cu}_{oxidation}\right)} \times 100\% \tag{4}$$

It was important to account for the loss of Cu by oxidation due to the long periods of off-time. The oxidation of the metallic copper can possibly happen both due to oxidation by the dissolved oxygen (reaction 5) and the comproportionation reaction between cupric ions and copper (reaction 6), which is driven by a difference in cuprous ion concentration between the surface and the bulk electrolyte.

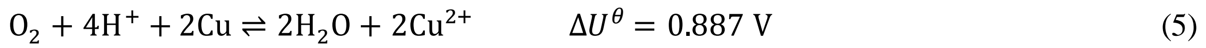

$$O_2 + 4H^+ + 2Cu \rightleftharpoons 2H_2O + 2Cu^{2+} \qquad \Delta U^\theta = 0.887\ \mathrm{V} \tag{5}$$

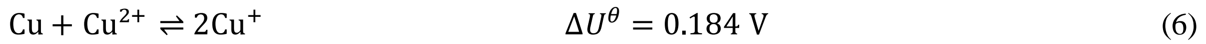

$$Cu + Cu^{2+} \rightleftharpoons 2Cu^+ \qquad \Delta U^\theta = 0.184\ \mathrm{V} \tag{6}$$

Both reactions 5 and 6 can be anticipated to proceed in the forward direction since ΔU^θ is positive. Based on thermodynamics, Cu should be oxidized by cupric ions until the surface concentration reaches a value at which overall reaction is not possible. Using the Nernst equation the equilibrium surface concentration of Cu^+ can be estimated by setting $\Delta U = 0$, which gives, according to equation 7, $c_{Cu^+,\ surface} = 6.13\times10^{-4}$ M.

$$U = 0 = (0.184\mathrm{V}) + \frac{RT}{2F}\ln\left(\frac{C^2_{Cu^+,\ surface}}{0.63\mathrm{M}}\right) \tag{7}$$

The oxidation rate of Cu can then be approximated by equation 8, where N_{Cu^+} is the cuprous-ion flux across the diffusion layer. The diffusion layer thickness δ_{diff} can be defined by equation 9, where ν is a kinematic viscosity, Ω is a rotation rate, and $D_{Cu^+} = 0.43\times10^{-5}$ $cm^2\ s^{-1}$ (D_{Cu^+} was assumed to be equal to the $D_{Cu^{2+}}$ reported by Noulty *et al.*).[38]

$$N_{Cu^+} = D_{Cu^+}\frac{c_{Cu^+,0}}{\delta_{diff}} \tag{8}$$

$$\delta_{diff} = 1.61\times D^{1/3}_{Cu^+}\times \nu^{1/6}\times \Omega^{-1/2} \tag{9}$$

The rate of oxidation of Cu due to etching by cupric-ions at 400 rpm is then predicted as 2.9 nm min^{-1}.

The oxidation rate of Cu by dissolved oxygen is more difficult to predict because the dissolved oxygen concentration is not known with precision, and large discrepancies between the measured rate and that expected from the oxygen reduction current were reported.[39] Therefore, the oxidation rate of Cu by O_2 was instead estimated by experiment. When 1 μm of copper film was plated and directly removed from the electrolyte (0.63 M $CuSO_4 \cdot 5H_2O$ and 0.3 M H_2SO_4) and rinsed immediately after the deposition, the measured film amount was 99% of the expectation, indicating a near 100% current efficiency of copper plating. However, when plated copper film was left in the electrolyte for 15 minutes at 400 rpm, only 89.9% of copper remained on the electrode due to oxidation. Then, the oxidation rate of copper at 400 rpm due to both reactions 5 and 6 was determined from equation 10.

$$\frac{1\,\mu\text{m}\times(0.99-0.899)}{15\text{ min}} = 6.1\text{ nm min}^{-1} \tag{10}$$

When copper film was left in 0.3 M H_2SO_4, 95% of the film remained. The oxidation rate of copper in sulfuric acid solution at 400 rpm was then equal to 2.7 nm min^{-1}. Since Cu is not susceptible to corrosion by H_2SO_4, the oxidation in 0.3 M H_2SO_4 was probably due to the presence of dissolved O_2. The measured oxidation rate was assumed to be constant and applied in the prediction of the weight percent of Ag in the alloy (see equation 4).

Measurement of the Cu-Ag alloy composition under various conditions

In the process of measuring silver concentrations with ICP-AES, it was discovered that the source of cupric ions ($CuSO_4 \cdot 5H_2O$) contained trace silver impurity. As shown in

Figure 3, the concentration of silver impurity in $CuSO_4 \cdot 5H_2O$ was in the range of our operating concentrations (non-linearity in the data was probably due to experimental uncertainty). After contacting several major chemical suppliers (such as Sigma-Aldrich, Fisher Scientific, and Alfa Aesar), it was found that $CuSO_4 \cdot 5H_2O$ is not tested for trace silver metal impurity and cannot be guaranteed as silver-free. Therefore, even the 99.995% trace metal basis $CuSO_4 \cdot 5H_2O$ contained silver impurity, as was revealed in our experiments and then confirmed by a representative from Sigma-Aldrich.[40] Also, silver concentration was found to vary across different lots of $CuSO_4 \cdot 5H_2O$. Therefore care was to be taken to account for Ag already present in $CuSO_4 \cdot 5H_2O$.

The control of silver content in the alloy was established under various conditions. Figure 4 demonstrates how the presence of chloride and organic additives (namely PEG and SPS) affected the incorporation of Ag in the film at various concentrations of silver in the electrolyte. In the absence of chloride and organic additives, experimental results agree with the theoretical estimates, shown by a straight line in Figure 4. In the presence of PEG and SPS, however, the incorporation of Ag was about 20% less than expected. The lower deposition rate of Ag in the presence of additives was possibly due to a chelating action of additives to Ag^+ ions. A similar impact of additives on a plating rate of Ag was also observed by Strehle *et al.*[22] The incorporation of Ag into the alloy was unaffected by the presence of 1 ppm (2.82×10^{-5} M) of chloride. However, when Cl concentration was 10 ppm, silver incorporation into the alloy leveled at around c_{Ag^+} = 2 μM. This behavior was consistent with measurements of Ag^+ solubility described above, where the saturation concentration of Ag was 1.9 μM at c_{Cl^-} = 10 ppm

It was hypothesized that frequency of the current pulse would not to affect composition of the alloy, because frequency does not alter total off- and on-times. Electroplating of film alloys at various frequencies was performed to confirm this hypothesis. Results showed little variation of Ag content at frequencies ranging from 0.5 – 5 Hz (not shown).

The impact of rotation speed on the weight percent of Ag in the alloy was investigated, and results are shown in Figure 5. Rotation of an RDE controls the flux of ions to the electrode's surface, and therefore enables to determine the effect of flow on the film composition. According to Levich equation, during mass-transfer-controlled deposition of silver, the reaction rate should be directly proportional of the square root of the rotation speed. This behavior was confirmed experimentally, as shown by Figure 5. Again, a decrease in measured silver content from estimated values (shown by the straight line) were attributed to the presence of organic additives in the electrolyte. A similar impact of additives on plating rate of Ag was demonstrated in Figures 4 as well.

Decreasing the duty cycle of the square pulse was anticipated to increase the Ag incorporation. Indeed, as shown in Figure 6, the amount of Ag increased at lower values of duty cycle and decreased at higher values. Although it was possible to increase the weight percent of Ag above 1 wt% of by lowering the duty cycle, there was a practical limit driven by the oxidation of Cu at long off-times (*i.e.* low duty cycles). The amount of Ag in the alloy was then limited practically, since it took increasingly longer times to deposit a certain film thickness. The experimental values again are lower than theoretical estimates due to the presence of organic additives in the electrolyte, as discussed above.

Measurement of surface quality and compositional depth profile

Cu-Ag films prepared by pulse-plating were found to exhibit significant roughness. The roughness of a pulse-plated sample from a bath containing PEG, SPS, and 10 ppm of Cl^- (Figure 7a) was about ten times more than DC-plated sample from the same bath (Figure 7b). It was found that adding a leveling agent, such as polyvinylpyrrolidone (PVP),[41] to the electrolyte could substantially reduce film roughness to the levels seen in Figure 7b. The electrodeposition of Cu-Ag alloys showed that PVP had minimal or no effect on the incorporation of Ag into the film.

The concentration of Cl in the electrolyte had a significant impact on the quality of the plated Cu-Ag films. Figure 8 shows SEM images of the Cu-Ag deposits with 0.3 wt% Ag plated at two different chloride concentrations: 1 ppm and 10 ppm. At $c_{Cl^-} = 1$ ppm (Figure 8a), deposits were discontinuous and contained voids; while, at $c_{Cl^-} = 10$ ppm (Figure 8b), films showed relatively uniform surface coverage with large grains. The discontinuous films likely have decreased trench filling ability. Annealing is usually used to obtain better material properties of deposits. Therefore, sample shown in Figures 8a was annealed at 250 ^{o}C for 30 minutes with a continuous Ar gas flow to investigate the effect of heat treatment. However, annealing this sample had almost no effect on the final quality of the film.

Furthermore, cross-sectional views showed that the deposits were about 33% thicker at the edges than at the center (not shown). This variation was consistent with the analysis of current distribution profile on an RDE. At the studied conditions the Tafel Wagner number (Wa_T) for an RDE can be defined by equation 11.[42] Hence, the Wagner number is equal to 0.73, for $a_c = 0.5$, $i_{avg} = 10$ mA cm^{-2}, and $k = 113.22$ mS cm^{-1}. According to Newman's

treatment of secondary current distribution[42] this Wagner number in fact predicts 33% thickness increase at the edge of a disk electrode.

$$Wa_T = \frac{RTk}{a_c F r i_{avg}} \qquad (11)$$

The compositional depth profiles of the Cu-Ag films were examined by ToF-SIMS. Figure 9 shows a profile of the Cu-Ag film plated from an electrolyte with PEG, SPS, PVP, $c_{Cl^-} = 10$ ppm, and $c_{Ag^+} = 1.7$ μM. Initially, there was a surface oxidation peak which decreased until the native oxide was sputtered away and the non-oxidized Cu-Ag alloy was reached. This surface oxide enhanced ionization efficiency of all trace elements, and did not indicate higher concentrations near the surface.[43] The disappearance of the oxide could be taken as where the oxygen peak plateaued, which also matched with where the Cu signal stabilized (not shown). The SIMS profile in figure 9 shows that the Ag as well as other impurities were uniformly distributed throughout the thickness of the film, probably implying no interface segregation. Annealing the samples slightly increased the thickness of the surface oxide, but the effect was minor. From the ToF-SIMS profile, the silver content was measured at about 0.3 wt%, which matches well with ICP-AES measurements.

Conclusions

This chapter examined electrodeposition of Cu-Ag alloys at a substantial chloride concentration by the application of pulsed plating. It was demonstrated that Ag incorporation into the alloy can be controlled by changing concentration of Ag^+, rotation speed, and duty cycle. The organic additives were found to decrease the deposition rate of Ag by about 20%. It was also discovered that $CuSO_4 \cdot 5H_2O$ from a number of major chemical suppliers contained Ag as impurity. The loss of Cu due to oxidation during off-

time considerably influenced the fraction of Ag in the alloy. The pulse-plating conditions created significant film roughness. However, addition of a leveling agent helped to reduce roughness of the plated Cu-Ag films. The chloride concentration was shown to have a critical impact on the behavior of a leveling agent. At 1 ppm of chloride, films contained voids and were discontinuous, while at 10 ppm of chloride continuous deposits with large grains were obtained.

List of Symbols

a_c	cathodic transfer coefficient
c	concentration, M or ppm or g L^{-1}
D	diffusion coefficient, cm^2 s^{-1}
δ_{diff}	diffusion layer thickness, cm
F	Faraday's constant, C mol^{-1}
k	conductivity, mS cm^{-1}
K_{sp}	solubility product
N	molar flux, mol cm^{-2}
r	radius, cm
R	universal gas constant, J mol^{-1} K^{-1}
T	temperature, K

U^{θ} standard reduction potential, V

υ kinematic viscosity, cm^2 s^{-1}

Ω Rotation speed, rpm

Wa_T tafel Wagner number

w weight, g

References

1. J.R. Lloyd, *Microelectron. Eng.*, **49**, 51 (1999).

2. S. R. Wilson, C. J. Tracy and J. L. Freeman, *Handbook of Multilevel Metallization for Intergrated Circuits*, p. 910, William Andrew (1994).

3. M. Tan, C. Guymon, D. R. Wheeler and J. N. Harb, *J. Electrochem. Soc.*, **154**, D78 (2007).

4. C.-K. Hu, M. Angyal, B. C. Baker, G. Bonilla, C. Cabral, D. F. Canaperi, S. Choi, L. Clevenger, D. Edelstein, L. Gignac, E. Huang, J. Kelly, B. Y. Kim, V. Kyei-Fordjour, S. L. Manikonda, J. Maniscalco, S. Mittal, T. Nogami, C. Parks, R. Rosenberg, A. Simon, Y. Xu, T. A. Vo and C. Witt, *AIP Conf. Proc.*, **1300**, 57 (2010).

5. S. Strehle, S. Menzel, A. Jahn, U. Merkel, J. W. Bartha and K. Wetzig, *Microelectron. Eng.*, **86**, 2396 (2009).

6. D. Padhi, S. Gandikota, H. B. Nguyen, C. McGuirk, S. Ramanathan, J. Yahalom and G. Dixit, *Electrochim. Acta*, **48**, 935 (2003).

7. C. K. Hu, B. Luther, F. B. Kaufman, J. Hummel, C. Uzoh and D. J. Pearson, *Thin Solid Films*, **262**, 84 (1995).

8. K. Barmak, C. Cabral, K. P. Rodbell and J. M. E. Harper, *J. Vac. Sci. & Tech. B,* **24**, 2485 (2006).

9. ITRS, *International Technology Roadmap for Semiconductors* (2011).

10. S. Strehle, J. W. Bartha and K. Wetzig, *Thin Solid Films*, **517**, 3320 (2009).

11. I. Volov and A. C. West, *J. Electrochem. Soc.*, **158**, D456 (2011)

12. A. C. West, S. Mayer and J. Reid, *Electrochem. and Solid-State Lett.*, **4**, C50 (2001).

13. P. C. Andricacos, C. Uzoh, J. O. Dukovic, J. Horkans and H. Deligianni, *IBM J. Res. Dev.*, **42**, 567 (1998).

14. J. W. Gallaway, M. J. Willey and A. C. West, *J. Electrochem. Soc.*, **156**, D287 (2009).

15. P. M. Vereecken, R. A. Binstead, H. Deligianni and P. C. Andricacos, *IBM J. Res. Dev.*, **49**, 3 (2005).

16. W.-P. Dow, H.-S. Huang, M.-Y. Yen and H.-H. Chen, *J. Electrochem. Soc.*, **152**, C77 (2005).

17. J. P. Healy, D. Pletcher and M. Goodenough, *J. Electroanal. Chem.*, **338**, 155 (1992).

18. J. J. Kelly and A. C. West, *J. Electrochem. Soc.*, **145**, 3477 (1998).

19. P. Taephaisitphongse, Y. Cao and A. C. West, *J. Electrochem. Soc.*, **148**, C492 (2001).

20. I. Volov, O. Mann, Y. Hoenersch, B. Wahl and A. C. West, *J. Sep. Sci.*, **34**, 2385 (2011).

21. J. A. Dean, Lange's Handbook of Chemistry (15th Edition), McGraw-Hill (1999).

22. S. Strehle, S. Menzel, J. W. Bartha and K. Wetzig, *Microelectron. Eng.*, **87**, 180 (2010).

23. P. E. Bradley and D. Landolt, *Electrochim. Acta*, **45**, 1077 (1999).

24. I. Baskaran, T. S. N. Sankara Narayanan and A. Stephen, *Mater. Lett.*, **60**, 1990 (2006).

25. S. D. Beattie and J. R. Dahn, *J. Electrochem. Soc.*, **150**, A894 (2003).

26. F. Mangolini, L. Magagnin and P. L. Cavallotti, *J. Electrochem. Soc.*, **153**, C623 (2006).

27. E. Beltowska-Lehman, P. Ozga and E. Chassaing, *Surf. and Coat. Tech.*, **78**, 233 (1996).

28. I. Volov, T. Saito and A. C. West, *J. Electrochem. Soc.*, **158**, D384 (2011).

29. R. G. Brennan, M. M. Phillips, L.-Y. O. Yang and T. P. Moffat, *J. Electrochem. Soc.*, **158**, D178 (2011).

30. M. Hayase, M. Taketani, T. Hatsuzawa and K. Hayabusa, *Electrochem. and Solid-State Lett.*, **6**, C92 (2003).

31. J. Mendez, R. Akolkar and U. Landau, *J. Electrochem. Soc.*, **156**, D474 (2009).

32. J. W. Gallaway and A. C. West, *J. Electrochem. Soc.*, **155**, D632 (2008).

33. J. W. Gallaway, M. J. Willey and A. C. West, *J. Electrochem. Soc.*, **156**, D146 (2009).

34. W.-P. Dow, M.-Y. Yen, C.-W. Liu and C.-C. Huang, *Electrochim. Acta*, **53**, 3610 (2008).

35. W. Schwarzacher and D. S. Lashmore, *IEEE T. Magn.*, **32**, 3133 (1996).

36. R. R. M. Johnston and M. Spiro, *J. Phys. Chem.*, **71**, 3784 (1967).

37. J. Hotlos and M. Jaskula, *J. Electroanal. Chem. and Interfac. Electrochem.*, **249**, 123 (1988).

38. R. A. Noulty and D. G. Leaist, *J. Solution Chem.*, **16**, 813 (1987).

39. M. Breathnach, S. Ahmed, R. Sharna, L. D. Burke and D. N. Buckley, *ECS Transactions*, **6**, 51 (2007).

40. G. Stachowiak, private communication with Sigma-Aldrich, in (2012).

41. M. J. Willey, J. Reid and A. C. West, *Electrochem. and Solid-State Lett.*, **10**, D38 (2007).

42. J. Newman and K. E. Thomas-Alyea, *Electrochem. Syst.*, p. 672, Wiley-Interscience (2004).

43. K. Franzreb, J. L., P. Williams, Surface Sci. **573**, 291 (2004).

Figure 1.

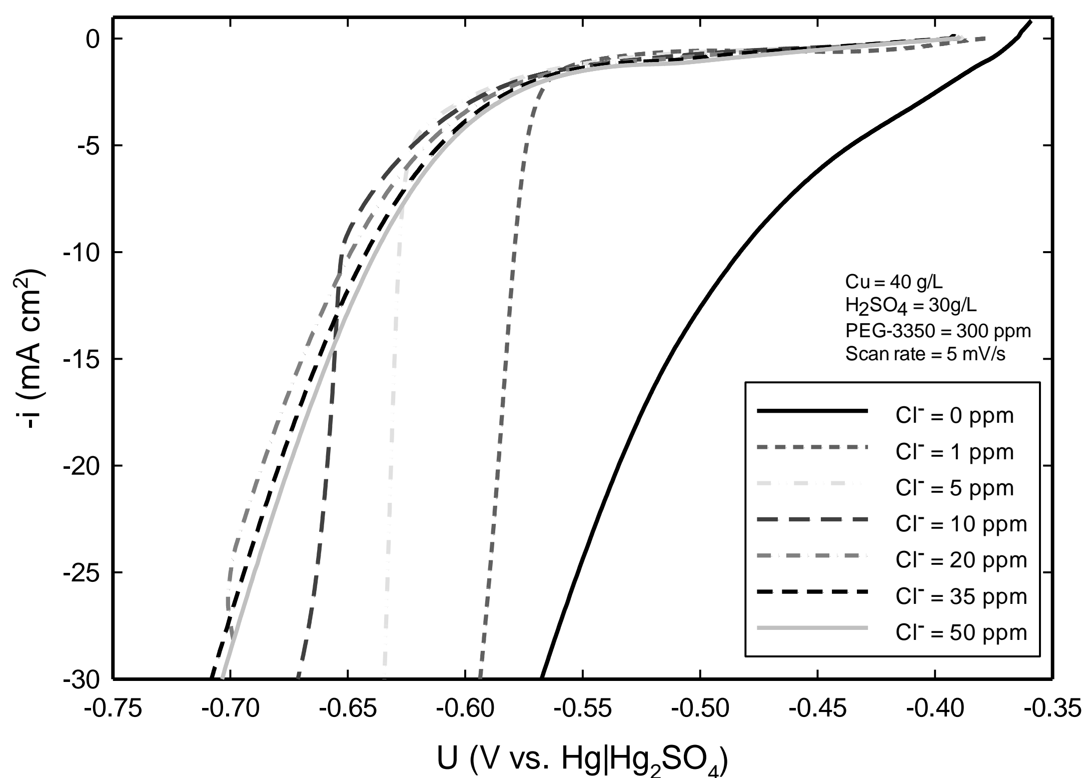

Figure 1. Linear sweep voltammetry results obtained at a sweep rate of 5 mV s^{-1}; the potential was swept from less to more negative. Data were obtained on a preplated with copper, platinum RDE at 100 rpm. Results illustrate the effect of PEG on the suppression of copper deposition at various concentrations of chloride.

Figure 2.

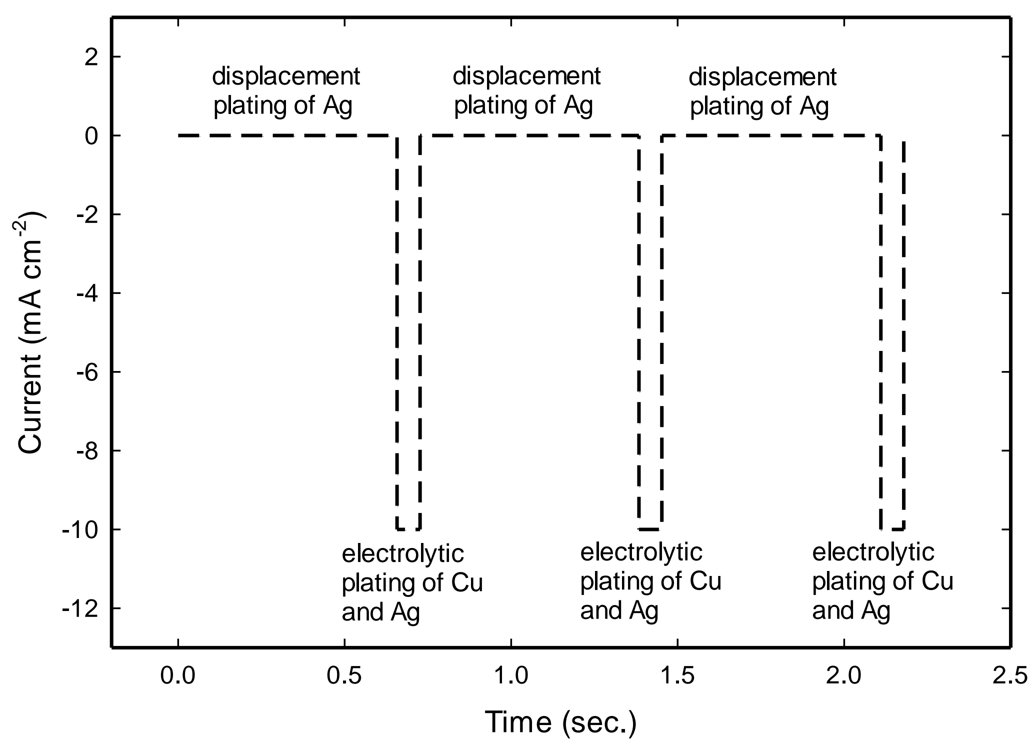

Figure 2. An example of the unipolar pulse-plating waveform that was employed for the deposition of Cu-Ag alloys. At zero current, Cu on the surface is replaced by silver; at negative current both Cu and Ag are galvanostatically plated. Duty cycle for the shown pulse is equal to 9.47% and frequency is 1.38 Hz.

Figure 3.

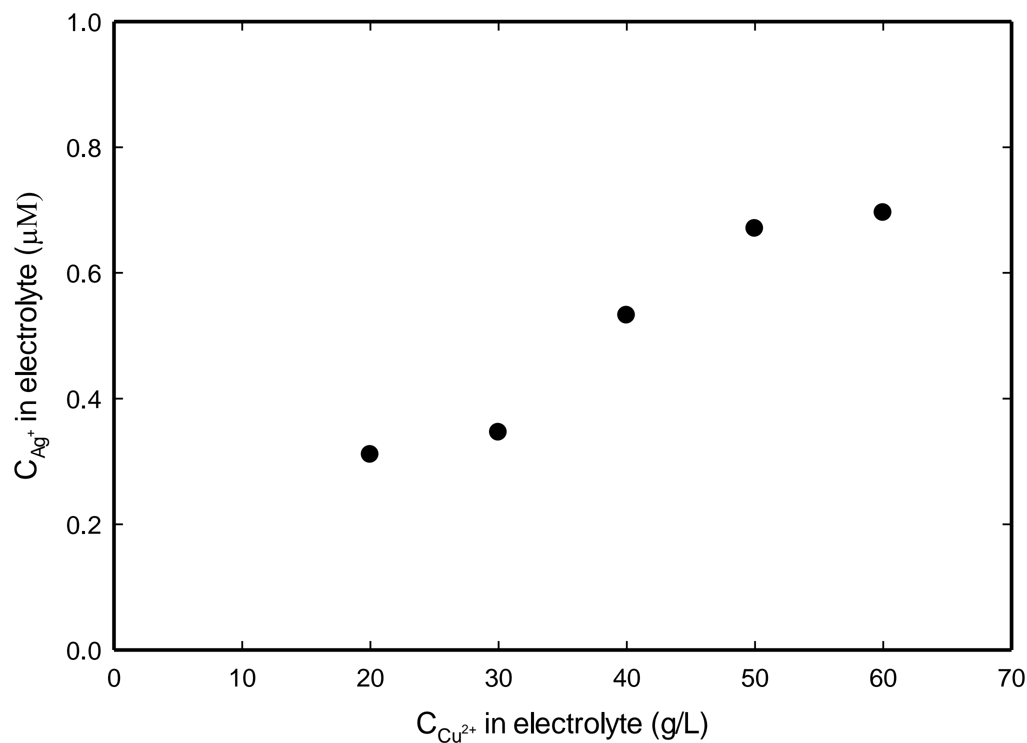

Figure 3. Concentration of Ag as a function of ionic copper from a specific lot of $CuSO_4 \cdot 5H_2O$. Films were plated at 400 rpm, 9.47% duty cycle, 1.38 Hz frequency. Figure shows the presence of Ag, even though Ag was not added to solution. This is because $CuSO_4 \cdot 5H_2O$ already contains Ag as an impurity.

Figure 4.

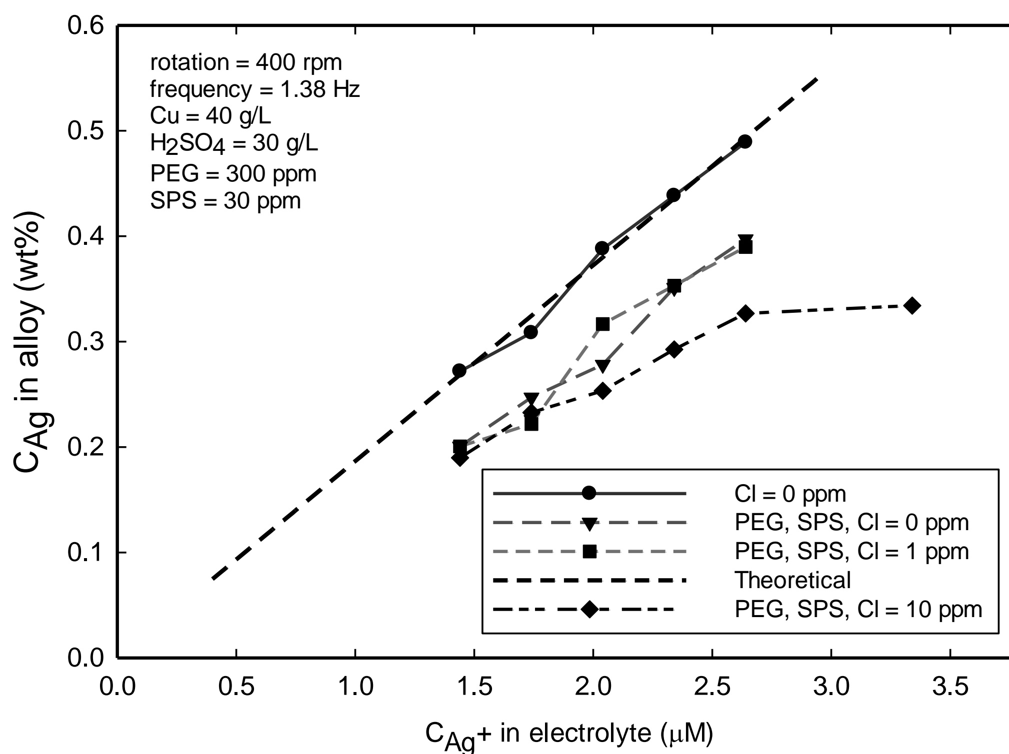

Figure 4. Composition of Ag in the alloy as a function of ionic Ag in the electrolyte, obtained at 400 rpm, 9.47% duty cycle, 1.38 Hz frequency, and i_{on} = -10 mA cm^{-2} (the nominal thickness is 226 nm). Straight line shows the theoretical values (assuming mass transfer controlled Ag deposition). The data demonstrates lower plating rate of Ag in the presence of PEG and SPS, and also how the solubility AgCl affects silver content in the film.

Figure 5.

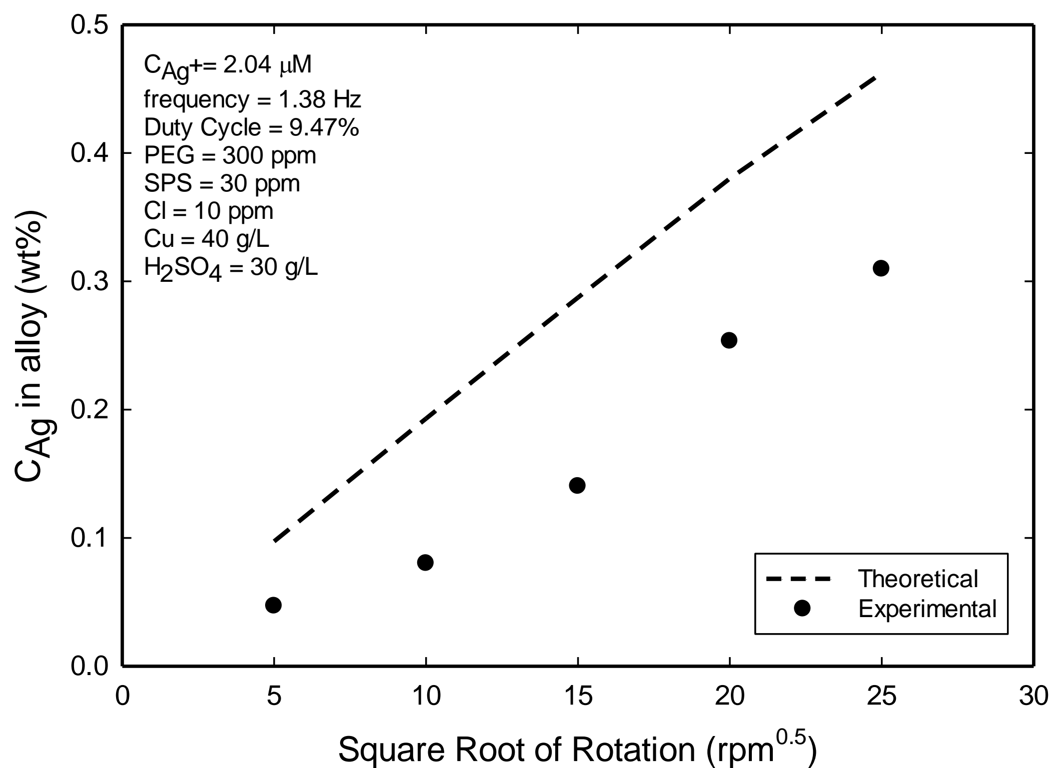

Figure 5. Composition of Ag in alloy as a function of rotation speed. The electrodeposition was performed at 1.38 Hz, 9.47% duty cycle, and i_{on} = -10 mA cm^{-2}. The straight line shows theoretical estimates assuming mass transfer controlled Ag deposition. The nominal thickness was kept at 226 nm.

Figure 6.

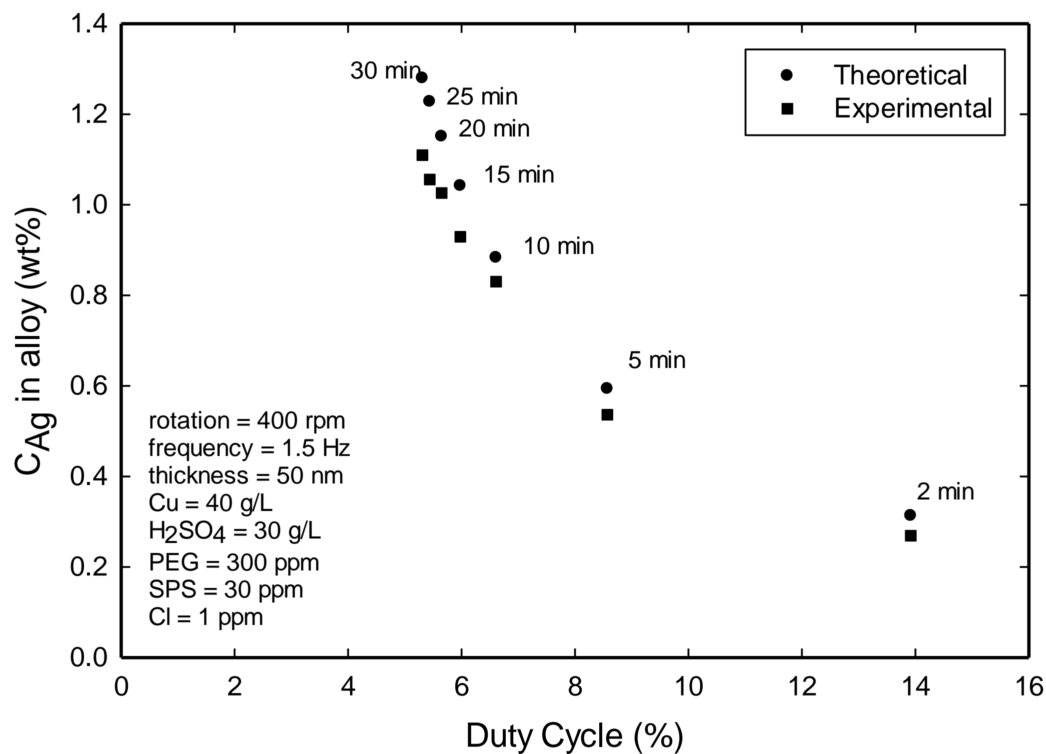

Figure 6. Effect of duty cycle on the variation of Ag in the alloy. The electrodeposition was performed at 400 rpm, 1.38 Hz, and i_{on} = -10 mA cm^{-2}, while keeping the nominal thickness at 50 nm. The times labeled above the data points indicate the off-time required to reach an estimated thickness of 50 nm.

Figure 7

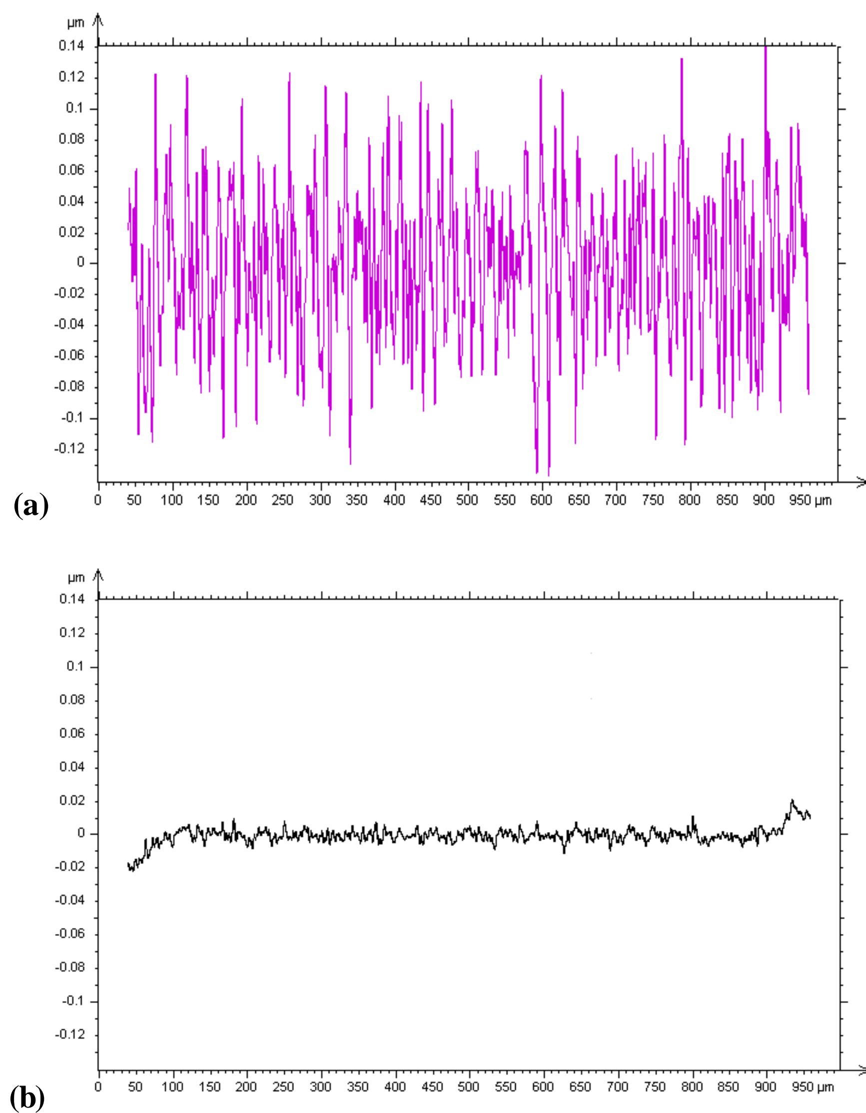

Figure 7. Roughness profile of the thin films plated at 400 rpm by (a) pulse-plating from bath with PEG, SPS, and Cl (10 ppm); (b) DC plating with PEG, SPS, and Cl (10 ppm). Pulse plating was done at duty cycle of 9.47% and frequency of 1.38 Hz.

Figure 8.

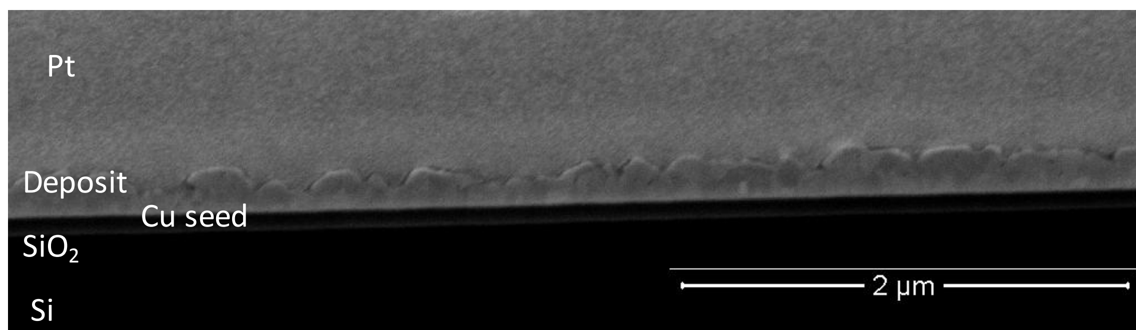

(a)

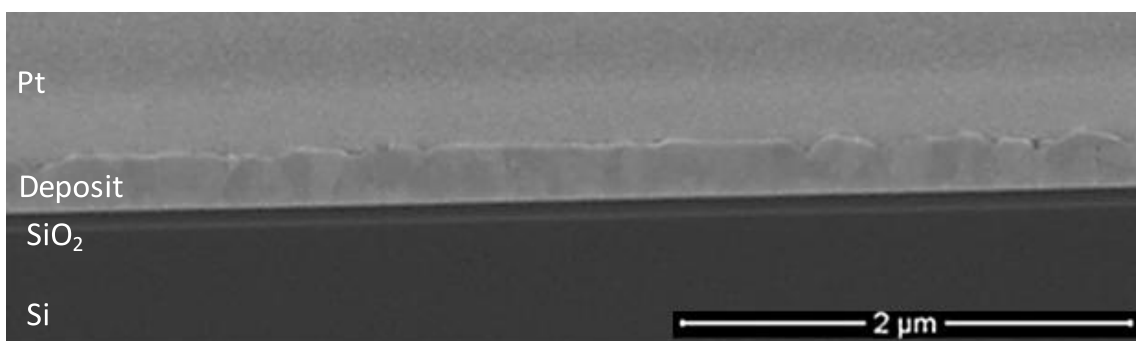

(b)

Figure 8. Scanning electron images taken at the center of the Cu-Ag alloy thin films before heat treatment. Samples were plated at 400 rpm and 9.47% duty cycle from the electrolyte containing PEG, SPS, PVP, $c_{Ag^+} = 1.7$ µM, at two different chloride concentrations. (a) cross-section view, at $c_{Cl^-} = 1$ ppm, nominal thickness 120 nm, 0.3 wt% Ag; (b) cross-section view, $c_{Cl^-} = 10$ ppm, nominal thickness 230 nm, 0.3 wt% Ag.

Figure 9.

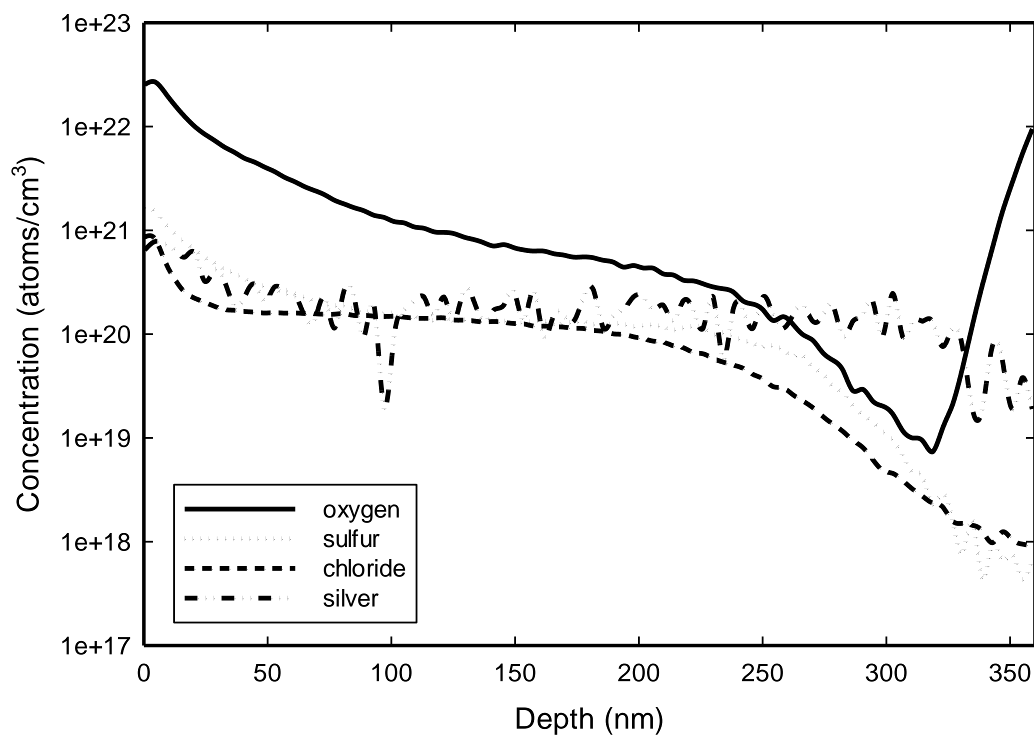

Figure 9. ToF-SIMS depth profile of the Cu-Ag film plated from an electrolyte with PEG, SPS, PVP, $c_{Cl^-} = 10$ ppm, and $c_{Ag^+} = 1.7$ µM. Film was deposited at 400 rpm and 9.47% duty cycle for a nominal thickness of 230 nm. Silver content shown in the figure is about 0.3 wt%.

Chapter 6

Electrodeposition of Copper-Tin Film Alloys for Interconnect Applications

Abstract

The electrodeposition of copper-tin alloy thin films was studied as a potential application for on-chip interconnection, where Cu-Sn alloys may be less susceptible to failure caused by electro- and stress-migration than pure copper. Alloys with variable Sn content were plated from acidic copper sulfate electrolytes by polarizing copper deposition into the region where Sn deposition became possible. The effective polarization was demonstrated by means of several halogen-polyether pairs, with Br-EPE (poly(ethylene glycol)-*block*-poly(propylene glycol)-*block*-poly(ethylene glycol)) pair exhibiting the strongest polarization. Alloy content of Sn between 0 – 7 at% was obtained above the reduction potential of Sn^{2+}, which can be attributed to UPD mechanism. Higher Sn content of up to 20 at% was achieved when Cu deposition was suppressed below the reduction potential of Sn^{2+} by the combination of Br^- and EPE. A positive correlation between Sn content and concentration of Sn^{2+} in the electrolyte was observed. At low rotation speeds of a disk electrode (*i.e.* 25 rpm versus 100 rpm) the tin content in the alloy was higher, possibly due to stronger suppression of copper deposition at low rotation speeds. The relationship between Sn content and the applied current density was specific to the employed additive chemistry.

---

* This work was done in collaboration with Xiaoxuan Sun, Greeshma Gadikota, Ping Shi

Introduction

Resistances to electromigration and stress migration are becoming dominant factors for enabling miniaturization of modern microelectronic devices.[1-3] Present generation devices utilize electrochemically deposited copper as a preferred material for interconnect fabrication.[4] The resistance of copper to electromigration and stress migration failure can be improved by alloying a small amount of another metal with copper, such as Sn, Ag, and Co. [2,5,6] The content of the alloying metal needs to be small in order to keep the electrical resistivity low.[7] For the application of Cu-Sn alloys in the interconnect fabrication, a controlled method for the deposition of Cu-Sn alloys needs to be established.

Acidic copper sulfate electrolytes have been successfully utilized for the on-chip metallization of copper.[8] The filling of surface features by electrodeposition without voids and with desired material properties is made possible by a combination of certain additives: suppressor, chloride, accelerator, and leveler.[9-13] Suppressors are typically polymers such as polyethylene glycol (PEG) that polarize Cu deposition in the presence of chloride ions.[14-16] The accelerator molecule is almost exclusively bis-(3-sulfopropyl) disulfide (SPS), which can alleviate suppression caused by the Cl-PEG pair.[17-20] The role of a leveling agent, such as polyvinylpyrrolidone (PVP) and Janus Green B, is to improve surface topography. [9,21]

The large difference between the standard reduction potentials of Cu^{2+} and Sn^{2+} ($\Delta E^o = 0.4\ V$) is a major challenge for electrodepositing Cu-Sn alloys. Although Cu-Sn deposition has been studied for multiple applications and from various electrolytes, [22-29] the electrochemical deposition of Cu-Sn alloys specifically for microelectronic applications has received limited attention. Padhi *et al.* used acidic copper sulfate electrolytes with commercial additives to obtain Cu-Sn deposits.[23] However, under the activation control

regime, they were not able to achieve the fraction of Sn above 0.3 at%. This small amount of Sn deposition was attributed to either physical incorporation of tin oxide or underpotential deposition (UPD) of tin. A study by Horkans *et al.* also attributed the production of alloys with minor amounts of Sn to the UPD mechanism.[27] Horkans *et al.* prepared Cu-Sn alloys with various amounts of Sn (0-8 at%) using a methane sulfonic acid electrolyte, which strongly inhibits Cu deposition. However, deposition in the copper sulfate and sulfuric acid electrolyte is probably necessary due to the widespread industrial acceptance of these electrolytes. An underpotential deposition of tin was also observed by Qiao *et al.* on a gold disk electrode.[30] Survila *et al.* attributed UPD of Sn to the formation of specific copper-rich phases, and even found Cu-Sn alloy phases that were specific to underpotential deposition of tin on copper.[29]

In this paper we investigate the co-deposition of Cu with Sn from acidic copper sulfate solutions in the presence of suppressor, accelerator, and leveler. In order to emulate state-of-the-art plating conditions, deposition of copper was performed at currents below the limiting current of Cu and without the use of complexing agents. To enable alloy formation, we used stronger halogen-suppressor pairs, rather than a conventional Cl-PEG, together with SPS. Stronger suppression allows for polarization of Cu deposition to a greater extent and makes co-deposition of Sn possible.

The stronger suppressor for Cu deposition used in the study is a block copolymer – EPE, which stands for poly(ethylene glycol)-*block*-poly(propylene glycol)-*block*-poly(ethylene glycol). Gallaway *et al.* demonstrated that not only is the Cl-EPE system more polarizing than Cl-PEG system, but it also leads to better filling performance when used with SPS.[31-33] The degree of inhibition among suppressor molecules has been linked to

length of the hydrocarbon chain, hydrophobicity, and steric effects.[29,33] A study by Hayase *et al.*[34] and Survila *et al.*[29] revealed that substituting Br^- for Cl^- leads to an additional polarization in suppressor-containing electroplating baths. Therefore, the ability to produce varying alloy compositions using Br^- was also investigated as part of this study.

Experimental

Polarization experiments on RDE.

A three electrode cell was used for the electrochemical investigation. The working electrode was a platinum rotating disk electrode (RDE) with 4 mm disk diameter (Pine Corporation); the counter electrode was a platinum wire; and the reference electrode was Ag|AgCl (BASi Re-5). Prior to each experiment, the platinum surface of the RDE was electrochemically pretreated in 0.5 M H_2SO_4 solution by cycling the electrode potential repeatedly between 1.2 V and -0.171 V at 1 V s^{-1} until a characteristic cyclic voltammogram was developed. Then, the electrode was transferred to additive-free copper sulfate electrolyte, wherein a thin layer of copper was preplated at - 40 mA cm^{-2} for 120 seconds at a rotation speed of 100 rpm. The polarization experiments were conducted by sweeping the potential from open-circuit potential at a scan rate of -5 mV s^{-1}. At the end of each experiment, the deposit was removed from the RDE surface by using concentrated nitric acid.

Electroplating of alloy films.

The electrochemical deposition of Cu-Sn films was conducted on wafer coupons, which were cleaved from 300 mm silicon wafer that had Ta/TaN barrier layer and PVD

plated copper-seed layer on the surface. Approximately 2.54×2.54 cm^2 coupon squares were cleared of dust by blowing pre-purified compressed nitrogen to the surface and attached to the coupon holder designed by Atotech USA, Inc. to approximate an RDE. The electrical contacts between the wafer segments and the coupon holder were made by using Cu adhesive tape. A well-defined circular surface area was achieved by applying precut Kapton tape. A hole in the Kapton tape was punched using a craft punch (Marvy Uchida), with 1.6 cm hole diameter (surface area 1.98 cm^2).

Prior to each deposition experiment, the holder was first attached to a rotatory shaft of the RDE stand, and after being rinsed with deionized (DI) water (18.2 MΩ·cm), it was immersed in about 200 ml of electrolyte contained in a 325 ml Pyrex crystallizing dish. The counterelectrode was a gold wire. Various currents were generated and controlled by FRA2 μAutolab Type III potentiostat/galvanostat (Metrohm Autolab B.V.) and General Purpose Electrochemical System (GPES) software. The nominal thickness of each deposit was 1 μm. After a deposition experiment, the coupon was rinsed with DI water and blown dry with compressed nitrogen. Then, the whole deposit (including the seed layer) was first dissolved in 1 ml of 35% concentrated nitric acid, and then diluted in DI water to make up 10 ml of volume for ICP-OES analysis which is discussed below. The above procedures for electroplating metal alloy films have been successfully implemented for studying Cu-Ag alloys.[6]

Electrolyte preparation

Electrolytes for all plating experiments were prepared using the following materials: $CuSO_4 \cdot 5H_2O$, 99+ % (Fisher Scientific, Acros Organics), H_2SO_4, 95-98% (EMD Chemicals,

Inc.), $SnSO_4$, 97+ % (Fisher Scientific, Acros Organics), PEG 3350 g mol^{-1} (Sigma-Aldrich), HCl, 12.1 M (VWR, BDH Aristar), HBr, 47%-49% (Alfa Aesar), SPS, 96% [35] (Raschig GmbH), PVP 29,000 g mol^{-1} (Sigma-Aldrich), EPE 2000 g L^{-1} (Sigma-Aldrich). For all experiments conducted in this study the concentration of PEG was 8.95×10^{-5} M, the concentration of SPS was 8.46×10^{-4} M, the concentration of PVP was 6.9×10^{-6} M, the concentration of EPE was 1.0×10^{-4} M, the concentration of Cl^- was 1.41×10^{-3} M, and the concentration of Br^- was 1.88×10^{-3} M. The organic additives (PEG, SPS, and PVP), bromide, and chloride were individually added to the plating bath from premade concentrated solutions that were dissolved in DI water. EPE could not be dissolved into a concentrated solution due to its low solubility of about 1.0×10^{-4} M.

Electrolytes with $SnSO_4$ required special preparation. In order to dissolve $SnSO_4$, $SnSO_4$ was first allowed to disperse in water for a few minutes and then concentrated H_2SO_4 was added to the murky mixture. Upon contact with H_2SO_4, the murky solution readily changed to transparent water-like solution, and at this point all $SnSO_4$ was considered dissolved. If $SnSO_4$ was added to a dilute H_2SO_4 solution (such as 0.5 M), the mixture remained murky for several days, even at 80^0C. It was also found that if $SnSO_4$ was completely dissolved in relatively low sulfuric acid solutions (*i.e.* 0.3 M H_2SO_4) a yellowish precipitate would start forming after about 6 hours. This precipitate could possibly be SnO_2, which is not soluble in acids and alkalis. Dissolving $SnSO_4$ at higher sulfuric acid concentrations, such as 1.5 M H_2SO_4, substantially slowed down formation of a precipitate to over a week.

Metrology

Inductively Coupled Plasma – Atomic Emission Spectroscopy, ICP-AES (Horiba JobinYvon) controlled by ACTIVAnalyst 5.4 software was used to determine the total amount of tin in the electroplated films. Tin concentrations were quantified by calibrating the signal intensities with known concentrations of tin. Calibration standards were prepared using 1000 ppm ICP standard of tin metal in 3% nitric acid (Ricca Chemical Company). The emission wavelength that was chosen for tin analysis is 242.949 nm.

Results and Discussion

Polarization of Cu and Sn deposition on RDE

In order to electrodeposit Cu-Sn alloys, it is necessary to selectively inhibit Cu deposition until the onset of Sn deposition. Various combinations of halogen with suppressor molecules, such as Cl-PEG, Cl-EPE, Br-PEG, and Br-EPE, were found to polarize the reduction of copper to a varying degree, with Br-EPE couple being the most suppressing (Figure 1). The polarization characteristics of these additive systems were substantially influenced by the concentrations of copper sulfate and sulfuric acid in the electrolyte. As shown in Figure 1, it was possible to increase the polarization of Cu^{2+} reduction by about 70 mV when 0.63 M of Cu^{2+} and 0.31 M of H_2SO_4 were substituted with 0.31 M Cu^{2+} and 150 1.53 M of H_2SO_4. Also, selection of a halogen molecule had a large effect on the polarization of copper deposition. It was found that when 1.41×10^{-3} M of Cl^- was replaced with 1.88×10^{-3} M of Br^- ions, the polarization of Cu^{2+} reduction increased by an additional 150 mV.

For the successful filling of sub-micron features, it is necessary to add an accelerator component, such as SPS, to a chloride-suppressor system [10,36]. Figure 2 shows the change in polarization of copper deposition when SPS is added to the four different halogen-suppressor systems: Cl-PEG, Cl-EPE, Br-PEG, and Br-EPE. In the presence of Cl^- ions, SPS depolarizes suppression in Cl-PEG and Cl-EPE systems by about 100 mV and 150 mV, respectively. However, in the presence of Br^- ions, SPS has a much smaller depolarizing effect on Br-PEG system and little to no effect on polarization by Br-EPE.

The polarization curves shown in Figure 3 reveal that in the absence of additives the reduction of Sn^{2+} begins at a potential of about -0.47 V *vs.* Ag|AgCl when $c_{Sn^{2+}}$= 84.3 mM and at about -0.5 V *vs.* Ag|AgCl when $c_{Sn^{2+}}$= 8.43 mM. This dependence on concentration is expected from the Nernst equation (Eqn. 1). Both curves reach a diffusion limited plateau at more negative potentials. Figure 3 also shows the impact of additives on polarization of tin deposition. As can be seen from the inset to Figure 3, Cl-EPE and Br-EPE do not seem to have a significant impact on the onset of tin reduction. However, the rate of reduction of Sn^{2+} is substantially hindered by these additives. Small cathodic currents seen at potentials higher than the reduction of Sn^{2+} could in part be due to UPD mechanism, as well as reductions of Sn^{4+} (Reaction 2) and/or dissolved oxygen. Although Sn^{4+} was not added to the electrolyte, it could be present via oxidation of Sn^{2+} ions by dissolved oxygen (Reaction 3). Since ΔE^{o} for Reaction 3 is positive, reaction will proceed spontaneously in the forward direction. The presence of Sn^{4+} ions could also potentially explain the appearance of precipitate in dilute sulfuric acid solutions (see experimental section).

$$\Delta E = \frac{RT}{nF}\log\left(c_{Sn^{2+},\ a}/c_{Sn^{2+},\ b}\right) \qquad (1)$$

$$Sn^{4+} + 2e^{-} \rightleftarrows Sn^{2+} \qquad (\ E^{o} = -0.05\ \mathrm{V\ vs.\ Ag|AgCl}) \qquad (2)$$

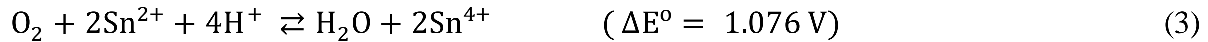

$$O_2 + 2Sn^{2+} + 4H^+ \rightleftarrows H_2O + 2Sn^{4+} \qquad (\Delta E^o = 1.076\ V) \qquad (3)$$

A study by Padhi *et al.* demonstrated that the addition of $SnSO_4$ to the additive-free copper electrolyte did not change the polarization behavior of Cu^{2+} deposition [23]. To measure the impact of $SnSO_4$ on the polarization of Cu^{2+} reduction in the presence of additives, linear sweep experiments were performed. Figure 4 shows that the polarization of Cu^{2+} reduction by Cl-PEG, Br-PEG, Cl-EPE, and Br-EPE was also almost unaffected in the presence of Sn^{2+} at 84.3 mM.

Co-deposition of Cu-Sn thin films

The co-deposition of Cu-Sn alloys was attempted utilizing a number of halogen-suppressor combinations. The atomic fraction of Sn in a Cu-Sn alloy was computed by dividing the molar concentration of Sn measured from ICP by the total number of moles deposited according to the Faraday's law (Eqn. 4).

$$c_{Sn}(at\%) = \frac{c_{Sn,\ ICP}}{\left(\frac{iAt}{nF}\right)} \times 100\% \qquad (4)$$

In equation 2, numerator $c_{Sn,\ ICP}$ is the concentration of Sn measured by ICP-AES, i is current density, A is the electrode surface area, n is the number of electrons transferred per ion in reaction, t the deposition time, and F is the Faraday's constant.

Based on Figures 2 and 3, only the Br-EPE pair polarized copper deposition enough to reach the deposition potential of Sn^{2+}. However, the co-deposition of Cu-Sn alloys with substantial Sn contents were obtained using a variety of different halogen-suppressor pairs possibly due to the existence of UPD of Sn.[27,30] Tin was not detected in the alloy when the electrolyte contained Cl-EPE-SPS (which polarized Cu^{2+} deposition by only about 0.2 V)

and 84.3 mM of Sn^{2+} ions. However, the deposition of Cu-Sn from a bath containing Cl-PEG couple (which polarized Cu^{2+} deposition by about 0.25 V at higher current densities) showed already a detectible but small incorporation of 0.06 at% Sn at 100 rpm and current densities up to -22 mA cm^{-2}. Decreasing the rotation speed from 100 rpm to 25 rpm in Cl-PEG system increased Sn content to 0.48 at%. This effect can possibly be attributed to stronger suppression rate of Cu^{2+} reduction by halogen-suppressor pairs at lower rotation speeds, as was both noted by Survila *et al.*[29] and observed in our experiments (not shown). When Cu deposition becomes more polarized, electrode potential shifts to negative and allows for higher rate of Sn deposition.

The Cl-EPE system polarized copper deposition more than Cl-SPS-EPE and Cl-PEG systems by about 0.3 V. The deposition of Cu-Sn alloy from a Cl-EPE-containing electrolyte at different current densities and $c_{Sn^{2+}}$ revealed that a substantial Sn content of over 6 at% could be achieved. Figure 5 shows that Sn composition in the alloy increased linearly with an increase in current density at three different $c_{Sn^{2+}}$. There was a positive correlation between Sn content in the alloy and the ionic concentration of Sn^{2+} in the Cl-EPE electrolyte. Figure 6 shows the effect of rotation speed on the Sn content. Analogous to Cl-EPE system, at low rotation speeds Sn contents were higher.

Figure 7 shows time variation of electrode potential under various current densities during coupon plating in the electrolyte containing Cl-EPE additive system and 84.3 mM of Sn^{2+}. Graphed potentials were corrected for ohmic drop according to Newman's treatment of primary current distribution on an RDE.[37] Electrode potentials became more negative with increasing current densities, approaching reduction potential of tin in the highest current

density range. This observation correlates well to an increase in the Sn content shown in Figure 5.

The Br-PEG pair polarized Cu deposition more than Cl-EPE pair did. However, the content of Sn utilizing the Br-EPE pair was less than in the presence of Cl-EPE. This observation suggests that the deposition of Sn was influenced by the halogen-suppressor combination in use. Figure 8 shows the effect of current density on incorporation rate of Sn during Cu-Sn deposition with Br-PEG pair at three different Sn^{2+} concentrations. There was almost an exponential dependence of Sn content on current density. Figure 9 shows the effect of rotation speed on Sn content from a bath containing Br-PEG additive system. As was seen for Cl-PEG and Cl-EPE systems, at low rotation speeds Sn content became higher.

Based on Figure 2, Br-EPE and Br-EPE-SPS systems were the most polarizing combinations for Cu deposition. Figure 10 shows that at 8.43 mM of Sn^{2+} in electrolytes, Sn content in the alloy ranged from about 0.3 – 2 at% depending on the applied current density. Addition of SPS to Br-EPE system did not alter the dependence of Sn content on current density. This result was consistent with polarization data, since SPS did not affect polarization of Cu in the Br-EPE-containing electrolyte. The alloying content of Sn also went through a maximum along the current density axis, possibly due to the varying kinetics of Cu^{2+} and Sn^{2+} deposition at changing overpotentials.

When the concentration of Sn^{2+} was increased from 8.43 mM to 84.3 mM, deposits had a distinctly silvery appearance, indicating a substantial incorporation of Sn in the alloy. These samples could not be analyzed with ICP-AES technique because of the precipitation in the samples (see experimental section). Therefore, Energy-Dispersive X-ray Spectroscopy

(EDX) was used instead to measure Sn content. Figure 10 shows the amount of Sn in these deposits. Sn content was significant, reaching almost 20 at% at -10 mA cm^{-2}.

The effect of having a leveling agent, PVP, along with Br-EPE-SPS is also shown in Figure 9. Based on polarization experiments, PVP depolarized the suppression caused by Br-EPE-SPS. Consistent with this effect, the incorporation of Sn in the alloy was less in the presence of PVP than in the absence of it. Figure 11 shows the effect of rotation speed on the alloy composition; as was seen in other systems, Sn content decreased with an increase in rotation speed.

Conclusions

The present study examined electrodeposition of Cu-Sn alloy thin films from acidic copper sulfate electrolytes by the application of additives that polarize Cu deposition to varying degrees. The most polarizing effect was achieved by utilizing the Br-EPE pair, compared to several other halogen-suppressor combinations. All additive combinations used in this paper exhibited stronger polarization of Cu deposition in electrolytes with higher sulfuric acid and lower Cu^{2+} concentration. It was demonstrated that Sn contents of 0 – 7 at% in the alloy occurred above the reduction potential of Sn^{2+}. This can possibly be due to underpotential deposition. When Cu deposition was suppressed by the Br^{-} and EPE pair, a high Sn content of up to 20 at% was achieved at 84.3 mM of Sn^{2}. The content of Sn in the Cu-Sn alloy was found to be a function of the applied current density, rotation speed, and the amount of Sn^{2+} ions present in the electrolyte. A positive correlation between the Sn content and concentration of Sn^{2+} in the electrolyte was observed; also the Sn content in the

alloy was higher at lower rotation speeds. The relationship between the Sn content and the applied current density was specific to the utilized additive combination.

References

1. C. M. Tan, Electromigration in ULSI Interconnections, World Scientific Publishing Company, 2012.
2. C.-K. Hu, M. Angyal, B. C. Baker, G. Bonilla, C. Cabral, D. F. Canaperi, S. Choi,L. Clevenger, D. Edelstein, L. Gignac, E. Huang, J. Kelly, B. Y. Kim, V. Kyei-Fordjour, S. L. Manikonda, J. Maniscalco, S. Mittal, T. Nogami, C. Parks, R. Rosenberg, A. Simon, Y. Xu, T. A. Vo, C. Witt, in E. Zschech, P. S. Ho, S. Ogawa (Editors), Stress-Induced Phenomena in Metallization: 11th International Workshop, 2010, p. 57.
3. A. Heryanto, K. L. Pey, Y. K. Lim, W. Liu, N. Raghavan, J. Wei, C. L. Gan, M. K. Lim, Tan, J. B., *J. App. Phys.* 109 (2011) 9.
4. International Technology Roadmap for Semiconductors, Interconnect Chapter (2009).
5. C. K. Hu, B. Luther, F. B. Kaufman, J. Hummel, C. Uzoh, D. J. Pearson, *Thin Solid Films* 262 (1995) 84.
6. I. Volov, E. Swanson, B. O'Brien, K. Dunn, A. C. West, *J. Electrochem. Soc*. 159 (2012) D677.
7. S. Strehle, J. W. Bartha, K. Wetzig, *Thin Solid Films* 517 (2009) 3320.
8. P. C. Andricacos, C. Uzoh, J. O. Dukovic, J. Horkans, H. Deligianni, *IBM J. Res. & Dev*. 42 (1998) 567.

9. J. J. Kelly, C. Tian, A. C. West, *J. Electrochem. Soc.* 146 (1999) 2540.

10. T. P. Moffat, D. Wheeler, S. K. Kim, D. Josell, *Electrochim. Acta* 53 (2007) 145.

11. T. P. Moffat, D. Wheeler, D. Josell, *J. Electrochem. Soc.* 151 (2004) C262.

12. K. Kondo, N. Yamakawa, Z. Tanaka, K. Hayashi, *J. Electroanal. Chem.* 559 (2003) 137.

13. I. Volov, T. Saito, A. C. West, *J. Electrochem. Soc.* 158 (2011) D384.

14. J. P. Healy, D. Pletcher, M. Goodenough, *J. Electroanal. Chem.* 338 (1992) 155.

15. J. J. Kelly, A. C. West, *J. Electrochem. Soc.* 145 (1998) 3477.

16. J. J. Kelly, A. C. West, *J. Electrochem. Soc.* 145 (1998) 3472.

17. M. Tan, J. N. Harb, *J. Electrochem. Soc.* 150 (2003) C420.

18. J. J. Kim, S.-K. Kim, Y. S. Kim, *J. Electroanal. Chem.* 542 (2003) 61.

19. I. Volov, O. Mann, Y. Hoenersch, B. Wahl, A. C. West, *J. Sep. Sci.* 34 (2011) 2385.

20. I. Volov, A. C. West, *J. Electrochem. Soc.* 158 (2011) D456.

21. M. J. Willey, J. Reid, A. C. West, *Electrochem. and S.-S. Lett.* 10 (2007) D38.

22. G. I. Medvedev, N. A. Makrushin, O. V. Ivanova, Russ. *J. App. Chem.* 77 (2004) 1104.

23. D. Padhi, S. Gandikota, H. B. Nguyen, C. McGuirk, S. Ramanathan, J. Yahalom, G. Dixit, *Electrochim. Acta* 48 (2003) 935.

24. A. Survila, Z. Mockus, S. Kanapeckate, V. Jasulaitiene, R. Juekenas, *Electrochim. Acta* 52 (2007) 3067.

25. O. Galdikiené, Z. Mockus, *J. App. Electrochem.* 24 (1994) 1009.

26. S. D. Beattie, J. R. Dahn, *J. Electrochem. Soc.* 150 (2003) A894.

27. J. Horkans, I. C. H. Chang, P. C. Andricacos, H. Deligianni, *J. Electrochem. Soc.* 142 (1995) 2244.

28. H. Nakano, S. Oue, D. Yoshihara, H. Fukushima, Y. Saka, S. Sawada, Y. Hattori, *Mat. Tran.* 52 (2011) 1237.

29. A. Survila, Z. Mockus, S. Kanapeckaite, D. Brazinskiene, Juskens, *J. Electrochem. Soc.* 159 (2012) D296.

30. Z. Qiao, W. Shang, X. Zhang, C. Wang, *Anal. and Bioanal. Chem.* 381 (2005) 1467.

31. J. W. Gallaway, M. J. Willey, A. C. West, *J. Electrochem. Soc.* 156 (2009) D146.

32. J. W. Gallaway, M. J. Willey, A. C. West, *J. Electrochem. Soc.* 156 (2009) D287.

33. J. W. Gallaway, A. C. West, *J. Electrochem. Soc*. 155 (2008) D632.

34. M. Hayase, M. Taketani, T. Hatsuzawa, K. Hayabusa, *Electrochem. and S.-S. Lett*. 6 (2003) C92.

35. R. G. Brennan, M. M. Phillips L.-Y. O. Yang, T. P. Moffat, *J. Electrochem. Soc.* 158 (2011) D178.

36. Y. Cao, P. Taephaisitphongse, R. Chalupa, A. C. West, *J. Electrochem. Soc.* 148 (2001) C466.

37. J. Newman, K. E. Thomas-Alyea, *Electrochem. Syst.*, p. 424, Wiley-Interscience (2004).

Figure 1

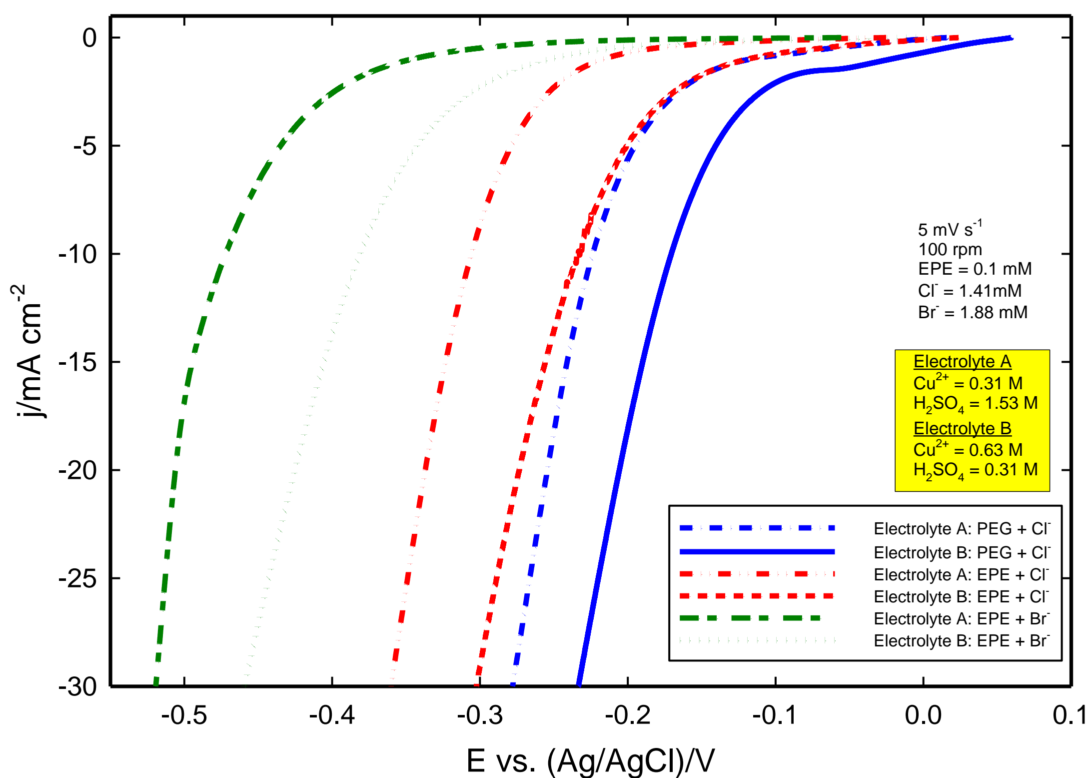

Figure 1. Linear sweep voltametry results conducted at a sweep rate of 5 mV s^{-1} and rotation speed of 100 rpm. Results show the polarization of copper deposition on preplated RDE in the presence of Cl-PEG, Cl-EPE or Br-EPE additive systems. Two different electrolyte compositions were used: Electrolyte A was composed of Cu^{2+} = 0.31 M and H_2SO_4 = 1.53 M and Electrolyte B was composed of Cu^{2+} = 0.63 M and H_2SO_4 = 0.31 M.

Figure 2

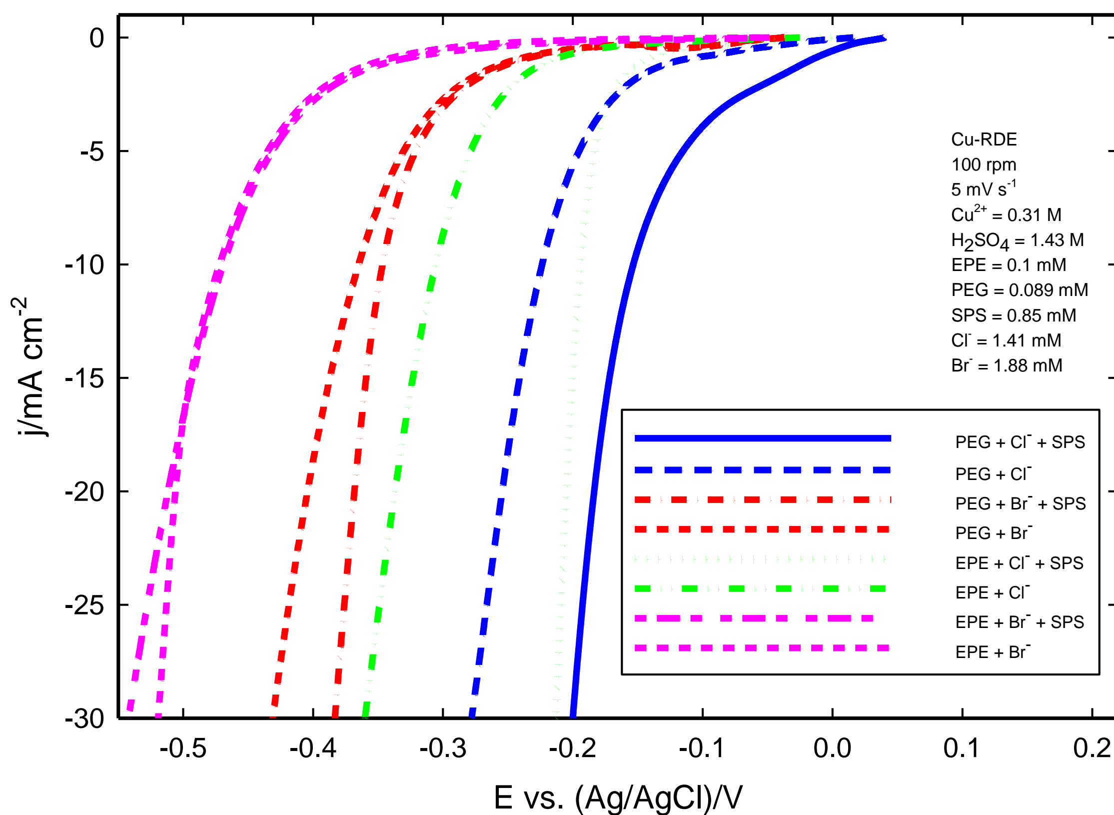

Figure 2. Linear sweep voltametry results conducted on preplated RDE at a sweep rate of 5 mV s^{-1} and rotation speed 100 rpm. Results show polarization of Cu deposition by Cl-PEG, Cl-EPE, Br-PEG, and Br-EPE systems with and without SPS. In the presence of Br^- ions, SPS has little to no effect on polarization of Cu^{2+} reduction.

Figure 3

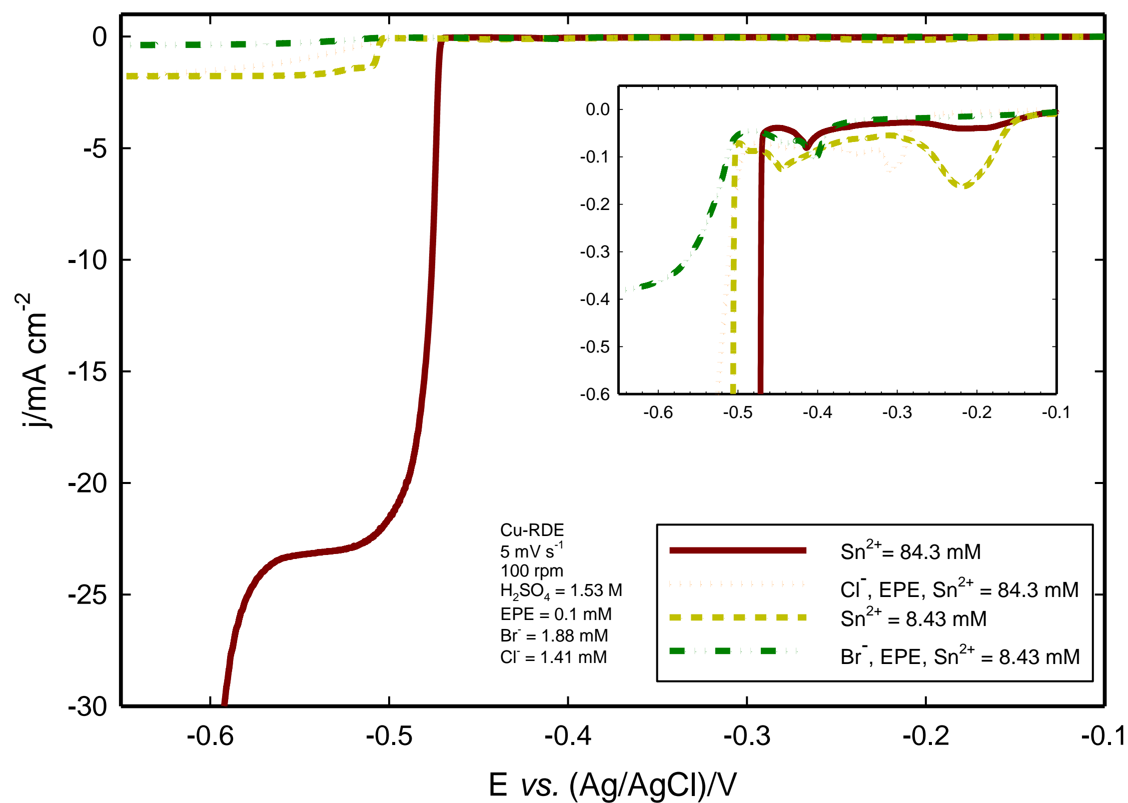

Figure 3. Linear sweep voltametry results conducted on preplated RDE at a sweep rate of 5 mV s^{-1} and rotation speed of 100 rpm. Experiments show the onset of Sn deposition and the influence of additives on polarization of Sn^{2+} deposition.

Figure 4

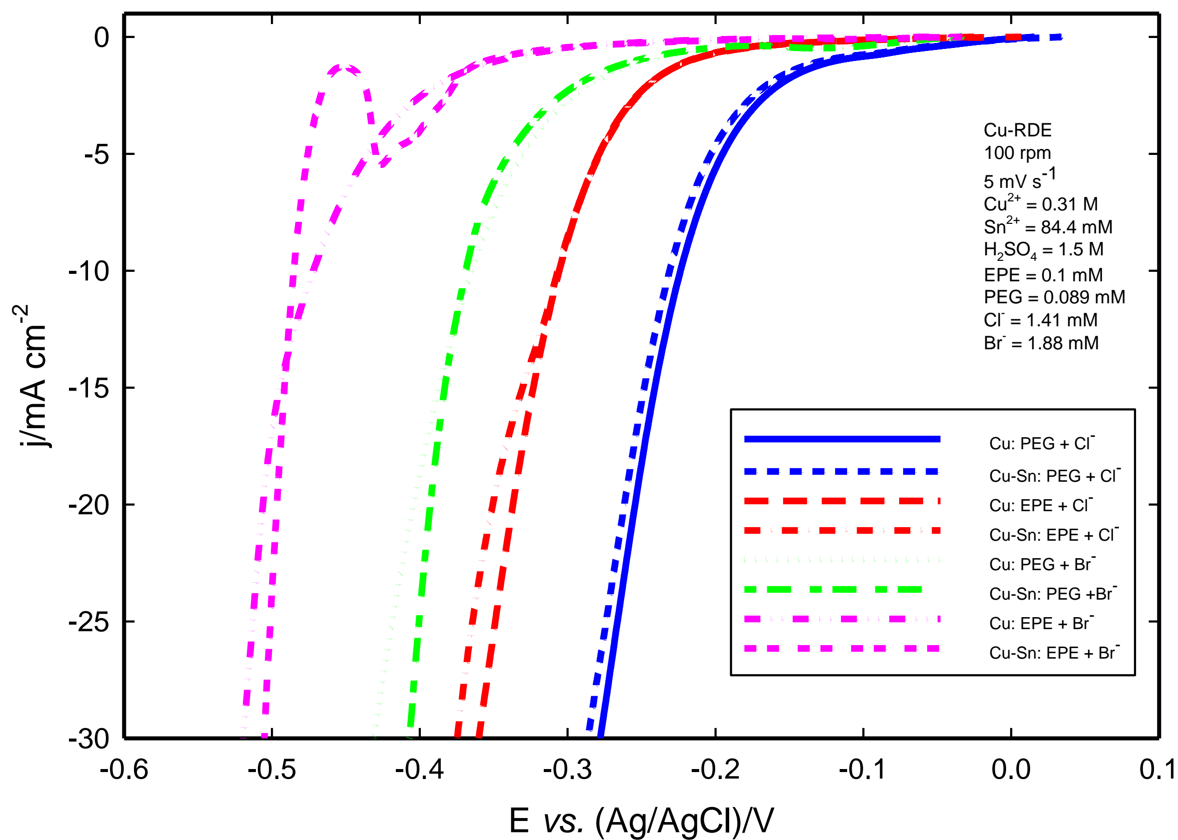

Figure 4. Linear sweep voltametry results conducted on preplated RDE at a sweep rate of 5 mV s^{-1} and rotation speed 100 rpm. Experiments show that polarization of Cu deposition by different halogen-suppressor pairs is almost unaffected by the presence Sn^{2+} ions at 84.3 mM.

Figure 5

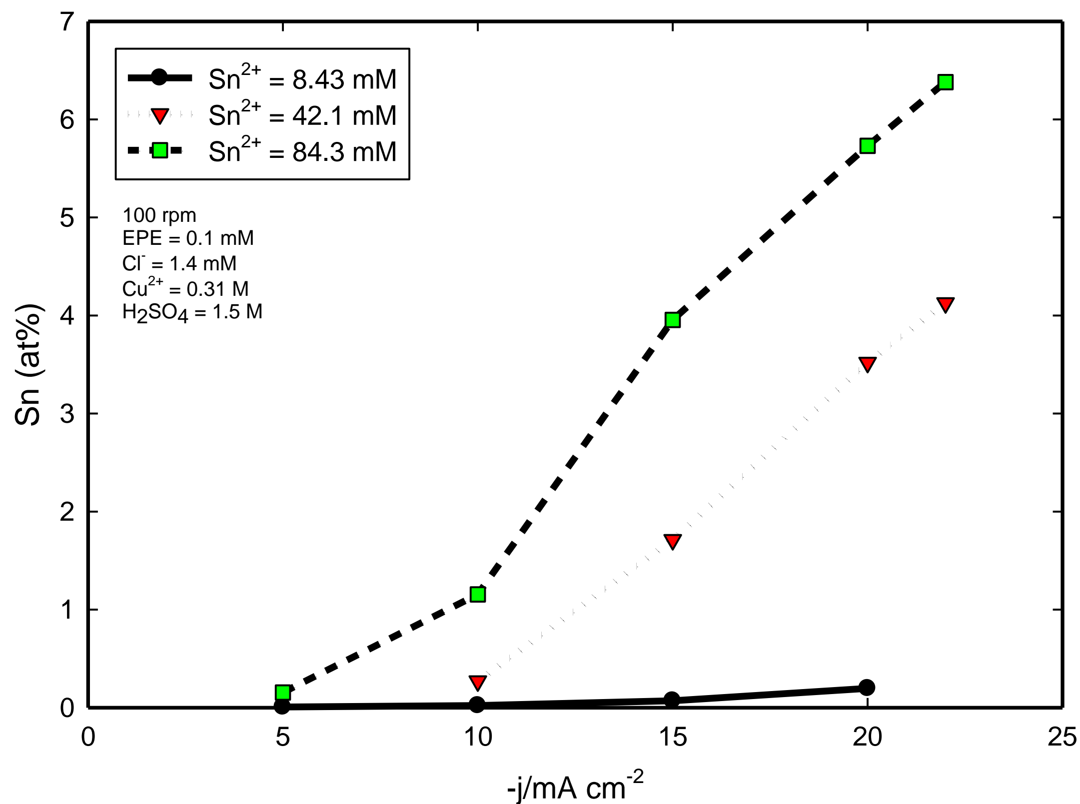

Figure 5. Composition of Sn in the Cu-Sn alloy as a function of current density and Sn^{2+} concentration in the electrolyte containing Cl-EPE additive system. Deposition was conducted at 100 rpm.

Figure 6

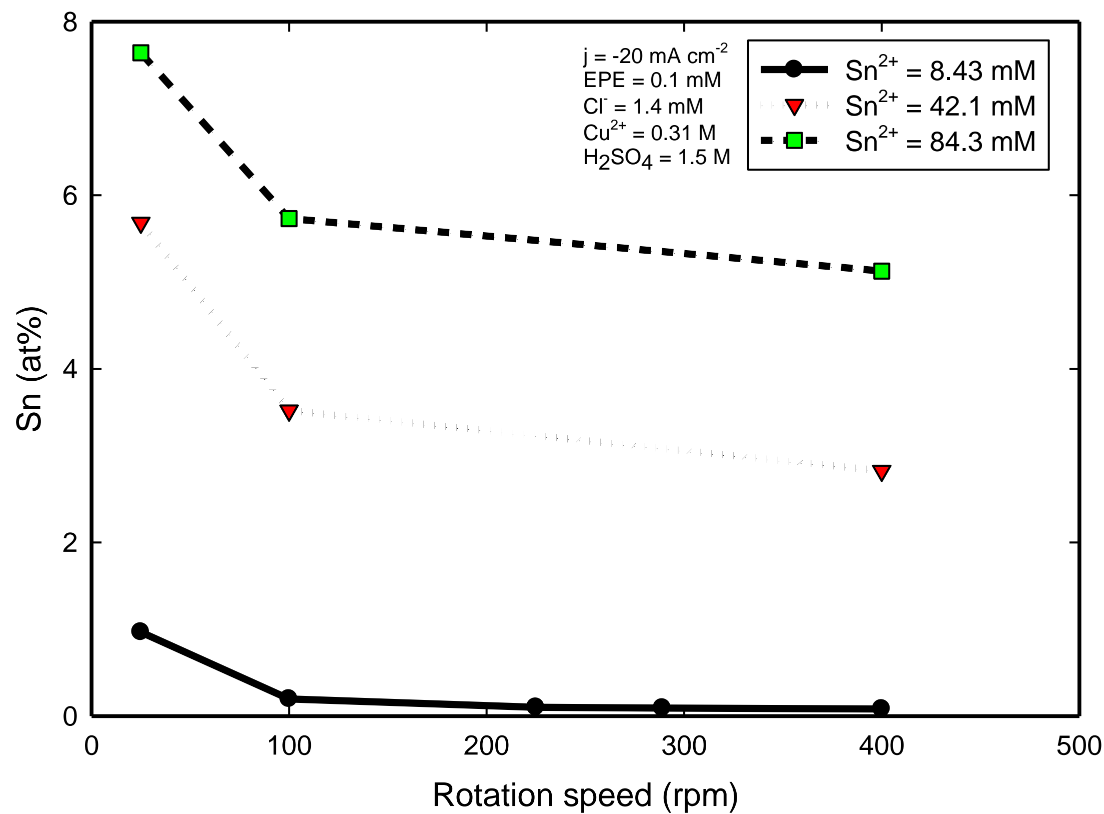

Figure 6. Composition of Sn in the Cu-Sn alloy as a function of rotation speed and Sn^{2+} concentration in the electrolyte containing Cl-EPE additive system. Deposition was conducted at j = -20 mA cm^{-2}.

Figure 7

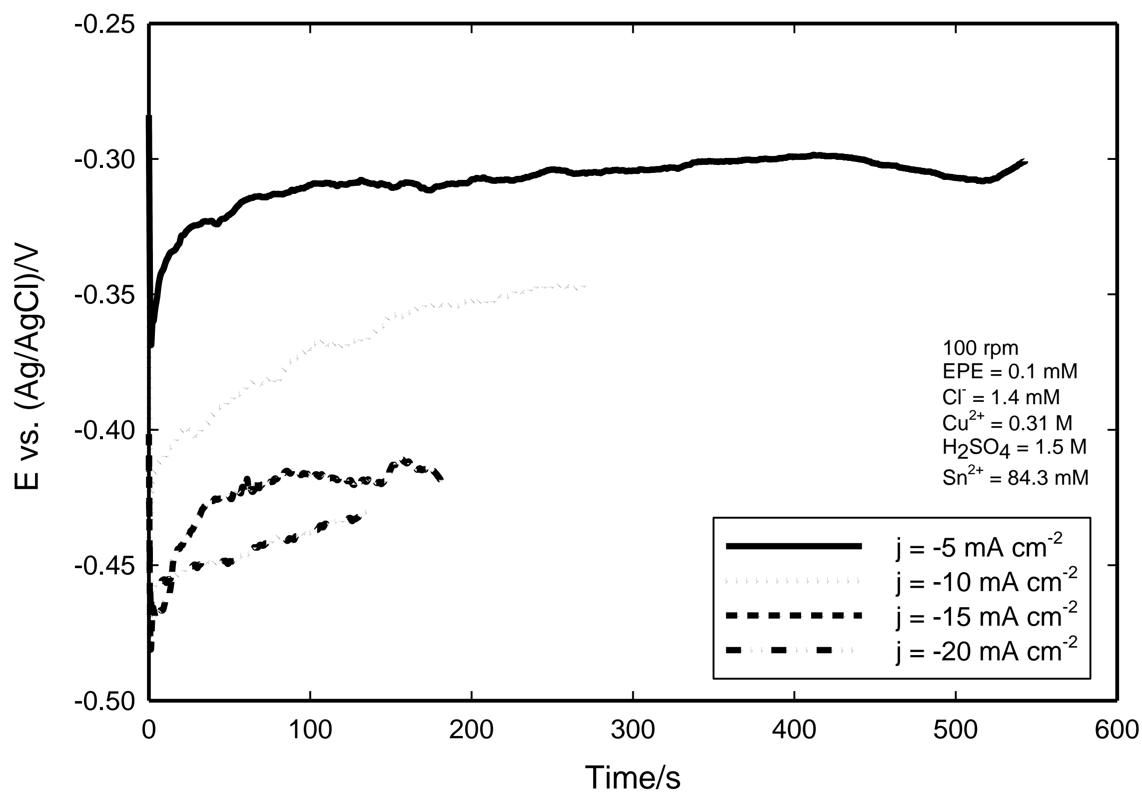

Figure 7. Time variation of electrode potential during coupon plating at various current densities. Electrolyte contained 84.3 mM Sn^{2+} and Cl-EPE additive system. Potential was corrected for ohmic drop. The nominal thickness of each deposit was 1 μm.

Figure 8

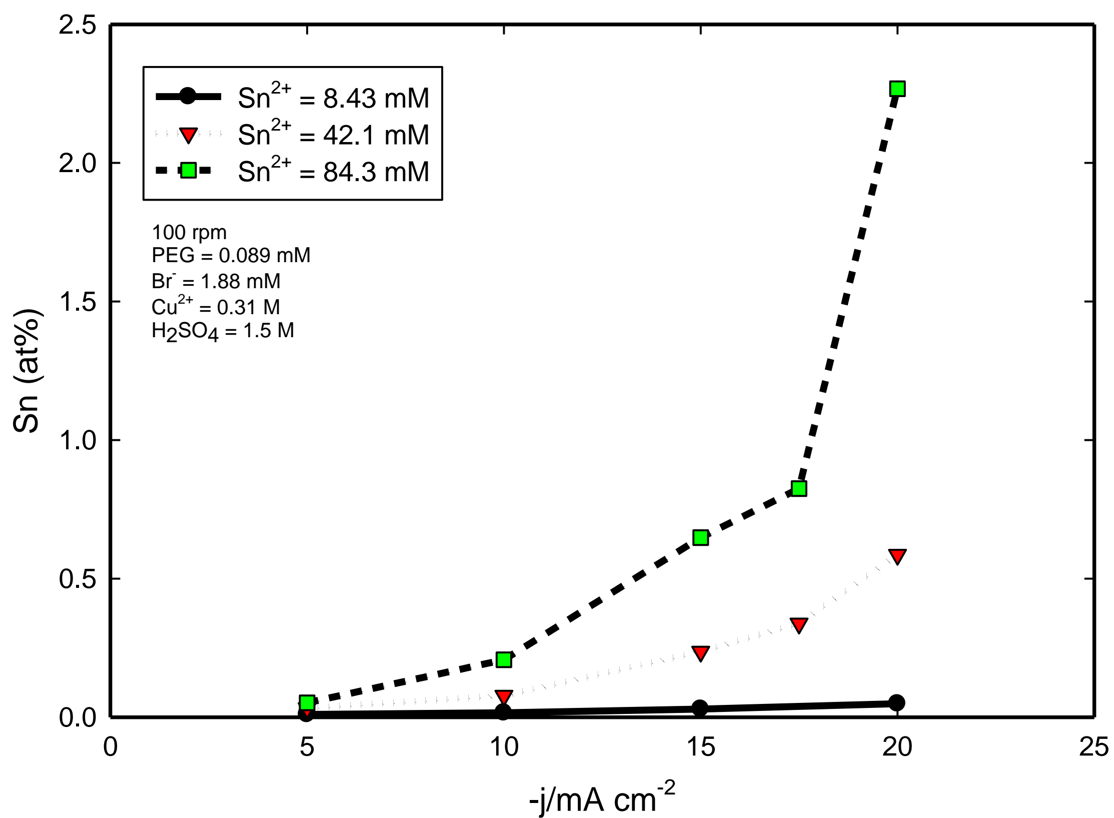

Figure 8. Composition of Sn in the Cu-Sn alloy as a function of current density and Sn^{2+} concentration in the electrolyte containing Br-PEG additive system. Deposition was conducted at 100 rpm.

Figure 9

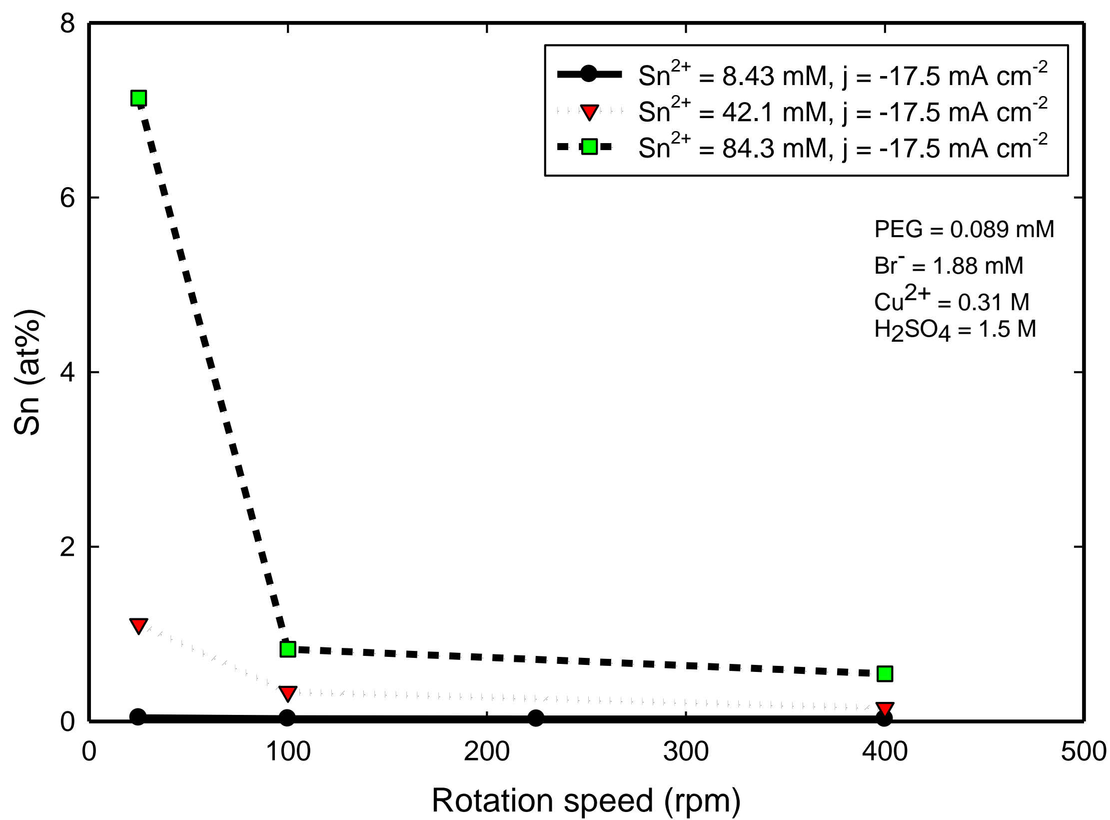

Figure 9. Composition of Sn in the Cu-Sn alloy as a function of rotation speed and Sn^{2+} concentration in the electrolyte containing Br-PEG additive system. See legend for the applied current density.

Figure 10

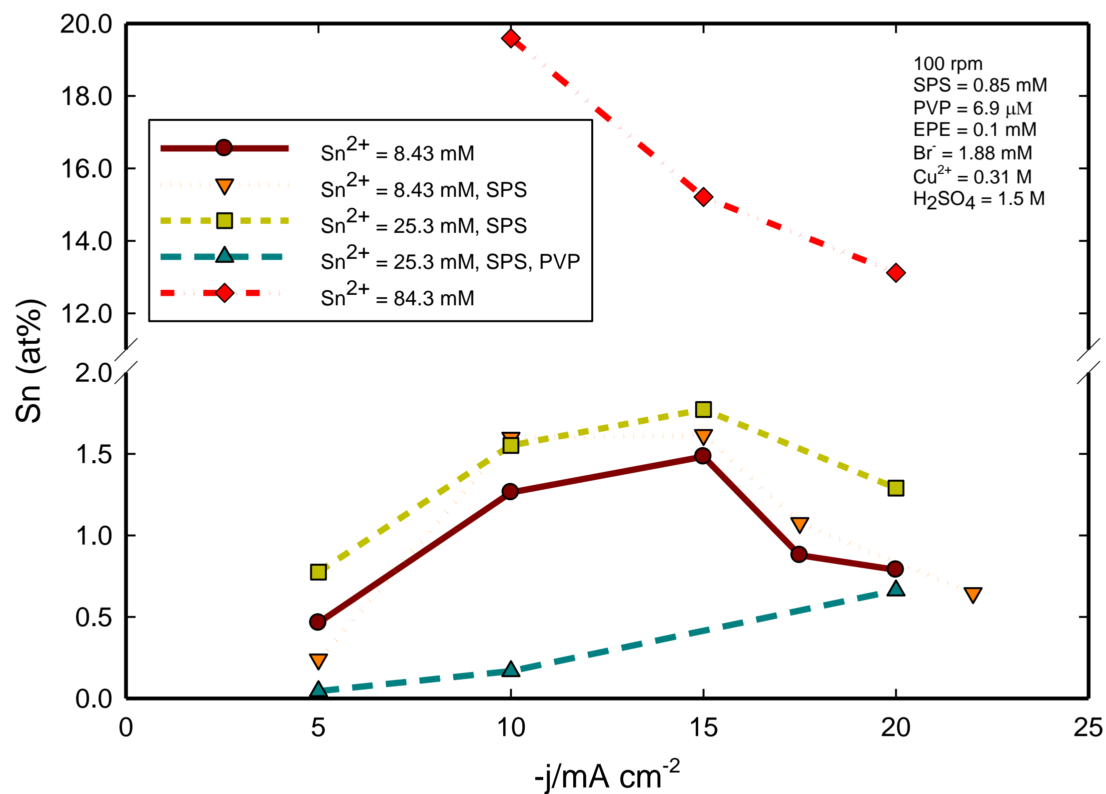

Figure 10. Composition of Sn in the Cu-Sn alloy as a function of current density and Sn^{2+} concentration in the electrolyte containing Br-EPE additive system. Deposition was conducted at 100 rpm.

Figure 11

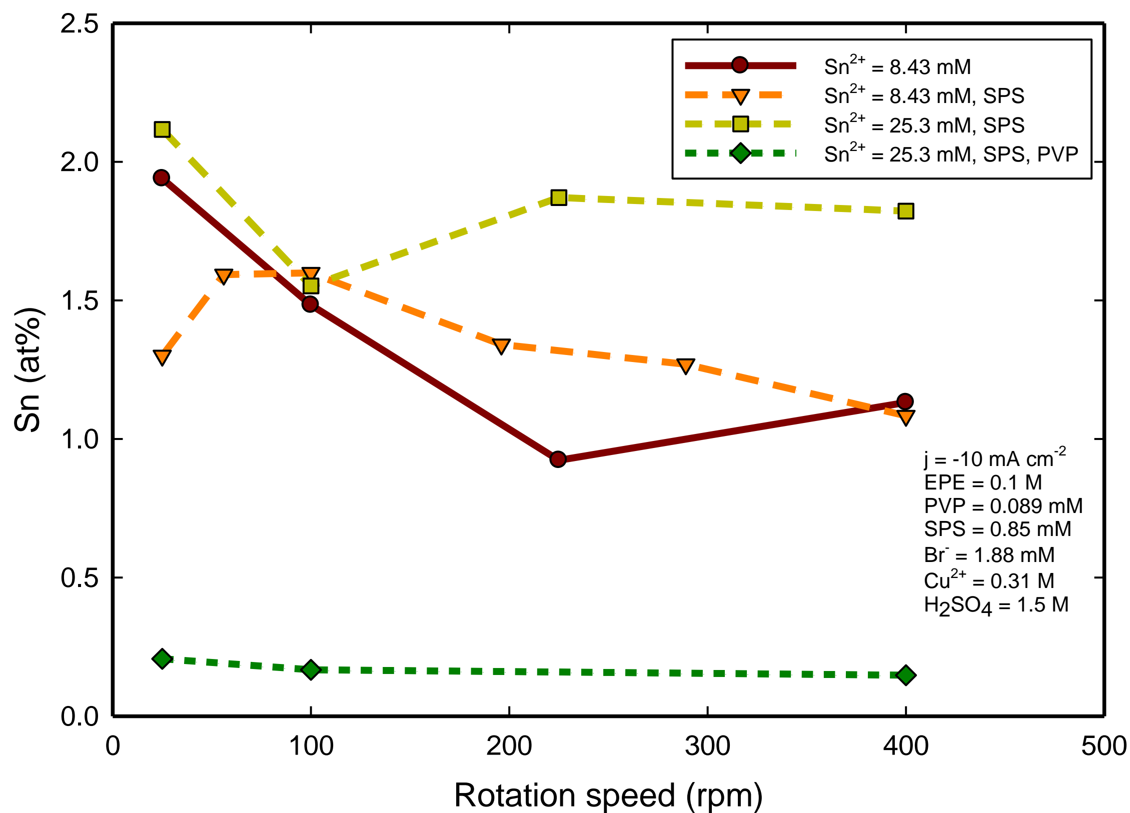

Figure 11. Composition of Sn in the Cu-Sn alloy as a function of rotation speed and Sn^{2+} concentration in the electrolyte containing Br-EPE additive system. Deposition was conducted at $j = -10$ mA cm^{-2}.

Chapter 7

Conclusions

First part of this research evaluated the impact of Fe^{3+}/Fe^{2+} redox couple on two representative organic additives (PEG and SPS), while second part focused on electrodeposition of copper alloys as a possible application in interconnect technology. Two alloys under investigation were copper-silver (Cu-Ag) and copper-tin (Cu-Sn) co-deposits. The objective of both projects was to extend copper interconnect technology to meet the challenges of present and future semiconductor device fabrication.

The inhibition of copper metal deposition by PEG as well as adsorption and desorption of PEG were not affected by the Fe^{3+}/Fe^{2+} redox couple. In contrast, the activity of SPS increased when the Fe^{3+}/Fe^{2+} couple was present in a copper-plating bath. During electrochemical analysis with HPLC, it was found that the Fe^{3+}/Fe^{2+} redox couple reacted with SPS to form MPS in the bulk solution. The Fe^{3+}/Fe^{2+} ratio was a method of varying the reducing power of the electrolyte, changing the concentration of MPS derived from SPS. The electrochemical response from adding either Fe^{2+} or 20 ppb MPS to copper electrolyte was almost identical, suggesting further that the enhanced acceleration by adding redox mediator was the result of elevation of bulk MPS concentration. The estimates of the standard reduction potential of SPS to MPS reduction, based on equilibrium calculation with

reference to HPLC results, predicted the reduction potential in the range between 0.3 – 0.4 V *vs.* SHE.

The study of SPS/MPS equilibrium in the presence of Fe^{3+}/Fe^{2+} redox couple was facilitated by the development a novel chromatographic method for the effective detection of SPS, MPS, monoxide-of-SPS, and dioxide-of-SPS from a copper electrolyte. A HPLC tool was coupled with an electrochemical detector, which enabled concentration sampling in a range of just a few parts per billion. This method can also prove crucial for a plating bath control, where a small amount of certain byproducts significantly affect performance of the electrolyte.

Electrodeposition of Cu-Ag alloys at a substantial chloride concentration by the application of pulsed plating was demonstrated. It was shown that Ag incorporation into the alloy can be controlled by varying pulse frequencies and duty cycles, electrode rotation speeds, and electrolyte concentrations. However, organic additives decreased incorporation of Ag into the alloy due to a possible complexing effect on silver ion. It was also discovered that $CuSO_4 \cdot 5H_2O$ from a number of major chemical suppliers contained Ag as impurity. The pulse-plating conditions created significant film roughness. However, addition of a leveling agent substantially reduced roughness of the Cu-Ag films. Chloride concentration was shown to have a critical impact on behavior of a leveling agent. At 1 ppm of chloride films contained voids and were discontinuous, while at 10 ppm of chloride continuous deposits with large grains were obtained.

The final chapter of this work examined electrodeposition of Cu-Sn alloy thin films from acidic copper sulfate electrolytes. Co-deposition of Sn with Cu was enabled by the polarization of copper deposition into the region where Sn deposition became possible. The

most polarizing effect was achieved by utilizing the Br-EPE pair, compared to several other halogen-suppressor combinations. All additive combinations used also exhibited stronger polarization of Cu deposition in electrolytes with higher sulfuric acid and lower Cu^{2+} concentration. The content of Sn in the Cu-Sn alloy was found to be a function of the applied current density, rotation speed, and the amount of Sn^{2+} present in the electrolyte. It was demonstrated that Sn content between 0 – 7 at% in the alloy occurred above the reduction potential of Sn^{2+}, possibly due to underpotential deposition. Higher Sn content of up to 20 at% was achieved when Cu deposition was suppressed below the deposition potential of Sn^{2+} by the combination of Br and EPE at 10 g L^{-1} of Sn^{2+}. A positive correlation between Sn content and concentration of Sn^{2+} in the electrolyte was observed. Higher tin content in the alloy also correlated to low rotation speeds. The relationship between the Sn content and the applied current density was specific to the utilized additive combination.